ISSN 1563 – 0277
eISSN 2617 – 4871

ӘЛ-ФАРАБИ атындағы ҚАЗАҚ ҰЛТТЫҚ УНИВЕРСИТЕТІ

ХАБАРШЫ

Математика, механика, информатика сериясы

КАЗАХСКИЙ НАЦИОНАЛЬНЫЙ УНИВЕРСИТЕТ имени АЛЬ-ФАРАБИ

ВЕСТНИК

Серия математика, механика, информатика

AL-FARABI KAZAKH NATIONAL UNIVERSITY

Journal of Mathematics, Mechanics and Computer Science

№4 (116)

Алматы
«Қазақ университеті»
2022

Зарегистрирован в Министерстве информации и коммуникаций Республики Казахстан, свидетельство №16508-Ж от 04.05.2017 г. (Время и номер первичной постановки на учет №766 от 22.04.1992 г.). Язык издания: английский. Выходит 4 раза в год.
Тематическая направленность: теоретическая и прикладная математика, механика, информатика.

Индексируется и участвует:

Научное издание
Вестник КазНУ. Серия "Математика, механика, информатика", № 4 (116) 2021.
Редактор – С.Е. Айтжанов. Компьютерная верстка – С.Е. Айтжанов

ИБ N 15229
Формат 60 × 84 1/8. Бумага офсетная. Печать цифровая. Объем 6,25 п.л.
Заказ N 13463. Издательский дом "Қазақ университеті"
Казахского национального университета им. аль-Фараби. 050040, г. Алматы, пр.аль-Фараби, 71, КазНУ.
Отпечатано в типографии издательского дома "Қазақ университеті".

1-бөлім **Раздел 1** **Section 1**

Математика **Математика** **Mathematics**

IRSTI 27.31.44 DOI: https://doi.org/10.26577/JMMCS.2022.v116.i4.01

B. O. Derbissaly
Institute of Mathematics and Mathematical Modeling, Almaty, Kazakhstan
e-mail: derbissaly@math.kz

ON GREEN'S FUNCTION OF SECOND DARBOUX PROBLEM FOR HYPERBOLIC EQUATION

A definition and justify a method for constructing the Green's function of the second Darboux problem for a two-dimensional linear hyperbolic equation of the second order in a characteristic triangle is given. In contrast to the (well-developed) theory of the Green's function for self-adjoint elliptic problems, this theory has not yet been developed. And for the case of asymmetric boundary value problems such studies have not been carried out. It is shown that the Green's function for a hyperbolic equation of the general form can be constructed using the Riemann-Green function for some auxiliary hyperbolic equation. The notion of the Green's function is more completely developed for Sturm-Liouville problems for an ordinary differential equation, for Dirichlet boundary value problems for Poisson equation, for initial boundary value problems for a heat equation. For many particular cases, the Greens' function has been constructed explicitly. However, many more problems require their consideration. In this paper, the problem of constructing the Green's function of the second Darboux problem for a hyperbolic equation was investigated. The Green's function for the hyperbolic problems differs significantly from the Green's function of problems for equations of elliptic and parabolic types.
Key words: Hyperbolic equation, initial-boundary value problem, second Darboux problem, boundary condition, Green function, a characteristic triangle, Riemann–Green function.

Б. О. Дербісалы
Математика және математикалық моделдеу институты , Алматы қ., Қазақстан
e-mail: derbissaly@math.kz

ГИПЕРБОЛАЛЫҚ ТЕҢДЕУ ҮШІН ЕКІНШІ ДАРБУ ЕСЕБІНІҢ ГРИН ФУНКЦИЯСЫ

Сипаттамалық үшбұрышта қарастырылатын екінші ретті екі өлшемді сызықтық гиперболалық теңдеу үшін Грин функциясын құру әдістемесі анықталды және негізделді. Өз-өзіне түйіндес эллиптикалық есептер үшін Грин функциясының (жақсы дамыған) теориясынан айырмашылығы, сипаттамалық шекаралық есептер үшін бұл теория әлі жетік әзірленбегендігінде. Ал симметриялық емес шекаралық есептер жағдайында мұндай зерттеулер жүргізілмеген. Жалпы түрдегі гиперболалық теңдеуге арналған Грин функциясын кейбір (арнайы жолмен құрылған) көмекші гиперболалық теңдеу үшін Риман-Грин функциясын қолдана отырып құруға болатындығы көрсетілді. Грин функциясының толығырақ тұжырымдамасы қарапайым дифференциалдық теңдеу үшін Штурм-Лиувиль есептері үшін, Пуассон теңдеуі үшін Дирихле шеткі есептері үшін, жылуөткізгіштік теңдеуі үшін бастапқы шекаралық есептер үшін жасалған. Көптеген дербес жағдайларда Грин функциясы айқын түрде құрылған. Алайда, басқа да көптеген есептер оларды қарастыруды талап етеді. Бұл мақалада гиперболалық теңдеу үшін екінші Дарбу есебінің Грин функциясын құру мәселесі зерттелді. Гиперболалық есептер үшін құрылған Грин функциясы эллиптикалық және параболалық есептер үшін құрылған Грин функциясынан айтарлықтай ерекшеленеді.

Түйін сөздер: Гиперболалық теңдеу, бастапқы-шекаралық есеп, екінші Дарбу есебі, шекаралық шарт, Грин функциясы, характеристикалық үшбұрыш, Риман–Грин функциясы.

Б. О. Дербисалы
Институт математики и математического моделирования, г. Алматы, Казахстан
e-mail: derbissaly@math.kz

О ФУНКЦИИ ГРИНА ВТОРОЙ ЗАДАЧИ ДАРБУ ДЛЯ ГИПЕРБОЛИЧЕСКОГО УРАВНЕНИЯ

Дано определение и обоснована методика построения функции Грина для второй задачи Дарбу для двумерного линейного гиперболического уравнения второго порядка, рассматриваемого в характеристическом треугольнике. В отличие от (хорошо разработанной) теории функции Грина для самосопряженных эллиптических задач, для характеристических граничных задач эта теория еще не подробно разработана. А для случая несимметрических граничных задач таких исследований не проводилось. Показано, что функция Грина для гиперболического уравнения общего вида может быть построена с использованием функции Римана-Грина для некоторого (специальным образом построенного) вспомогательного гиперболического уравнения. Наиболее полно понятие функции Грина разработано для задач Штурма-Лиувилля для обыкновенного дифференциального уравнения, для краевых задач Дирихле для уравнения Пуассона, для начально-краевых задач для уравнения теплопроводности. Для многих частных случаев функция Грина была построена в явном виде. Однако, еще многие задачи требуют своего рассмотрения. В настоящей статье исследована задача о построении функции Грина для второй задачи Дарбу для гиперболического уравнения. Функция Грина для гиперболических задач существенно отличается от функций Грина задач для уравнений эллиптического и параболического типа.

Ключевые слова: Гиперболическое уравнение, начально-краевая задача, вторая задача Дарбу, граничное условие, функция Грина, характеристический треугольник, функция Римана–Грина.

1 Introduction

In $S \subset \mathbb{R}^n$ let us consider some a linear differential equation

$$Lu(x) = f(x),\ x \in S, \tag{1}$$

with homogeneous boundary conditions

$$Qu(x) = 0,\ x \in S. \tag{2}$$

If a solution of this problem exists, is unique and can be represented in the integral form

$$u(x) = \int\limits_S G_Q(x,y)f(y)dy, \tag{3}$$

then the kernel of this integral operator (3), that is, the function $G_Q(x,y)$, is called the Green's function of problem (1), (2).

It is also said that the Green's function for each fixed $y \in S$ satisfies the equation

$$LG_Q(x,y) = \delta(x-y),\ x \in S, \tag{4}$$

and the boundary conditions (2). Here $\delta(x-y)$ is the Dirac delta function. Equation (4) should be understood in the sense of generalized functions.

It is known that if the operator of problem (1), (2) has eigenfunctions $\{u_k(x)\}_{k=1}^{\infty}$ forming the Riesz basis in $L_2(S)$, then the solution of the problem can be represented as

$$u(x) = \sum_{k=1}^{\infty} \frac{1}{\lambda_k} \langle f, v_k \rangle_{L_2(S)} u_k(x), \tag{5}$$

where $\langle \cdot, \cdot \rangle_{L_2(S)}$ is a scalar product in $L_2(S)$, λ_k are eigenvalues of the operator, $\{v_k(x)\}_{k=1}^{\infty}$ is a biorthogonal system to $\{u_k(x)\}_{k=1}^{\infty}$. Formula (5) is called the spectral representation of the solution or the spectral representation of the inverse operator.

Representing the scalar product as an integral, we obtain the integral representation (3) of the solution of the problem, where

$$G_Q(x, y) = \sum_{k=1}^{\infty} \frac{1}{\lambda_k} u_k(x) \overline{v_k(y)} \tag{6}$$

is the Green's function of problem (1), (2). In the case when problem (1), (2) is self-adjoint, the system of its eigenfunctions forms an orthogonal basis. Therefore, we can choose $v_k(x) = u_k(x)$. In this case, it is easy to see from (6) that the Green's function is the symmetric function: $G_Q(x, y) = G_Q(y, x)$.

For series of characteristic problems for a wave equation and a wave equation with potential (despite the fact that these problems are solved by the method of separation of variables) all eigenvalues and eigenfunctions are constructed in the works of T. Sh. Kal'menov [1], [2] and M. A. Sadybekov [3]- [5]. Therefore, for these problems the Green's function can be constructed in the form of series (6). Although the presence of the Green's function is guaranteed for any self-adjoint problem, and it can be constructed in the form of series (6), the use of infinite series for constructing a solution of the problem is not very convenient. Therefore, the construction of the Green's function in the form of finite sums is actual.

We are interested in the integral representation of Green's function of the second Darboux problem for a general hyperbolic equation of the second order, since all the properties of Green's function of this problem come from the integral representation of Green's function.

The main difference between this paper and others, that in contrast to the previous works of other authors ([6]- [15] and others), we conduct the investigation and construction of the Green's function without the assumption of its symmetry. Also, unlike other authors, in this paper we will give a definition of the Green's function and a method for constructing it for the case of general coefficients.

2 Formulation of the problem

Let $\Omega = \{(\xi, \eta) :\ 0 \le \xi \le 1,\ \xi \le \eta \le 1\}$. The following hyperbolic equation is considered in Ω:

$$\frac{\partial^2 u}{\partial \xi \partial \eta} + a(\xi, \eta) \frac{\partial u}{\partial \xi} + b(\xi, \eta) \frac{\partial u}{\partial \eta} + c(\xi, \eta) u = f(\xi, \eta), \quad (\xi, \eta) \in \Omega, \tag{7}$$

with the initial condition

$$(u_\xi - u_\eta)(\xi, \xi) = \nu(\xi),\ 0 \le \xi \le 1, \tag{8}$$

and the boundary condition

$$u(0,\xi)=\tau(\xi),\ 0\le\xi\le 1. \tag{9}$$

We will assume that $a,b,a_\xi,b_\eta,c,f\in C\left(\overline{\Omega}\right);\ \nu,\tau\in C^1\left([0,1]\right)$ and

$$a(\xi,\xi)=b(\xi,\xi),\ 0\le\xi\le 1. \tag{10}$$

In [16] it was shown that equality (10) we can always get.

Also, we assume

$$a_\xi(\xi,\xi)=b_\eta(\xi,\xi),\ 0\le\xi\le 1. \tag{11}$$

3 Green's function of the problem (7)-(9)

Definition 1 *Green's function of the problem* (1)-(3) *let us call the function* $G(\xi,\eta;\xi_1,\eta_1)$, *which for every fixed* $(\xi_1,\eta_1)\in\Omega$, *satisfies the homogeneous equation*

$$L_{(\xi,\eta)}G(\xi,\eta;\xi_1,\eta_1)=0,\ (\xi,\eta)\in\Omega,\ at\,\xi\ne\xi_1,\ \eta\ne\eta_1,\ \eta\ne\xi_1,\ \xi\ne\eta_1; \tag{12}$$

and the next boundary conditions

$$(G_\xi-G_\eta)(\xi,\xi;\xi_1,\eta_1)=0,\ 0\le\xi\le 1,\ (\xi_1,\eta_1)\in\Omega; \tag{13}$$

$$G(0,\xi;\xi_1,\eta_1)=0,\ 0\le\xi\le 1,\ (\xi_1,\eta_1)\in\Omega; \tag{14}$$

and on the above characteristic lines, the following conditions must be met: the values of the derivatives of the Green function in directions parallel to these characteristics must coincide in adjacent regions; i.e.,

$$\frac{\partial G(\xi_1+0,\eta;\xi_1,\eta_1)}{\partial\eta}+a(\xi_1,\eta)G(\xi_1+0,\eta;\xi_1,\eta_1)$$
$$=\frac{\partial G(\xi_1-0,\eta;\xi_1,\eta_1)}{\partial\eta}+a(\xi_1,\eta)G(\xi_1-0,\eta;\xi_1,\eta_1),\ at\ \eta\ne\eta_1,\ \eta\ne\xi_1; \tag{15}$$

$$\frac{\partial G(\eta_1+0,\eta;\xi_1,\eta_1)}{\partial\eta}+a(\eta_1,\eta)G(\eta_1+0,\eta;\xi_1,\eta_1)$$
$$=\frac{\partial G(\eta_1-0,\eta;\xi_1,\eta_1)}{\partial\eta}+a(\eta_1,\eta)G(\xi_1-0,\eta;\xi_1,\eta_1),\ at\ \eta\ne\eta_1,\ \eta\ne\xi_1; \tag{16}$$

$$\frac{\partial G(\xi,\eta_1+0;\xi_1,\eta_1)}{\partial\xi}+b(\xi,\eta_1)G(\xi,\eta_1+0;\xi_1,\eta_1)$$
$$=\frac{\partial G(\xi,\eta_1-0;\xi_1,\eta_1)}{\partial\xi}+b(\xi,\eta_1)G(\xi,\eta_1-0;\xi_1,\eta_1),\ at\ \xi\ne\xi_1\ \xi\ne\eta_1; \tag{17}$$

$$\frac{\partial G(\xi,\xi_1+0;\xi_1,\eta_1)}{\partial\xi}+b(\xi,\xi_1)G(\xi,\xi_1+0;\xi_1,\eta_1)$$

$$= \frac{\partial G(\xi, \xi_1 - 0; \xi_1, \eta_1)}{\partial \xi} + b(\xi, \xi_1) G(\xi, \xi_1 - 0; \xi_1, \eta_1) \text{ at } \xi \neq \xi_1 \; \xi \neq \eta_1; \tag{18}$$

and the "corner condition"

$$G(\xi_1 - 0, \eta_1 - 0; \xi_1, \eta_1) - G(\xi_1 + 0, \eta_1 - 0; \xi_1, \eta_1)$$

$$+G(\xi_1 + 0, \eta_1 + 0; \xi_1, \eta_1) - G(\xi_1 - 0, \eta_1 + 0; \xi_1, \eta_1) = 1. \tag{19}$$

must be satisfied as the regions meet at $(\xi, \eta) = (\xi_1, \eta_1)$.

4 Existence and uniqueness of the Green's function of the problem (7)-(9)

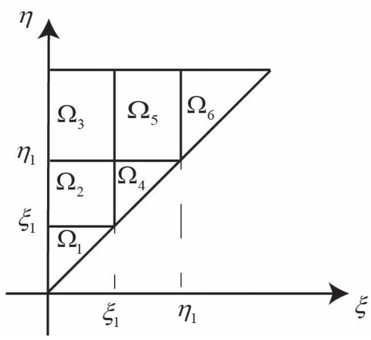

Figure 1: Splitting the domain Ω.

Theorem 1 *The function* $G(\xi, \eta; \xi_1, \eta_1)$ *that satisfies the conditions* (12)-(19) *exists and is unique.*

Proof. To show that a function $G(\xi, \eta; \xi_1, \eta_1)$, which satisfies the conditions (12)-(19) exists and unique, we divide the domain Ω into several subdomains (see Figure (1)) and consider the following problems sequentially. Let (ξ_1, η_1) be an arbitrary point of the domain Ω.

In the domain $\Omega_1 = \{(\xi, \eta) : 0 < \xi < \xi_1, \xi < \eta < \xi_1\}$ we consider the problem

$$L_{(\xi,\eta)} G = 0, \; (\xi, \eta) \in \Omega_1; \tag{20}$$

$$(G_\xi - G_\eta)(\xi, \xi; \xi_1, \eta_1) = 0, \; 0 \leq \xi \leq \xi_1; \tag{21}$$

$$G(0, \xi; \xi_1, \eta_1) = 0, \; 0 \leq \xi \leq \xi_1, \; (\xi_1, \eta_1) \in \Omega_2. \tag{22}$$

The problem (20)-(22) is a second Darboux problem and has a unique solution

$$G(\xi, \eta; \xi_1, \eta_1) \equiv 0, \; (\xi, \eta) \in \Omega_1. \tag{23}$$

In the domain $\Omega_2 = \{(\xi, \eta) : 0 \leq \xi \leq \xi_1, \xi_1 \leq \eta \leq \eta\}$ let us consider the problem

$$L_{(\xi,\eta)}G = 0,\ (\xi, \eta) \in \Omega_2; \tag{24}$$

$$G(0, \xi; \xi_1, \eta_1) = 0,\ \xi_1 \leq \xi \leq \eta_1,\ (\xi_1, \eta_1) \in \Omega_2. \tag{25}$$

From (23) we have the next equality

$$\frac{\partial G(\xi, \xi_1 + 0; \xi_1, \eta_1)}{\partial \xi} + b(\xi, \xi_1)G(\xi, \xi_1 + 0; \xi_1, \eta_1) = 0,\ 0 \leq \xi \leq \xi_1. \tag{26}$$

Integrating (26) by ξ we have

$$G(\xi, \xi_1 + 0; \xi_1, \eta_1) = \exp\left(-\int_0^\xi B(t, \xi_1)dt\right) C_1(\xi_1, \eta_1),\ 0 \leq \xi \leq \xi_1. \tag{27}$$

Substituting $\xi = 0$ in (27), using condition (14) we have that $C_1(\xi_1, \eta_1) \equiv 0$ and

$$G(\xi, \xi_1 + 0; \xi_1, \eta_1) = 0,\ 0 \leq \xi \leq \xi_1. \tag{28}$$

The problem (24),(25),(28) is a Goursat problem and has a unique solution

$$G(\xi, \eta; \xi_1, \eta_1) \equiv 0,\ (\xi, \eta) \in \Omega_2. \tag{29}$$

Therefore from (29) in the domain $\Omega_3 = \{(\xi, \eta) : 0 \leq \xi \leq \xi_1, \eta_1 \leq \eta \leq 1\}$, we get the problem

$$L_{(\xi,\eta)}G = 0,\ (\xi, \eta) \in \Omega_3; \tag{30}$$

$$G(0, \xi; \xi_1, \eta_1) = 0,\ \eta_1 \leq \xi \leq 1,\ (\xi_1, \eta_1) \in \Omega_3; \tag{31}$$

$$\frac{\partial G(\xi, \eta_1 + 0; \xi_1, \eta_1)}{\partial \xi} + b(\xi, \eta_1) \cdot G(\xi, \eta_1 + 0; \xi_1, \eta_1) = 0,\ 0 \leq \xi \leq \xi_1. \tag{32}$$

Integrating (32) by ξ we have

$$G(\xi, \eta_1 + 0; \xi_1, \eta_1) = \exp\left(-\int_0^\xi b(t, \eta_1)dt\right) C_2(\xi_1, \eta_1),\ 0 \leq \xi \leq \xi_1. \tag{33}$$

Substituting $\xi = 0$ in (33), using condition (14) we have that $C_2(\xi_1, \eta_1) \equiv 0$ and

$$G(\xi, \eta_1 + 0; \xi_1, \eta_1) = 0,\ 0 \leq \xi \leq \xi_1. \tag{34}$$

Therefore, the problem (30),(31),(34) is a Goursat problem and has a unique solution

$$G(\xi, \eta; \xi_1, \eta_1) \equiv 0,\ (\xi, \eta) \in \Omega_3. \tag{35}$$

In the domain $\Omega_4 = \{(\xi, \eta) : 0 \leq \xi \leq \xi_1, \xi \leq \eta \leq \eta_1\}$ we get the problem

$$L_{(\xi,\eta)}G = 0,\ (\xi, \eta) \in \Omega_4; \tag{36}$$

$$(G_\xi - G_\eta)(\xi, \xi; \xi_1, \eta_1) = 0,\ \xi_1 \leq \xi \leq \eta_1. \tag{37}$$

From (29) we have

$$\frac{\partial G(\xi_1+0,\eta;\xi_1,\eta_1)}{\partial \eta}+a(\xi_1,\eta)G(\xi_1+0,\eta;\xi_1,\eta_1)=0,\ \xi_1\leq\eta\leq\eta_1. \tag{38}$$

Integrating (38) by η we get

$$G(\xi_1+0,\eta;\xi_1,\eta_1)=\exp\left(-\int_{\xi_1}^{\eta}a(\xi_1,t)dt\right)C_3(\xi_1,\eta_1),\ \xi_1\leq\eta\leq\eta_1. \tag{39}$$

Substituting $\eta=\xi_1$ in (39), using condition (14) we have that $C_3(\xi_1,\eta_1)\equiv 0$ and

$$G(\xi_1+0,\eta;\xi_1,\eta_1)=0,\ \xi_1\leq\eta\leq\eta_1. \tag{40}$$

This problem (36),(37),(40) is a second Darboux problem and has a unique solution

$$G(\xi,\eta;\xi_1,\eta_1)\equiv 0,\ (\xi,\eta)\in\Omega_4. \tag{41}$$

Therefore, from (35), (41) in the domain $\Omega_5=\{(\xi,\eta):\xi_1\leq\xi\leq\eta_1,\eta_1\leq\eta\leq 1\}$ our problem is a Goursat problem

$$L_{(\xi,\eta)}G=0,\ (\xi,\eta)\in\Omega_5; \tag{42}$$

$$\frac{\partial G(\xi_1+0,\eta;\xi_1,\eta_1)}{\partial \eta}+a(\xi_1,\eta)G(\xi_1+0,\eta;\xi_1,\eta_1)=0,\ \eta_1\leq\eta\leq 1; \tag{43}$$

$$\frac{\partial G(\xi,\eta_1+0;\xi_1,\eta_1)}{\partial \xi}+b(\xi,\eta_1)G(\xi,\eta_1+0;\xi_1,\eta_1)=0,\ \xi_1\leq\xi\leq\eta_1; \tag{44}$$

$$G(\xi_1+0,\eta_1+0;\xi_1,\eta_1)=1. \tag{45}$$

The problem (41)-(45) has a unique solution, and it is easy to see that its solution coincides with the Riemann-Green function, that is,

$$G(\xi,\eta;\xi_1,\eta_1)=R(\xi,\eta;\xi_1,\eta_1),\ (\xi,\eta)\in\Omega_5. \tag{46}$$

Therefore from (46) in the domain $\Omega_6=\{(\xi,\eta):\eta_1\leq\xi\leq 1,\xi\leq\eta\leq 1\}$ we get the problem

$$L_{(\xi,\eta)}G=0,\ (\xi,\eta)\in\Omega_6; \tag{47}$$

$$(G_\xi-G_\eta)(\xi,\xi;\xi_1,\eta_1)=0,\ \eta_1\leq\xi\leq 1; \tag{48}$$

$$\frac{\partial G(\eta_1+0,\eta;\xi_1,\eta_1)}{\partial \eta}+b(\eta_1,\eta)G(\eta_1+0,\eta;\xi_1,\eta_1)$$
$$=\frac{\partial R(\eta_1,\eta;\xi_1,\eta_1)}{\partial \eta}+b(\eta_1,\eta)R(\eta_1,\eta;\xi_1,\eta_1),\ \eta_1\leq\eta\leq\xi_1. \tag{49}$$

The problem (47)-(49) is a second Darboux problem and has a unique solution.

Thus, we have shown that for any $(\xi_1,\eta_1)\in\Omega$ and $(\xi,\eta)\in\Omega$ the Green's function that satisfies the conditions (12)-(19) exists and unique. The theorem is proved.

5 Construction of the Green's function of the problem (7)-(9)

As can be seen from the proof of Theorem (1), the Green's function $G(\xi,\eta;\xi_1,\eta_1)=0$ in the domains Ω_1, Ω_2, Ω_3, Ω_4. And in the domain Ω_5 it coincides with the Riemann function (46).

Let us find a representation of the Green's function in the domain Ω_6. To construct the Green's functions, we will continue the coefficients of equation (47) in $\Omega_6^*=\{(\xi,\eta):\eta_1\le\xi\le 1,\ \eta_1\le\eta\le\xi\}$ such a way that the following conditions

$$A(\xi,\eta)=\begin{cases}a(\xi,\eta), & (\xi,\eta)\in\Omega_6,\\ b(\eta,\xi), & (\xi,\eta)\in\Omega_6^*,\end{cases}$$

$$B(\xi,\eta)=\begin{cases}b(\xi,\eta), & (\xi,\eta)\in\Omega_6,\\ a(\eta,\xi), & (\xi,\eta)\in\Omega_6^*,\end{cases}$$

$$C(\xi,\eta)=\begin{cases}c(\xi,\eta), & (\xi,\eta)\in\Omega_6,\\ c(\eta,\xi). & (\xi,\eta)\in\Omega_6^*\end{cases}$$

are met. Actually, show that coefficients of (47) have the following symmetry:

$$A(\xi,\eta)=B(\eta,\xi),\ C(\xi,\eta)=C(\eta,\xi),\ (\xi,\eta)\in\Omega_6. \tag{50}$$

From (50) we have

$$A(\eta,\xi)=\begin{cases}a(\eta,\xi), & (\eta,\xi)\in\Omega_6,\\ b(\xi,\eta), & (\eta,\xi)\in\Omega_6^*,\end{cases}=\begin{cases}b(\xi,\eta), & (\xi,\eta)\in\Omega_6,\\ a(\eta,\xi), & (\xi,\eta)\in\Omega_6^*,\end{cases}=B(\xi,\eta).$$

If we have chosen (ξ,η) from Ω_6, then (η,ξ) will be from Ω_6^*.

From (4) and (5) we get

$$A(\xi,\xi)=B(\xi,\xi),\ A_\xi(\xi,\xi)=B_\eta(\xi,\xi),\ \eta_1\le\xi\le 1.$$

If the coefficients $a,b,a_\xi,b_\eta,c\in C\left(\overline{\Omega}\right)$ then in virtue of (50) coefficients $A(\xi,\eta)$, $B(\xi,\eta)$, $C(\xi,\eta)$ in the domain $\widetilde{\Omega_6}=\Omega_6\cup\Omega_6^*=\{(\xi,\eta):\eta_1\le\xi\le 1,\ \eta_1\le\eta\le 1\}$ have the following smoothness

$$A,B,A_\xi,B_\eta,C\in C\left(\overline{\widetilde{\Omega_6}}\right). \tag{51}$$

Let (ξ_1,η_1) be an arbitrary point of the domain Ω. In order to construct the Green function in the domain Ω_6, consider the problem:

$$\frac{\partial^2 G_1}{\partial\xi\partial\eta}+A(\xi,\eta)\frac{\partial G_1}{\partial\xi}+B(\xi,\eta)\frac{\partial G_1}{\partial\eta}+C(\xi,\eta)G_1=0,\ (\xi,\eta)\in\widetilde{\Omega}_6; \tag{52}$$

$$\begin{aligned}&\frac{\partial G_1(\eta_1+0,\eta;\xi_1,\eta_1)}{\partial\eta}+b(\eta_1,\eta)G_1(\eta_1+0,\eta;\xi_1,\eta_1)\\ &=\frac{\partial R(\eta_1,\eta;\xi_1,\eta_1)}{\partial\eta}+b(\eta_1,\eta)R(\eta_1,\eta;\xi_1,\eta_1),\ \eta_1\le\eta\le\xi_1;\end{aligned} \tag{53}$$

$$\frac{\partial G_1(\xi,\eta_1+0;\xi_1,\eta_1)}{\partial\xi}+a(\xi,\eta_1)G_1(\xi,\eta_1+0;\xi_1,\eta_1)$$
$$=\frac{\partial R(\xi,\eta_1;\xi_1,\eta_1)}{\partial\xi}+a(\xi,\eta_1)R(\xi,\eta_1;\xi_1,\eta_1),\ \eta_1\le\xi\le\xi_1. \tag{54}$$

The problem (52)-(54) is a Goursat problem. Its solution exists and unique. We are interested in the representation of the function $G_1(\xi,\eta;\xi_1,\eta_1)$.

Lemma 1 *If the function $G_1(\xi,\eta;\xi_1,\eta_1)$ is the solution to the problem* (52)-(54)*, then for any $(\xi,\eta)\in\widetilde{\Omega}_6$ we have $G_1(\xi,\eta;\xi_1,\eta_1)=G_1(\eta,\xi;\xi_1,\eta_1)$.*

To show that the function $G_1(\eta,\xi;\xi_1,\eta_1)$ satisfies the equation (52), in (52) replace $\xi=\eta_2$, $\eta=\xi_2$, $(\eta_2,\xi_2)\in\Omega_6^*$ and after using the symmetry conditions of coefficients, we get that $G_1(\eta,\xi;\xi_1,\eta_1)$ satisfies the equation (52).

Also doing the substitution of $\xi=\eta_2$ in (53) and using the symmetry conditions of coefficients, we get the condition (54). Similarly, by replacing $\eta=\xi_2$ in (54) and using the symmetry conditions of coefficients, we get the condition (53).

Thus, we have shown that the function $G_1(\eta,\xi;\xi_1,\eta_1)$ is also a solution to the problem (52)-(54). Since the solution to problem (52)-(54) is unique, then

$$G_1(\xi,\eta;\xi_1,\eta_1)=G_1(\eta,\xi;\xi_1,\eta_1),\ (\xi,\eta)\in\widetilde{\Omega}_6.$$

Solution of the problem (52)-(54) we search in the following form

$$G_1(\xi,\eta;\xi_1,\eta_1)=R(\xi,\eta;\xi_1,\eta_1)+g(\xi,\eta;\xi_1,\eta_1),(\xi,\eta)\in\widetilde{\Omega}_6.$$

Then we get the following problem

$$\frac{\partial^2 g}{\partial\xi\partial\eta}+A(\xi,\eta)\frac{\partial g}{\partial\xi}+B(\xi,\eta)\frac{\partial g}{\partial\eta}+C(\xi,\eta)g=0,\ (\xi,\eta)\in\widetilde{\Omega}_6; \tag{55}$$

$$\frac{\partial g(\eta_1,\eta;\xi_1,\eta_1)}{\partial\eta}+b(\eta_1,\eta)g(\eta_1,\eta;\xi_1,\eta_1)=0,\ \eta_1\le\eta\le\xi_1; \tag{56}$$

$$\frac{\partial g(\xi,\eta_1;\xi_1,\eta_1)}{\partial\xi}+a(\xi,\eta_1)g(\xi,\eta_1;\xi_1,\eta_1)=0,\ \eta_1\le\xi\le\xi_1. \tag{57}$$

It is easy to see that the solution to the problem (55)-(57) has the form

$$g(\xi,\eta;\xi_1,\eta_1)=R(\eta,\xi;\xi_1,\eta_1),\ (\xi,\eta)\in\widetilde{\Omega}_6.$$

Lemma 2 *Let (ξ,η) be an arbitrary point of the domain Ω. By internal variables (ξ_1,η_1) the Green's function of the problem* (7)-(9) *has the following properties:*

$$L^*_{(\xi_1,\eta_1)}G(\xi,\eta;\xi_1,\eta_1)=0,\ (\xi_1,\eta_1)\in\Omega,\ \text{at}\ \xi_1\ne\xi,\ \xi_1\ne\eta,\ \eta_1\ne\xi; \tag{58}$$

$$(G_{\xi_1}-G_{\eta_1})(\xi,\eta;\xi_1,\xi_1)+(a-b)(\xi_1,\xi_1)G(\xi,\eta;\xi_1,\xi_1)=0,\ 0\le\xi_1\le1; \tag{59}$$

$$G(\xi,\eta;0,\eta_1)=0,\ 0\le\eta_1\le1; \tag{60}$$

$$\frac{\partial G(\xi,\eta;\xi-0,\eta_1)}{\partial \eta_1} - a(\xi,\eta_1)G(\xi,\eta;\xi-0,\eta_1) = 0,\ at\ \eta_1 \neq \eta,\ \eta_1 \neq \xi; \tag{61}$$

$$\frac{\partial G(\xi,\eta;\xi_1,\eta-0)}{\partial \xi_1} - b(\xi_1,\eta)G(\xi,\eta;\xi_1,\eta-0) = 0,\ at\ \xi_1 \neq \xi; \tag{62}$$

$$\frac{\partial G(\xi,\eta;\xi_1,\xi-0)}{\partial \xi_1} - b(\xi_1,\xi)\ G(\xi,\eta;\xi_1,\xi-0)$$

$$= \frac{\partial G(\xi,\eta;\xi_1,\xi+0)}{\partial \xi_1} - b(\xi_1,\xi)G(\xi,\eta;\xi_1,\xi+0); \tag{63}$$

$$G(\xi,\eta;\xi-0,\eta-0) - G(\xi,\eta;\xi+0,\eta-0)$$

$$+G(\xi,\eta;\xi+0,\eta+0) - G(\xi,\eta;\xi-0,\eta+0) = 1; \tag{64}$$

$$G(\xi,\eta;\xi,\xi-0) - G(\xi,\eta;\xi,\xi+0) - G(\xi,\eta;\xi-0,\xi) = 0. \tag{65}$$

Properties (58)-(65) are easy to get out of the construction of the Green's function of problem (7)-(9). Under these conditions (58)-(65) it is possible to uniquely restore the Green's function of problem (7)-(9).

Using properties (58)-(65) we can use it to write the integral representation of the solution to problem (7)-(9). To do this, we consider the following integral

$$\iint_{\Omega_{(\xi\eta)}} G(\xi,\eta;\xi_1,\eta_1)f(\xi_1,\eta_1)d\xi_1 d\eta_1$$

$$= \iint_{\Omega_{(\xi\eta)}} G(\xi,\eta;\xi_1,\eta_1)\left(\frac{\partial^2 u}{\partial \xi_1 \partial \eta_1} + a\frac{\partial u}{\partial \xi_1} + b\frac{\partial u}{\partial \eta_1} + cu\right) d\xi_1 d\eta_1. \tag{66}$$

Applying Green's theorem in a plane [17] and using the conditions (8), (9) properties of Green's function (58)-(65), from (66) we get the following representation of the solution to problem (7)-(9) in the domain $\Omega_{(\xi\eta)} = \Omega_5 \cup \Omega_6$:

$$u(\xi,\eta) = \frac{1}{2}\left(G(\xi,\eta;0,\xi+0) - G(\xi,\eta;0,\xi-0)\right)\tau(\xi) + \frac{1}{2}G(\xi,\eta;0,\eta-0)\tau(\eta)$$

$$+\frac{1}{2}\int_0^{\xi} G(\xi,\eta;\xi_1,\eta_1)\nu(\xi_1)d\xi_1 + \iint_{\Omega_{(\xi\eta)}} G(\xi,\eta;\xi_1,\eta_1)f(\xi_1,\eta_1)d\xi_1 d\eta_1.$$

6 Conclusion

In this paper, an integral representation of the Green function for a general second-order hyperbolic equation for the second Darboux problem is constructed, since all the properties of the Green function of this problem follow from the integral representation of the Green function. It is shown that the main difference between this work and other previous works by other authors, we conduct research and build a function Green's solution of this problem without using the symmetry conditions of the lower coefficients. In addition, unlike other authors, it is in the article that we will give a definition of the Green function and a method for constructing it for cases of general coefficients.

References

[1] Kalmenov T. Sh. On the Spectrum of a Self-Adjoint Problem for the Wave Equation // Vestnik Akad. Nauk. Kazakh. SSR. - 1982. - V. 2. - P. 63-66. [in Russian]

[2] Kal'menov T. Sh. Spectrum of a boundary - value problem with translation for the wave equation // Differential equations. - 1983. - V. 19, No. 1. - P. 64 - 66. [in Russian]

[3] Sadybekov M. A., Orynbasarov E. M. Baseness of the system of the eigenfunctions and associated functions with displacement of Lavrentev-Bitsadze equation // Doklady Mathematics. - 1992. - V. 324, No. 6. - P. 1152-1154. [in Russian]

[4] Orynbasarov E. M., Sadybekov M. A. The basis property of the system of eigen- and associated functions of a boundary value problem with shift for the wave equation // Math. Notes. - 1992. - V. 51, No. 5. - P. 482-484. [in Russian]

[5] Yessirkegenov N. A., Sadybekov M. A. Spectral properties of boundary-value problem with a shift for wave equation // Russian Math. (Iz. VUZ). - 2016. - V. 60, No. 3. - P. 41-46.

[6] Kreith K. Symmetric Green's functions for a class of CIV boundary value problems // Canad. Math. Bull. - 1988. - V. 31. - P. 272-279.

[7] Kreith K. Establishing hyperbolic Green's functions via Leibniz's rule // SIAM Rev. - 1991. - V. 33. - P. 101-105.

[8] Kreith K. A self-adjoint problem for the wave equation in higher dimensions // Comput. Math. Appl. - 1991. - V. 21. - P. 129-132.

[9] Kreith K. Mixed selfadjoint boundary conditions for the wave equation // Differential equations and its applications (Budapest), Colloq. Math. Soc. Janos Bolyai, 62, North-Holland, Amsterdam. - 1991. - P. 219-226.

[10] Iraniparast N. A method of solving a class of CIV boundary value problems // Canad. Math. Bull. - 1992. - V. 35, No. 3. - P. 371-375.

[11] Iraniparast N. A boundary value problem for the wave equation // Int. J. Math. Math. Sci. - 1999. - V. 22, No. 4. - P. 835-845.

[12] Iraniparast N. A CIV boundary value problem for the wave equation // Appl. Anal. - 2000. - V. 76, No. 3-4. - P. 261-271.

[13] Haws L. Symmetric Green's functions for certain hyperbolic problems // Comput. Math. Appl. - 1991. - V. 21, No. 5. - P. 65-78.

[14] Iraniparast N. Boundary value problems for a two-dimensional wave equation // Journal of Computational and Applied Mathematics. - 1994. - V. 55. - P. 349-356.

[15] Iraniparast N. A selfadjoint hyperbolic boundary-value problem // Electronic Journal of Differential Equations, Conference. - 2003. - V. 10. - P. 153-161.

[16] Derbissaly B. O, Sadybekov M. A. On Green's function of Darboux problem for hyperbolic equation // Bulletin of KazNU. Series of mathematics, mechanics, computer science. - 2021. - V. 111, No. 3. - P. 79-94.

[17] Riley K.F, Hobson M.P., Bence S.J. Mathematical methods for physics and engineering // Cambridge University Press, 2010.

Список литературы

[1] Кальменов Т. Ш. О спектре самосопряженной задачи для волнового уравнения // Вестник АН КазССР. - 1982. - Т. 2. - С. 63-66.

[2] Кальменов Т. Ш. Спектр краевой задачи со смещением для волнового уравнения // Дифференц. уравнения. - 1983. - Т. 19, Н. 1. -С. 64 - 66.

[3] Садыбеков М. А., Орынбасарова Е. М. Базисность системы корневых функций краевой задачи со смещением для уравнения Лаврентьева–Бицадзе // Докл. РАН. - 1992. - Т. 324, Н. 6. - С. 1152-1154.

[4] Орынбасаров Е. М., Садыбеков М. А: Базисность системы собственных и присоединенных функций краевой задачи со смещением для волнового уравнения // Матем. заметки. - 1992. - Т. 51, Н. 5. - С. 86-89.

[5] Yessirkegenov N. A., Sadybekov M. A. Spectral properties of boundary-value problem with a shift for wave equation // Russian Math. (Iz. VUZ). - 2016. - V. 60, No. 3. - P. 41-46.

[6] Kreith K. Symmetric Green's functions for a class of CIV boundary value problems // Canad. Math. Bull. - 1988. - V. 31. - P. 272-279.

[7] Kreith K. Establishing hyperbolic Green's functions via Leibniz's rule // SIAM Rev. - 1991. - V. 33. - P. 101-105.

[8] Kreith K. A self-adjoint problem for the wave equation in higher dimensions // Comput. Math. Appl. - 1991. - V. 21. - P. 129-132.

[9] Kreith K. Mixed selfadjoint boundary conditions for the wave equation // Differential equations and its applications (Budapest), Colloq. Math. Soc. Janos Bolyai, 62, North-Holland, Amsterdam. - 1991. - P. 219-226.

[10] Iraniparast N. A method of solving a class of CIV boundary value problems // Canad. Math. Bull. - 1992. - V. 35, No. 3. - P. 371-375.

[11] Iraniparast N. A boundary value problem for the wave equation // Int. J. Math. Math. Sci. - 1999. - V. 22, No. 4. - P. 835-845.

[12] Iraniparast N. A CIV boundary value problem for the wave equation // Appl. Anal. - 2000. - V. 76, No. 3-4. - P. 261-271.

[13] Haws L. Symmetric Green's functions for certain hyperbolic problems // Comput. Math. Appl. - 1991. - V. 21, No. 5. - P. 65-78.

[14] Iraniparast N. Boundary value problems for a two-dimensional wave equation // Journal of Computational and Applied Mathematics. - 1994. - V. 55. - P. 349-356.

[15] Iraniparast N. A selfadjoint hyperbolic boundary-value problem // Electronic Journal of Differential Equations, Conference. - 2003. - V. 10. - P. 153-161.

[16] Derbissaly B. O, Sadybekov M. A. On Green's function of Darboux problem for hyperbolic equation // Bulletin of KazNU. Series of mathematics, mechanics, computer science. - 2021. - V. 111, No. 3. - P. 79-94.

[17] Riley K.F, Hobson M.P., Bence S.J. Mathematical methods for physics and engineering // Cambridge University Press, 2010.

IRSTI 27.31.17 DOI: https://doi.org/10.26577/JMMCS.2022.v116.i4.02

J. Ferreira[1], **M. Shahrouzi**[2] **Sebastião Cordeiro**[3] **Daniel V. Rocha**[4]

[1]Federal Fluminense University, Volta Redonda-RJ, Brazil
[2]Jahrom University, Jahrom, Iran
[3]Federal University of Pará, Abaetetuba, Brazil
[4]Federal University of Pará (UFPA), Belem, Brazil
e-mail: *jorge_ferreira@id.uff.br

BLOW UP OF SOLUTION FOR A NONLINEAR VISCOELASTIC PROBLEM WITH INTERNAL DAMPING AND LOGARITHMIC SOURCE TERM

This paper is concerned with blow up of weak solutions of the following nonlinear viscoelastic problem with internal damping and logarithmic source term

$$|u_t|^\rho u_{tt} + M(\|u\|^2)(-\Delta u) - \Delta u_{tt} + \int_0^t g(t-s)\Delta u(s)ds + u_t = u|u|_R^{p-2} \ln |u|_R^k$$

with Dirichlet boundary initial conditions in a bounded domain $\Omega \subset R^n$. In the physical point of view, this is a type of problems that usually arises in viscoelasticity. It has been considered with power source term first by Dafermos [3], in 1970, where the general decay was discussed. We establish conditions of p, ρ and the relaxation function g, for that the solutions blow up in finite time for positive and nonpositive initial energy. We extend the result in [15] where is considered $M = 1$ and external force type $|u|^{p-2}u$ in it. Further we estate and sketch the proof of a result of local existence of weak solution that is used in the proof of the theorem on blow up. The idea underlying the proof of local existence of solution is based on Faedo-Galerkin method combined with the Banach fixed point method.

Key words: Nonlinear Viscoelastic Equation, Logarithmic Source, Blow Up, Local existence.

Ж. Феррейра[1], М. Шахрузи[2], Себастьяо Кордейро[3], Даниел В. Роча[4]
[1]Флуминенсе Федералдық университеті, Вольта Редонда-РЖ қ., Бразилия
[2]Джахром университеті, Джахром қ., Иран
[3]Пара федералды университеті, Абаэтетуба қ., Бразилия
[4]Пара Федералдық университеті, Белем қ., Бразилия
e-mail: *jorge_ferreira@id.uff.br

Ішкі демпферлік және логарифмдік көзді сызықты емес тұтқыр серпімді есеп шешімінің қирауы

Бұл жұмыс $\Omega \subset R^n$ шектелген облыста бастапқы және Дирихле шартымен қойылған тұтқыр-серпімді ішкі демпфірлік және логарифмдік сызықты емес мүшелері бар

$$|u_t|^\rho u_{tt} + M(\|u\|^2)(-\Delta u) - \Delta u_{tt} + \int_0^t g(ts)\Delta u(s)ds + u_t = u|u|_R^{p-2} \ln |u|_R^k$$

есебінің әлсіз шешімдерінің қирауын зерттеуге арналған. Физикалық тұрғыдан алғанда, бұл әдетте тұтқыр серпімділікте пайда болатын мәселелердің бір түрі. Оны қуат көзі терминімен алғаш рет 1970 жылы Дафермос [3] қарастырды, онда жалпы ыдырау талқыланған. Мұнда оң және теріс бастапқы энергия үшін шешімдердің ақырлы уақытта қирауы туралы p, ρ және g релаксация функциясына шарттар алынды . Нәтижені [15] үшін де кеңейттік, мұнда $M = 1$ алынды және оған сыртқы күштің түрі $|u|^{p-2}u$. Біз қирау теоремасын дәлелдеуінде қолданылатын әлсіз локалдік шешімнің шешімділігін дәлелін келтіреміз. Локалдік шешімнің болуын дәлелдейтін идея Фаедо-Галеркин әдісіне негізделген және Банахтың бекітілген нүкте әдісімен біріктірілген.
Түйін сөздер: Тұтқырсерпімді сызықты емес теңдеу, логарифмдік көз, шешімнің қирауы, локалдік бар болу.

Ж. Феррейра[1], М. Шахрузи[2], Себастьяо Кордейро[3], Даниел В. Роча[4]
[1]Федеральный университет Флуминенсе, г. Вольта-Редонда-Р.Дж., Бразилия
[2]Джахромский университета, г. Джахром, Иран
[3]Федеральный университет Пара, г. Абаэтетуба, Бразилия
[4]Федерального университета Пара, г. Белем, Бразилия
e-mail: *jorge_ferreira@id.uff.br

Разрушение решения нелинейной вязкоупругой задачи с внутренним затуханием и логарифмическим источником

Эта статья посвящена разрушению слабых решений следующих нелинейных вязкоупругая задача с внутренним демпфированием и логарифмическим исходным членом

$$|u_t|^\rho u_{tt} + M(\|u\|^2)(-\Delta u) - \Delta u_{tt} + \int_0^t g(ts)\Delta u(s)ds + u_t = u|u|_R^{p-2}\ln|u|_R^k$$

с граничными начальными условиями Дирихле в ограниченной области $\Omega \subset R^n$. С физической точки зрения это тип проблем, которые обычно возникают в вязкоупругости. Впервые он был рассмотрен с термином источника энергии Дафермосом [3] в 1970 году, где обсуждался общий распад энергии. Устанавливаются условия p, ρ и функции релаксации g, при которых решения разрушаются за конечное время при положительной и неположительной начальной энергии. Мы распространяем результат на [15], где рассматривается $M = 1$ и в нем внешняя сила типа $|u|^{p-2}u$. Далее мы сформулируем и набросаем доказательство результата локального существования слабого решения, используемого в доказательстве теоремы о разрушении. Идея, лежащая в основе доказательства локального существования решения, основана на сочетании метода Фаэдо-Галеркина с методом неподвижной точки банаха.
Ключевые слова: Нелинейное уравнение вязкоупругости, логарифмический источник, разрушение, локальное существование.

1 Introduction

In elasticity the existing theory accounts for materials which have a capacity to store mechanical energy with no dissipation (of the energy). On the other hand, a Newtonian viscous fluid in a nonhydrostatic stress state has a capacity for dissipating energy without storing it. Materials which are outside the scope of these two theories would be those for which some, but not all, of the work done to deform them, can be recovered. Such materials possess a capacity of storage and dissipation of mechanical energy. This is the case of viscoelastic materials.

Viscoelastic materials are those for which the behavior combines liquid-like and solid-like characteristics. Viscoelasticity is important in areas such as biomechanics; power industry or heavy construction; Synthetic polymers; Wood; Human tissue, cartilage; Metals at high temperature; Concrete.

Polymers, for instance, are viscoelastic materials since they exhibit an intermediate position between viscous liquids and elastic solids. The formulation of Boltzmann's superposition principle leads to a memory term involving a relaxation function of exponential type. But, it has been observed that relaxation functions of some viscoelastic materials are not necessarily of this type. See [13, 14]. In this work, we are concerned with the following initial boundary value problem:

$$\begin{cases} |u_t|^{\rho}_{\mathbb{R}} u_{tt} + M(\|u\|^2)(-\Delta u) - \Delta u_{tt} + \int_0^t g(t-s)\Delta u(s)ds + u_t \\ = u|u|^{p-2}_{\mathbb{R}} \ln |u|^k_{\mathbb{R}} \quad \text{in} \quad \Omega \times (0,\infty) \\ u = 0 \quad \text{on} \quad \partial\Omega \times [0,\infty) \\ u(x,0) = u_0(x) \quad \text{in} \quad \Omega \\ u_t(x,0) = u_1(x) \quad \text{in} \quad \Omega. \end{cases} \tag{1}$$

where $\Omega \subset \mathbb{R}^n$ $(n \geq 1)$ is a bounded domain with a smooth boundary $\partial\Omega$, $p > 2$, $\rho > 0$ and $k > 0$ are constants and $g : \mathbb{R}^+ \to \mathbb{R}^+$ and $M : [0,\infty) \to \mathbb{R}$ are C^1 functions, respectively, left to be defined later.

As mentioned in [9], the logarithmic nonlinearity appears in several branches of physics such as inflationary cosmology, nuclear physics, optics, and geophysics. With all this specific underlying meaning in physics, the global-in-time well-posedness of solution to the problem of evolution equation with such logarithmic-type nonlinearity captures lots of attention. See [9] for the references related to each branch listed above.

The dispersive term Δu_{tt} arises in the study of extensional vibrations of thin rods, see Love [7], via the model

$$u_{tt} - \Delta u - \Delta u_{tt} = f$$

and was studied by one of the authors in [11]. The function $M(\lambda)$ in (1) has its motivation in the mathematical description of vibration of an elastic stretched string, modeled by the equation

$$u_{tt} - M\Big(\int_\Omega |\nabla u|^2 dx\Big)\Delta u = 0,$$

which for $M(\lambda) \geq m_0 > 0$ was studied in [2, 4, 5, 10, 12].

Concerning blow-up results, Messaoudi [8] considered the equation

$$u_{tt} - \Delta u + \int_0^t g(t-s)\Delta u(s)ds + au_t|u_t|^{m-2} = b|u|^{r-2}u$$

and proved that any weak solution with negative initial energy blows up in finite time if $r < m$ and $\int_0^\infty g(s)ds \leq \frac{r-2}{r-2+\frac{1}{r}}$. Also, Liu [6] studied the equation

$$u_{tt} - \Delta u + \int_0^t g(t-s)\Delta u(s)ds - \omega\Delta u_t + \mu u_t = |u|^{r-2}u$$

where he proved that the solution with nonpositive initial energy as well as positive initial energy blows up in finite time.

Our blow up result is motivated by the viscoelastic wave equation with delay considered by [15]

$$|u_t|^\rho u_{tt}\Delta u - \Delta u_{tt} + \int_0^t g(t-s)\Delta u(s)ds + \mu_1 u_t(x,t) + \mu_2 u_t(x,t-\tau) = b|u|^{p-2}u.$$

We implemented the technique employed in it, in order to extend his/her problem to the case of logarithmic source term and M variable.

This work is divided as follows. The section 2 presents the notation and results underlying the methods used in this paper. In section 3 is stated and proved a result of blow up for locally defined solutions.

2 Preliminaries and assumptions

For simplicity of notations hereafter we denote by $|\cdot|$ the Lebesgue Space $L^2(\Omega)$-norm, $\|\cdot\| := \int_\Omega |\nabla(\cdot)|^2_{\mathbb{R}^n}dx$ the Sobolev space $H^1_0(\Omega)$-norm, $\|\cdot\|_r := \|\cdot\|_{L^r(\Omega)}$ and $|\cdot|_{\mathbb{R}}$ and $|\cdot|_{\mathbb{R}^n}$ for absolute value of a real number and the norm of a vetor in $\mathbb{R}^n$, respectively.

Lemma 1 *There exists $C > 0$ such that*

$$\|u\|_r^s \leq C\Big(\|u\|^2 + \|u\|_r^r\Big)$$

for any $u \in H^1_0(\Omega)$ and $2 \leq s \leq r$.

We start setting some hypotheses for the problem (1). Firstly, we shall assume that

$$0 < \rho \leq \frac{2}{n-2} \quad \text{if } n \geq 3, \quad \text{or } \rho > 0 \text{ if } n = 1,2, \tag{2}$$

$$2 < p \leq \frac{2(n-1)}{n-2} \quad \text{if } n \geq 3, \quad \text{or } p > 2 \text{ if } n = 1,2. \tag{3}$$

Secondly, we assume:

(H.1) $M \in C^1([0,\infty),\mathbb{R})$ is such that $M(\lambda) \geq m_0$, $\forall \lambda \in [0,\infty)$, where $m_0 > 0$.

(H.2) $g : \mathbb{R}^+ \to \mathbb{R}^+$ is a Lebesgue integrable and absolutely continuous function such that

$$1 - \int_0^\infty g(s)ds =: l > 0.$$

(H.3) There exist positive constants ξ_1 and ξ_2 verifying

$$-\xi_1 g(t) \leq g'(t) \leq -\xi_2 g(t) \quad \text{for almost all } t \geq 0.$$

We will need the very useful relation

$$\begin{aligned}\int_0^t g(t-\tau)(\nabla u(\tau), \nabla u_t(t))d\tau &= \frac{1}{2}(g' \diamond \nabla u)(t) - \frac{1}{2}(g \diamond \nabla u)'(t) \\ &+ \frac{d}{dt}\left\{\frac{1}{2}\left(\int_0^t g(s)ds\right)|\nabla u(t)|^2\right\} - \frac{1}{2}g(t)|\nabla u(t)|^2 \end{aligned} \tag{4}$$

that can be checked directly, where

$$(g \diamond y)(t) = \int_0^t g(t-s)|y(t) - y(s)|^2 ds$$

Let us denote $\hat{M}(s) = \int_0^s M(\tau)d\tau$. If $u(t), u_t(t) \in H_0^1(\Omega)$, then we define the total energy functional of equation (1):

$$\mathcal{E}(t) := \frac{1}{\rho+2}\|u_t(t)\|_{\rho+2}^{\rho+2} + \frac{1}{2}\left(\hat{M}(\|u\|^2) - \int_0^t g(s)ds\|u\|^2\right) + \frac{1}{2}\|u_t\|^2$$
$$+ \frac{k}{p^2}\int_\Omega |u|^p dx + \frac{1}{2}(g \diamond \nabla u)(t) - \frac{1}{p}\int_\Omega |u|_{\mathbb{R}}^p \ln |u|_{\mathbb{R}}^k dx. \tag{5}$$

From (4) and (H.3) one deduce that

$$\mathcal{E}'(t) = -|u_t(t)|^2 + \frac{1}{2}(g' \diamond \nabla u)(t) = \frac{1}{2}g(t)|\nabla u(t)|^2 \leq 0. \tag{6}$$

Using (H.1), (H.2), we infer

$$\mathcal{E}(t) \geq \frac{m_0+l-1}{2}\|u\|^2 + \frac{1}{2}(g \diamond \nabla u)(t) - \frac{c_s^{p+1}}{p}\|u\|^{p+1}$$
$$\geq F(\sqrt{(m_0+l-1)\|u\|^2 - (g \diamond \nabla u)(t)})$$

where c_s is the constant obtained from Sobolev embedding $H_0^1(\Omega) \hookrightarrow L^{p+1}(\Omega)$, and $F(x) = \frac{1}{2}x^2 - \frac{1}{p}B_1^{p+1}x^{p+1}$, with $B_1 = \frac{c_s}{(m_0+l-1)^{1/2}}$.

Remark 1 *As noticed in [15], F is increasing in $(0, \lambda_1)$, decreasing in (λ_1, ∞), and F has a maximum at $\lambda_1 = B_1^{-\frac{p+1}{p-1}}$ with the maximum value $E_1 = F(\lambda_1) = \frac{p-1}{2(p+1)}\lambda_1^2$.*

Lemma 2 ([15]) *Supposing (2), (3), (H.1) and (H.2), and that $(m_0+l-1)\|u_0\|^2 > \lambda_1^2$ and $E(0) < E_1$, then there exists $\lambda_2 > \lambda_1$ such that, for all $t \in [0, T)$,*

$$(m_0+l-1)\|u\|^2 + (g \diamond \nabla u)(t) \geq \lambda_2^2 \tag{7}$$

and

$$\|u\|_{p+1}^{p+1} \geq \frac{B_1^p}{p}\lambda_2^{p+1}. \tag{8}$$

3 Blow up

Theorem 1 *Assume that (2), (3), (H.1) and (H.2), and that $m_0+l-1 > 0$. Let $f \in L^2(0, T; H^{-1}(\Omega))$ and $u_0, u_1 \in H_0^1(\Omega)$. Then there exists a unique weak solution u for the problem*

$$\begin{cases} M(\|u\|^2)(-\Delta u) - \Delta u_{tt} + \int_0^t g(t-s)\Delta u(s)ds + u_t = f \\ u(0) = u_0, \quad u_t(0) = u_1. \end{cases} \tag{9}$$

Further, u_{tt} belongs to the class $L^\infty(0, T; H_0^1(\Omega))$.

Proof. Employ the Faedo-Galerkin method and Aubin-Lions Lemmas as in reference [1]. □

For our purposes hereafter, let us define

$$\mathbf{W} := \Big\{ w : w, w_t \in C(0,T; H_0^1(\Omega)), w_{tt} \in L^\infty(0,T; H_0^1(\Omega)) \Big\}$$

equipped with the norm

$$\|w\|_{\mathbf{W}}^2 := \alpha \|w\|^2_{L^\infty(0,T;H_0^1(\Omega))} + \delta \|w_t\|^2_{L^\infty(0,T;H_0^1(\Omega))} + \gamma \|w_{tt}\|^2_{L^2(0,T;H_0^1(\Omega))},$$

where $\alpha := \frac{m_0+l-1}{2}$, $\delta := \frac{1}{\sqrt{T}}$ and $\gamma := \frac{1}{\sqrt[4]{T}}$. □

It is easy to check that $\mathbf{W}$ is a Banach space with the norm $\|\cdot\|_{\mathbf{W}}$.

Theorem 2 *Let $u_0, u_1 \in H_0^1(\Omega)$ and assume that (H.1)-(H.3) and* (2) *and* (3) *are valid. Then the problem* (1) *has a local weak solution u in $\mathbf{W}$ for T small enough.*

Sketch of the proof. Let $M > 0$ and $T > 0$ and denote $\mathbf{Z}(M,T)$ the class of functions w belonging to $\mathbf{W}$, satisfying $w(0) = u_0$, $w_t(0) = u_1$ and $\|w\|_{\mathbf{W}} \le M$. Let us consider the application $A : \mathbf{Z}(M,T) \to \mathbf{W}$ defined in the following way. For each $v \in \mathbf{Z}(M,T)$, take $u := A[v]$ as the unique solution of the problem (9) with $f = v|v|_{\mathbb{R}}^{p-2} \ln |v|_{\mathbb{R}}^k - |v_t|_{\mathbb{R}}^\rho v_{tt}$. One can prove that with the hypotheses for p and ρ, A is a contraction from $\mathbf{Z}(M,T)$ to itself if M is large and T small enough. Apply next the Banach fixed point Theorem. □

In order to establish our result, an extra assumption on g is required:

(H.4)

$$\int_0^\infty g(s)ds < \frac{m_0 \zeta}{1+\zeta},$$

with $\zeta := \Big((p-2) - \beta(p-1)\Big)\Big(p - \beta(p-1)\Big)$, where $0 < \beta < \frac{p-2}{p-1}$ is a fixed number.

Theorem 3 *Assume that* (2), (3), *(H.1) and (H.2), and that $(m_0 + l - 1)\|u_0\|^2 > \lambda_1^2$ and $E(0) < \beta E_1$ and $\rho < p - 2$. Also assume that $\hat{M}(\tau) \le M(\tau)\tau$. Suppose that $u_0, u_1 \in H_0^1(\Omega)$. Then the solution u of* (1) *blows up in finite time.*

Proof. By contradiction we suppose there exists $K_1 > 0$ such that

$$\|u(t)\|^2 \le K_1 \ , \forall t \ge 0.$$

Set

$$H(t) = E_2 - \mathcal{E}(t),$$

where $E_2 \in (E(0), \beta E_1)$. By Lemma 6, we obtain $H(t) > 0$ and $H'(t) \ge 0$, $\forall t \ge 0$. Also, since $E_1 = \frac{p-1}{2(p+1)}\lambda_1^2$, then

$$\begin{aligned} H(t) &\le \beta E_1 - \frac{1}{2}\Big((m_0 + l - 1)\|u\|^2 + (g \diamond \nabla u)(t)\Big) + \frac{1}{p}\int_\Omega |u|_{\mathbb{R}}^p \ln |u|_{\mathbb{R}}^k dx \\ &\le E_1 - \frac{1}{2}\lambda_1^2 + \frac{1}{p}\int_\Omega |u|_{\mathbb{R}}^p \ln |u|_{\mathbb{R}}^k dx \le \frac{1}{p}\int_\Omega |u|_{\mathbb{R}}^p \ln |u|_{\mathbb{R}}^k dx. \end{aligned} \tag{10}$$

Define

$$L(t) = H^{1-\sigma}(t) + \frac{\varepsilon}{\rho+1}\int_\Omega |u_t|_{\mathbb{R}}^{\rho} u_t u dx + \varepsilon \int_\Omega \nabla u_t \nabla u dx + \frac{\varepsilon}{2}\int_\Omega u^2 dx, \tag{11}$$

where ε is chosen small enough for that $L(0) > 0$. Taking derivative of (11) and using (5), we get

$$L'(t) = (1+\sigma)L^{-\sigma}L' + \varepsilon\Big\{ - M(\|u\|^2)\|u\|^2 + \int_0^t g(t-s)(\nabla u(s), \nabla u(t))ds$$
$$+ \int_\Omega |u|_{\mathbb{R}}^p \ln |u|_{\mathbb{R}}^k dx\Big\} + \frac{\varepsilon}{\rho+1}\int_\Omega |u_t|_{\mathbb{R}}^{\rho+2} dx + \varepsilon\int_\Omega |\nabla u_t|_{\mathbb{R}^n}^2 dx. \tag{12}$$

It is easy to check the following inequality

$$\varepsilon \int_0^t g(t-s)(\nabla u(s), \nabla u(t))ds \geq \left(1 - \frac{1}{4\eta}\right)\int_0^t g(s)\|u\|^2 - \eta(g \diamond \nabla u)(t) \tag{13}$$

holds for all $\eta \geq 0$.

Employing the inequalities (13) into (12) we obtain

$$L'(t) \geq (1-\sigma)H^{-\sigma}H' + \varepsilon\frac{1}{\rho+1}\|u_t\|_{\rho+2}^{\rho+2} - \varepsilon\eta(g \diamond \nabla u)(t)$$
$$+ \varepsilon\Big[- M(\|u\|)\|u\|^2 + \left(1 - \frac{1}{4\eta}\right)\int_0^t g(s)ds\Big]\|u\|^2$$
$$+ \varepsilon\int_\Omega |u|_{\mathbb{R}}^p \ln |u|_{\mathbb{R}}^k dx + \varepsilon\int_\Omega |\nabla u_t|_{\mathbb{R}^n}^2 dx. \tag{14}$$

Adding $\varepsilon p(H(t) - E_2 + E(t))$ into (14), and regarding the equation of the total energy in (5) and that $\hat{M}(\tau) \geq M(\tau)\tau$, $\forall t \geq 0$, it follows

$$L'(t) \geq (1-\sigma)H^{-\sigma}H' + \varepsilon\left(\frac{1}{\rho+1} + \frac{p}{\rho+2}\right)\|u_t\|_{\rho+2}^{\rho+2} + \varepsilon\left(\frac{p}{2} - \eta\right)(g \diamond \nabla u)(t)$$
$$+ \varepsilon\Big[- M(\|u\|^2)\|u\|^2 + \frac{p}{2}\hat{M}(\|u\|^2) - \left(\frac{p-2}{2} + \frac{1}{4\eta}\right)\int_0^t g(s)ds\|u\|^2\Big]$$
$$+ \frac{\varepsilon k}{p}\int_\Omega |u|_{\mathbb{R}}^p dx + \varepsilon\left(1 + \frac{1}{2}\right)\int_\Omega |\nabla u_t|_{\mathbb{R}^n}^2 dx + \varepsilon p H(t) - \varepsilon p E_2$$
$$\geq (1-\sigma)H^{-\sigma}H' + \varepsilon\left(\frac{1}{\rho+1} + \frac{p}{\rho+2}\right)\|u_t\|_{\rho+2}^{\rho+2} + \varepsilon\left(\frac{p}{2} - \eta\right)(g \diamond \nabla u)(t)$$
$$+ \varepsilon\Big[\frac{(p-2)m_0}{2}\|u\|^2 - \left(\frac{p-2}{2} + \frac{1}{4\eta}\right)\int_0^t g(s)ds\|u\|^2\Big]$$
$$+ \frac{\varepsilon k}{p}\int_\Omega |u|_{\mathbb{R}}^p dx + \varepsilon\left(1 + \frac{1}{2}\right)\int_\Omega |\nabla u_t|_{\mathbb{R}^n}^2 dx + \varepsilon p H(t) - \varepsilon(p+1)E_2 \tag{15}$$

Taking now η to satisfy

$$\frac{1-l}{2\Big[(p-2)-\beta(p-1)\Big](m_0+l-1)} < \eta < \frac{p(1-\beta)}{2}+\beta, \tag{16}$$

which is possible by (H.4). Noticing that $\hat{M}(\tau) \leq M(\tau)\tau$ and that $(m_0+l-1)\|u\|^2 + (g \diamond \nabla u)(t) \geq \lambda_2^2$ (Lemma 2), we get

$$\begin{aligned}
&\frac{(p-2)m_0}{2}\|u\|^2 - \left(\frac{p-2}{2}+\frac{1}{4\eta}\right)\int_0^t g(s)ds\|u\|^2 + \left(\frac{p}{2}-\eta\right)(g\diamond\nabla u)(t) - (p+1)E_2 \\
&\geq \frac{\beta(p-1)}{2}\Big((m_0+l-1)\|u\|^2 + (g\diamond\nabla u)(t)\Big) - (p+1)E_2 \\
&= \frac{\beta(p-1)}{2}\frac{\lambda_1^2-\lambda_2}{\lambda_2^2}\Big((m_0+l-1)\|u\|^2 + (g\diamond\nabla u)(t)\Big) \\
&+ \frac{\beta(p-1)}{2}\frac{\lambda_1^2}{\lambda_2^2}\Big((m_0+l-1)\|u\|^2 + (g\diamond\nabla u)(t)\Big) - (p+1)E_2 \\
&\geq c_1\Big((m_0+l-1)\|u\|^2 + (g\diamond\nabla u)(t)\Big) + c_2
\end{aligned}$$

where $c_1 = \frac{\beta(p-1)}{2}\frac{\lambda_1^2-\lambda_2}{\lambda_2^2}$ and $c_2 = \frac{\beta(p-1)}{2}\lambda_1^2 - (p+1)E_2$. From $E_2 < \beta E_1$ and $E_1 = \frac{p-1}{2(p+1)}\lambda_1^2$, we have

$$c_2 = \frac{\beta(p-1)}{2}\lambda_1^2 - (p+1)E_2 > \beta\Big(\frac{(p-1)\lambda_1^2}{2} - (p+1)E_1\Big) = 0.$$

By the above estimates we deduce there exists $K > 0$ such that

$$L'(t) \geq K\Big(H(t) + \|u_t\|_{\rho+2}^{\rho+2} + \|u\|_p^p + \|u\|^2 + \|u_t\|^2\Big). \tag{17}$$

Next steps are aimed to estimate $L(t)^{\frac{1}{1-\sigma}}$. Let

$$0 < \sigma < \frac{1}{\rho+2} - \frac{1}{p}. \tag{18}$$

From Hölder inequality and Young's inequality we obtain:

$$\Big(\Big|\int_\Omega |u_t|_{\mathbb{R}}^\rho u_t u dx\Big|\Big)^{\frac{1}{1-\sigma}} \leq \|u_t\|_{\rho+2}^{\frac{\sigma+1}{1-\sigma}}\|u\|_{\rho+2}^{\frac{1}{1-\sigma}} \leq C_3\|u_t\|_{\rho+2}^{\frac{\sigma+1}{1-\sigma}}\|u\|_p^{\frac{1}{1-\sigma}} \tag{19}$$

$$\leq c_4\Big(\|u_t\|_{\rho+2}^{\frac{\sigma+1}{1-\sigma}\mu} + \|u\|_p^{\frac{1}{1-\sigma}\theta}\Big), \tag{20}$$

where $\frac{1}{\mu} + \frac{1}{\theta} = 1$. Choosing $\mu = \frac{(1-\sigma)(\rho+2)}{\rho+1} > 1$, it follows from (18) that $\frac{\theta}{1-\sigma} = \frac{\rho+2}{(1-\sigma)(\rho+2)-(\rho+1)} < p$. Thus, Lemma 1 implies

$$\Big(\Big|\int_\Omega |u_t|_{\mathbb{R}}^\rho u_t u dx\Big|_{\mathbb{R}}\Big)^{\frac{1}{1-\sigma}} \leq c_5\left(\|u_t\|_{\rho+2}^{\rho+2} + \|u\|^2 + \|u\|_p^p\right). \tag{21}$$

Similarly as derived in (20), we also obtain

$$\begin{aligned}\left(\int_\Omega |\nabla u_t \nabla u|_{\mathbb{R}} dx\right)^{\frac{1}{1-\sigma}} &\leq c_6 \left(\|u_t\|^{2(1-\sigma)} + \|u\|^{\frac{2(1-\sigma)}{1-2\sigma}}\right)^{\frac{1}{1-\sigma}} \\ &\leq c_7 \left(\|u_t\|^2 + \|u\|^{\frac{2}{1-2\sigma}}\right)^{\frac{1}{1-\sigma}}. \end{aligned} \tag{22}$$

Notice that

$$\|u\|^{\frac{2}{1-2\sigma}} \leq K_1^{\frac{2}{1-2\sigma}} \leq K_1^{\frac{2}{1-2\sigma}} \frac{H(t)}{H(0)} = c_8 H(t). \tag{23}$$

Therefore, from (21), (22) and (23) we infer that

$$L(t)^{\frac{1}{1-\sigma}} \leq c_9 \Big(H(t) + \|u_t\|_{\rho+2}^{\rho+2} + \|u\|_p^p + \|u\|^2 + \|u_t\|^2 \Big). \tag{24}$$

Combining 24 with (17) it yelds

$$L'(t) \geq c_{10} L(t)^{\frac{1}{1-\sigma}}. \tag{25}$$

Integrating (25) from 0 to t, we have

$$L(t) \geq \left(L(0)^{\frac{-\sigma}{1-\sigma}} - \frac{c_{11}}{1-\sigma} t \right)^{-\frac{1-\sigma}{\sigma}}. \tag{26}$$

This is a contradiction with the supposition that $\|u\|$ is globally bounded in t. Hence, the proof is complete. □

4 Conclusion

This work deals with a nonlinear viscoelastic problem with internal damping and logarithmic source term, which is an improvement of the problem considered in [15] in the case of absence of the term involving delay. By admitting the initial energy to be even positive, the problem becomes slightly difficult, what makes necessary a study of the growth of the terms of the total energy separately (Lemma 2). This work also states and sketches the proof of local existence of solution assumed to exist in the Theorem 3.

5 Acknowledgment

The authors would like to express their gratitude to the anonymous referee for their constructive comments and suggestions that allowed to improve this manuscript.

References

[1] Cavalcanti M.M., Domingos Cavalcanti V.N., Ferreira J. *Existence and uniform decay for a non-linear viscoelastic equation with strong damping*, *Mathematical Methods In Applied Sciences.* 24(14), (2001): 1043–1053.

[2] Cordeiro S.M.S., Pereira D.C., Ferreira J., Raposo C.A. *Global solutions and exponential decay to a Klein-Gordon equation of Kirchhoff-Carrier type with strong damping and nonlinear logarithmic source term*, *Partial Differential Equations in Applied Mathematics*, Vol.3, (2021):6 p.

[3] Dafermos C. M. *Asymptotic stability in viscoelasticity*, *Arch. Rational Mech. Anal.*, 37, (1970): 297–308.

[4] Liu, W., Li, G., Hong, L. *General Decay and Blow-Up of Solutions for a System of Viscoelastic Equations of Kirchhoff Type with Strong Damping*, *Journal of Function Spaces*, (2014): 21 p.

[5] Lions J.-L. *On some questions in boundary value problems of mathematical physics*, IM-UFRJ, (1978).

[6] Liu W. *Global existence, asymptotic behavior and blow-up of solutions for a viscoelastic equation with strong damping and nonlinear source*, *Topological Methods in Nonlinear Analysis*, Vol. 36, no. 1, (2010): 153–178.

[7] Love A.H.*A treatise on the mathematical theory of elasticity*, Dover New York, (1944).

[8] Messaoudi S. A. *Blow up and global existence in a nonlinear viscoelastic wave equation*, *Mathematische Nachrichten*, Vol. 260 (1), (2003): 58–66.

[9] Mezoua N., Mahmoud Boulaaras S.M., Allahem A. *Global Existence of Solutions for the Viscoelastic Kirchhoff Equation with Logarithmic Source Terms*, Hindawi Complexity, (2020), 25 p.

[10] Nishihara K. *On a global solution of some quasilinear hyperbolic equation*, *Tokyo Journal of Math.*, Vol. 7, (1984):437–459.

[11] Pereira D.C., Izaguirre R.M. *Sobre uma equações de vibrações não lineares*, Proceedings of 23 seminario brasileiro de Analise, Campinas, Sao Paulo, (1986): 155-158.

[12] Pohozaev S.I. *On a class of quasillnear hyperbolic equations. Mat USSR Sbornik*, Vol.25, no. 1, (1975): 145–148.

[13] Salim A.M., Tatar N. *Global existence and uniform stability of solutions for a quasilinear viscoelastic problem*, *Mathematical Methods In The Applied Sciences*, Vol. 30, (2007):665–680.

[14] Salim A.M., Tatar N. *Global Existence and Asymptotic Behavior for a Nonlinear Viscoelastic Problem*, *Mathematical Sciences Research Journal*, Vol. 7, no. 4, (2003): 136–149.

[15] Wu ST. *Blow-Up of Solution for A Viscoelastic Wave Equation with Delay*, *Acta Math Sci.*, 39, (2019): 329–338.

2-бөлім **Раздел 2** **Section 2**

Механика **Механика** **Mechanics**

IRSTI 27.39.21 DOI: https://doi.org/10.26577/JMMCS.2022.v116.i4.03

O. Khabidolda[1*], S.K. Akhmediyev[2], N.I. Vatin[3], R. Muratkhan[1], N.K. Medeubaev[1],

[1]Karaganda University named after Academician E.A. Buketov, Karaganda, Kazakhstan
[2]Karaganda Technical University, Karaganda, Kazakhstan
[3]Peter the Great St.Petersburg Polytechnic University, St.Petersburg, Russia
[*]e-mail: oka-kargtu@mail.ru

GENERALIZED FORMULA FOR ESTIMATING THE OSCILLATION FREQUENCY RESPONSE OF A CANTILEVER BAR WITH POINT MASSES

This paper presents a study of natural oscillations of a cantilever bar with five point masses with variable geometric and stiffness parameters (distances between locations of the masses, coefficients of variability of the bending stiffness of the bar sections). Using the exact method of forces based on the Mohr formula, there have been obtained expressions in general form for calculating the main unit coefficients of the secular equation, which makes it possible to perform calculations and to determine the oscillation frequency response of natural oscillations with a wide range of changes in the initial parameters of the physical and geometric state of cantilever bars. A numerical example has been given to illustrate the proposed theoretical approaches. The results have been compared with the results based on calculating a similar cantilever bar with one (reduced by masses) degree of freedom. A graphical dependence of the oscillation frequency response value on changing the value of the bending stiffness along the length of the cantilever bar gas been obtained. The theoretical provisions and applied results presented in the work will be widely used both in the practical design of bar systems and in scientific research in the field of mechanics of a deformable solid body.

Key words: cantilever bar, point masses, variable bending stiffness, main unit coefficients, oscillations frequency response for natural oscillations, graphical dependence of the oscillation frequency response, reduced mass, calculation reliability, calculation nomogram.

Ө. Хабидолда[1*], С.К. Ахмадиев[2], Н.И. Ватин[3], Р. Муратхан[1], Н.К. Медеубаев[1]
[1]Академик Е.А. Бөкетов атындағы Қарағанды университеті, Қарағанды қ., Қазақстан
[2]Қарағанды техникалық университеті, Қарағанды қ., Қазақстан
[3]Ұлы Петр Санкт-Петербург политехникалық университеті, Санкт-Петербург қ., Ресей
[*]e-mail: oka-kargtu@mail.ru

НҮКТЕЛІК МАССАЛАРЫ БАР КОНСОЛЬДІ ӨЗЕКТІҢ НЕГІЗГІ ЖАҒДАЙЫН БАҒАЛАУҒА АРНАЛҒАН ЖАЛПЫЛАНҒАН ФОРМУЛА

Бұл мақалада айнымалы геометриялық және қатаңдық параметрлері мен бес нүктелі массалары бар консоль өзегінің өзіндік тербелістеріне зерттеу жүргізілді (массалардың орналасуы арасындағы қашықтық, өзектер бөлімдерінің иілу қатаңдығының өзгеру коэффициенттері). Мора формуласына негізделген күштердің нақты әдісі ғасырлық теңдеудің негізгі бірлік коэффициенттерін есептеу үшін өрнектің жалпы түрінде алынады, бұл консольдік өзектердің физика-геометриялық күйінің бастапқы параметрлерінің өзгеруінің кең диапазонында табиғи тербелістердің негізгі жағдайын анықтауға есептеулер жүргізуге мүмкіндік береді.

Ұсынылған теориялық тәсілдерді суреттеу үшін сандық мысал келтірілген. Есептеу нәтижелерін салыстыру үшін еркіндік дәрежесі бірге тең ұқсас консольді өзекті (масса бойынша берілген) есептеу негізінде жүргізілді. Консольді өзектің иілу қатаңдығы мен өзек бойының ұзындығының өзгеруіне байланысты графикалық тәуелділік алынды. Жұмыста келтірілген теориялық ережелер мен қолданбалы нәтижелерді өзектік жүйелерді практикалық жобалау кезінде және деформацияланатын қатты дене механикасы саласындағы ғылыми зерттеулерде де кеңінен қолданылады.
Алынған теориялық және практикалық нәтижелер ғимараттар мен әртүрлі инженерлік құрылыстардағы тұтас арқалықтар құрылымын жобалау кезінде қолданыла алады.

Түйін сөздер: : Консольді өзек, нүктелік масса, айнымалы иілу қатаңдығы, негізгі бірлік коэффициенттер, өзіндік тербелістің негізгі жағдайы, негізгі жағдайдың графикалық тәуелділігі, келтірілген масса, есептеудің сенімділігі, есептеу номограммасы.

О. Хабидолда[1*], С.К. Ахмедиев[2], Н.И. Ватин[3], Р. Муратхан[1], Н.К. Медеубаев[1]
[1]Карагандинский университет имени академика Е.А. Букетова, г. Караганда, Казахстан
[2] Карагандинский технический университет, г. Караганда, Казахстан
[3] Санкт-Петербургский политехнический университет Петра Великого, г. Санкт-Петербург, Россия
*e-mail: oka-kargtu@mail.ru

ОБОБЩЕННАЯ ФОРМУЛА ДЛЯ ОЦЕНКИ ОСНОВНОГО ТОНА КОНСОЛЬНОГО СТЕРЖНЯ С ТОЧЕЧНЫМИ МАССАМИ

В данной работе выполнено исследование собственных колебаний консольного стержня с пятью точечными массами с переменными геометрическими и жесткостными параметрами (расстояния между местами расположения масс, коэффициентами переменности изгибных жесткостей участков стержней). Точным методом сил на основе формулы Мора получены в общем виде выражения для вычисления главных единичных коэффициентов векового уравнения, что позволяет производить расчеты на определение основного тона собственных колебаний при широком диапазоне изменения исходных параметров физико-геометрического состояния консольных стержней. Приведен численный пример для иллюстрации предлагаемых теоретических подходов. Выполнено сравнение результатов расчета на основе расчета аналогичного консольного стержня с одной (приведенной по массам) степенью свободы. Получена графическая зависимость величины основного тона от изменения значения изгибной жесткости по длине консольного стержня. Приведенные в работе теоретические положения и прикладные результаты найдут широкое применение как в практическом проектировании стержневых систем, так и в научных исследованиях в области механики деформируемого твердого тела.

Ключевые слова: Консольный стержень, точечные массы, переменная изгибная жесткость, главные единичные коэффициенты, основной тон собственных колебаний, графическая зависимость основного тона, приведенная масса, достоверность расчета, номограмма расчета.

1 Introduction

In the process of designing high-rise buildings (multi-storey structures) and tower-type structures (various support structures), in order to calculate them for pulsation from the dynamic effect of wind load, it is necessary to know the magnitude of the oscillation frequency response of free (natural) oscillations.

For this, various exact and approximate analytical and numerical methods are used.

In this paper, an approximate analytical method is proposed for calculating the oscillation frequency response of cantilever bars with step-variable bending stiffness along its length with point masses, which makes it possible to estimate the magnitude of the oscillation frequency response with sufficient engineering accuracy.

A certain number of works were dealing with the topic proposed by the authors of this article: for example, in work [1] the oscillatory processes of a statically determinate bar system with one degree of freedom are considered by the Runge-Kutta method in the MatCad program; there was compared the effect of the inelastic resistance of the material coefficient on the displacement of the concentrated mass.

Calculation for harmonic oscillations is also described in the works by Aizenberg Ya.N., Gvozdev A.A., Birbraer A.P., Shulman S.G., Rabinovich I.M., Barshtein M.F., Korenev B.G., Timoshenko S.P. and many others [2-8].

Study [9] considers special properties of the bending shapes of bars of constant bending stiffness to determine the value of the fundamental tone.

In work [10], nonlinear free oscillations of coating structures are considered based on studying the characteristic quadratic equation obtained by the matrix method.

In paper [11], a mixed form of the finite element method was used to calculate bar systems for free oscillations.

Papers [12, 13] consider the numerical implementation of the finite element method in calculations for free and forced oscillations; the matrices of stiffness, masses, examples of calculating beam systems of the Bernoulli-Euler and Timoshenko type are given, a new concept of "dynamic matrix"is introduced.

The purpose and objective of this work is to study the stress-strain state of cantilever bars with several point masses for natural oscillations with determining the oscillation frequency response in a wide range of changes of geometric and physical and mechanical parameters of the system under study.

In this case, the problem of obtaining an analytical expression for calculating the main unit coefficients of the secular equation in general form has been solved, which makes it possible to operate mathematically with geometric dimensions and bending stiffness when calculating various cantilever bars.

One of the objectives of the study is to illustrate the generalized formula obtained by the authors using the example of calculating the oscillation frequency response of a cantilever bar.

A graphic dependence (nomogram) of the oscillation frequency response of natural oscillations has also been obtained with changing the bending stiffness along the length of the bar.

2 Theoretical provisions and calculation methods

Coefficients $k_1,\ k_2,\ k_3,\ k_4$,determining the variability of the step-variable bending stiffness along the height of the bar at five levels (floors) of the structure;

Coefficients $a_1,\ a_2,\ a_3,\ a_4$ determining the differences in the size of sections (floors) along the height of the cantilever rod;

Coefficients $b_1,\ b_2,\ b_3,\ b_4$ determining the differences in the values of concentrated masses.

By changing the values of the above coefficients over a wide range, it is possible to study free oscillations, that is, to determine the value of the oscillation frequency response of the five-step-variable bending stiffness of the cantilever bar with different lengths, and the bending stiffness of its five steps (floors) with different values of five concentrated point masses located at the joints of steps (floors) along the height of the structure.

Let us calculate the values of the main coefficients $\delta_{ii}(i = 1,\ 2,\ 3,\ 4,\ 5)$according to the Vereshchagin rule, multiplying the corresponding single diagrams of the moments (Figure 1, b, c, d, e, f). Then, in generalized form, we obtain:

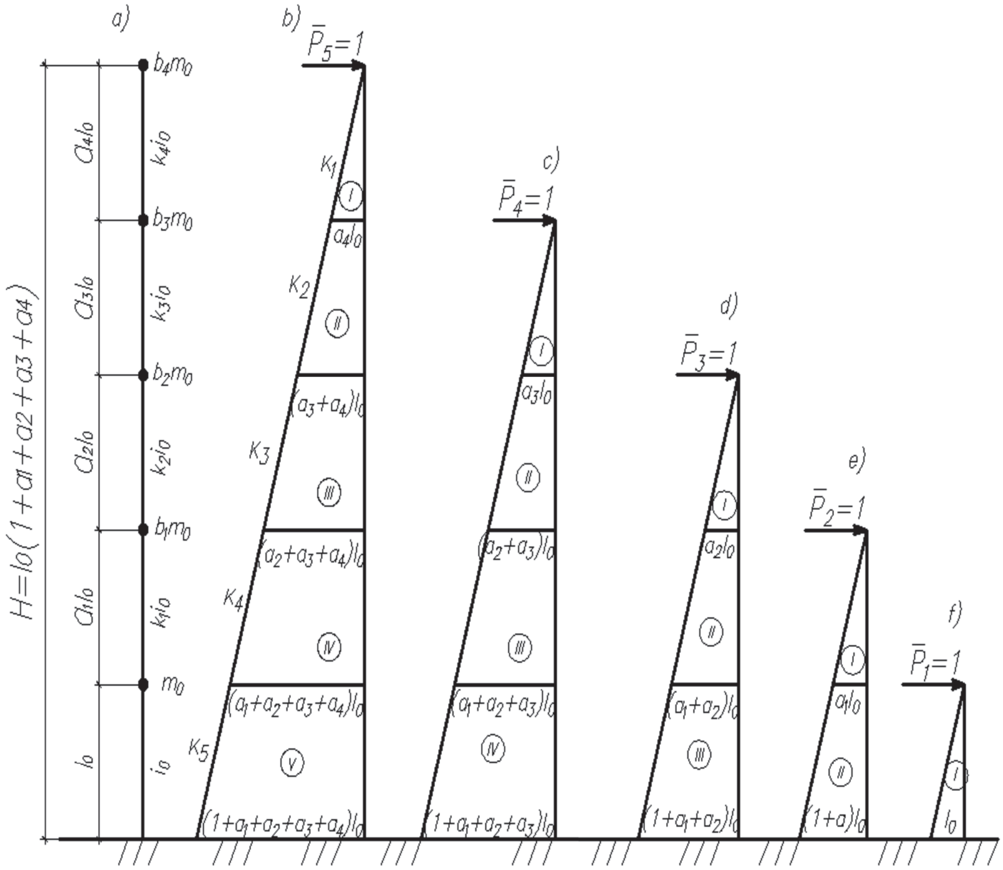

Figure 1: Towards the calculation of the cantilever bar for free oscillations: a) – the calculated scheme; b) – diagram $\overline{M}_5$; c) – diagram $\overline{M}_4$; d) – diagram $\overline{M}_3$; e) – diagram $\overline{M}_2$; f) – diagram $\overline{M}_1$

$$
\begin{aligned}
&\delta_{ii} = \tfrac{1}{E_iJ_i}(\overline{M}_i)\cdot(\overline{M}_i) = \tfrac{l_0^3}{l_0 i_0}\left[\tfrac{1}{k_{i-1}}\left(0.33a_{i-1}^3\right)\right] + \\
&+\tfrac{1}{k_{i-2}}\left[0.5a_{i-1}a_{i-2}(2a_{i-1}+a_{i-2}) + 0.1667(a_{i-2})^2(3a_{i-1}+2a_{i-2})\right] + \\
&+\tfrac{1}{k_{i-3}}\left[0.5(a_{i-2}+a_{i-1})a_{i-3}(2a_{i-2}+a_{i-1}) + a_{i-3} + 0.1667(a_{i-3})^2 3\left[(a_{i-2}+a_{i-1})+2a_{i-3}\right]\right] + \\
&+\tfrac{1}{k_{i-4}}\left[0.5(a_{i-2}+a_{i-1}+a_{i-3})\left[2(a_{i-2}+a_{i-1}+a_{i-3})+a_{i-4}\right] + \right.\\
&\left.+0.1667(a_{i-4})^2 3\left[(a_{i-2}+a_{i-1}+a_{i-3})+2a_{i-4}\right]\right] + \\
&+\left[0.5(a_{i-2}+a_{i-1}+a_{i-3}+a_{i-4})\left[2(a_{i-2}+a_{i-1}+a_{i-3}+a_{i-4})+1\right] + \right.\\
&\left.+0.1667\left[3(a_{i-2}+a_{i-1}+a_{i-3}+a_{i-4})+2\right]\right].
\end{aligned}
\tag{1}
$$

According to generalized formula (1) let's calculate the main coefficients:

a) $\delta_{55}(i=5)$

$$\begin{array}{l}\delta_{55}=\frac{l_0^2}{i_0}\left[\frac{1}{k_4}\left(0.3333a_4^3\right)\right]+\frac{1}{k_3}\left[0.5a_3a_4(2a_4+a_3)+0.1667(a_3)^2(3a_4+2a_3)\right]+\\+\frac{1}{k_2}\left[0.5(a_3+a_4)a_2\left[2(a_3+a_4+a_2\right]+0.1667(a_2)^2 3\left[(a_3+a_4)+2a_2\right]\right]+\\+\frac{1}{k_1}\left[0.5(a_3+a_4+a_2)\left[2(a_3+a_4+a_2)+a_1\right]+0.1667(a_1)^2 3\left[(a_3+a_4+a_2)+2a_1\right]\right]+\\+\left[0.5(a_3+a_4+a_2+a_1)+\left[2(a_3+a_4+a_2+a_1)+1\right]+0.1667\left[3(a_3+a_4+a_2+a_1)+2\right]\right]\end{array}$$

b) $\delta_{44}(i=4)$

$$\begin{array}{l}\delta_{44}=\frac{l_0^2}{i_0}\left[\frac{1}{k_3}\left(0.3333a_3^3\right)\right]+\frac{1}{k_2}\left[0.5a_3a_2(2a_3+a_2)+0.1667(a_2)^2(3a_3+2a_2)\right]+\\+\frac{1}{k_1}\left[0.5(a_3+a_2)\left[2(a_3+a_2)+a_1\right]+0.1667(a_1)^2\left[3(a_3+a_2)+2a_2\right]\right]+\\+\left[0.5(a_1+a_2+a_3)\left[2(a_1+a_2+a_3)+1\right]+0.1667\left[3(a_1+a_2+a_3)+2\right]\right]\end{array}$$

c) $\delta_{33}(i=3)$

$$\begin{array}{l}\delta_{33}=\frac{l_0^2}{i_0}\left[\frac{1}{k_2}\left(0.3333a_2^3\right)\right]+\frac{1}{k_1}\left[0.5a_2a_1(2a_2+a_1)+0.1667(a_1)^2(3a_2+2a_1)\right]+\\+\left[0.5(a_3+a_2)\left[3(a_1+a_2)+2\right]+0.1667\left[3(a_1+a_2)+2\right]\right]\end{array}. \tag{2}$$

d) $\delta_{22}(i=2)$

$$\delta_{22}=\frac{l_0^2}{i_0}\left[\frac{1}{k_1}\left(0.3333a_1^3\right)\right]+\left[0.5(a_1)^2(2a_1+1)+0.1667\left[3(a_1+2)\right]\right];$$

e) $\delta_{11}(i=1)$

$$\delta_{11}=\frac{l_0^2}{i_0}\left(0.3333\right).$$

Let's calculate the point masses values (Figure 1, a).

$$m_1=m_0;\;\; m_2=b_1m_0;\;\; m_3=b_2m_0;\;\; m_4=b_3m_0;\;\; m_5=b_4m_0;$$

According to the formula presented in [1], let's calculate the approximate value of the oscillation frequency response for free oscillations of the cantilever bar:

$$\frac{1}{\omega_1^2}=m_1\delta_{11}+m_2\delta_{22}+m_3\delta_{33}+m_4\delta_{44}+m_5\delta_{55} \tag{3}$$

Let's substitute the values calculated in (1, 2) into expression (3).

Based on the proposed generalized formulas for the cantilever bar (Figure 1, a), let's calculate a numerical example with the following initial data (Figure 2, a):

$$a_1=a_2=a_3=a_4=1;\;\; m_0=43.3\,kg\cdot s^2/cm;$$

$$l_0=3.5\,m;\;\; b_1=1.0254;\;\; b_2=0.9931;\;\; b_3=0.8799;\;\; b_4=0.836;$$

$$i_0^*=8.06\cdot 10^8 kg/cm;\;\; i_{AB}=3i_0^*=24.18\cdot 10^8=i_0;$$

$$k_1=0.8;\;\; k_2=0.6;\;\; k_3=0.4;\;\; k_4=0.2$$

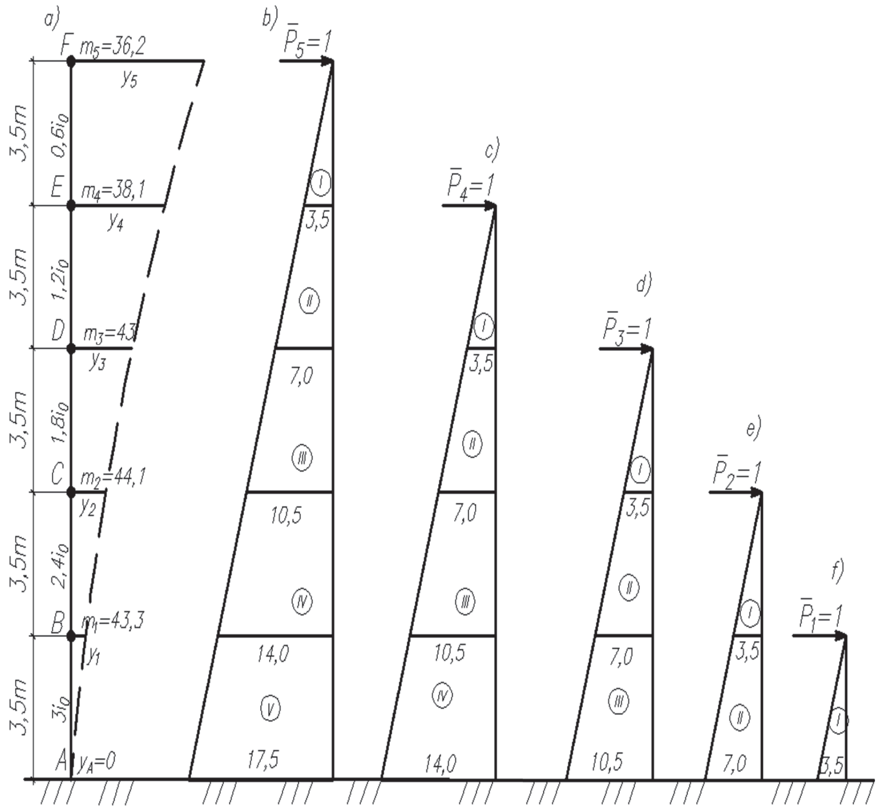

Figure 2: Towards the calculation of the cantilever bar (example): a) – the preset scheme; b) - diagram $\overline{M}_5$; c) - diagram $\overline{M}_4$; d) – diagram $\overline{M}_3$; e) – diagram $\overline{M}_2$; f) – diagram $\overline{M}_1$

3 Results

Based on the above theoretical calculations, we obtain the following results for which we calculate the values of the main coefficients $\delta_{ii}(i = 1,\ 2,\ 3,\ 4,\ 5)$ using formulas (2)

$$
\begin{aligned}
\delta_{55} &= \frac{1}{li_0}(23.82 + 83.56 + 150.8676 + 220.371 + 290.57) = \frac{768.992 \cdot 10^4}{li_0} = 27.26 \cdot 10^{-4};\\
\delta_{44} &= \frac{1}{li_0}(768.992 - 290.57) = \frac{478.422 \cdot 10^4}{li_0} = 16.96 \cdot 10^{-4};\\
\delta_{33} &= \frac{1}{li_0}(478.4221 - 220.371) = \frac{258.051 \cdot 10^4}{li_0} = 9.1475 \cdot 10^{-4};\\
\delta_{22} &= \frac{1}{li_0}(258..05 - 150.87) = \frac{107.18 \cdot 10^4}{li_0} = 3.8 \cdot 10^{-4};\\
\delta_{11} &= \frac{1}{li_0}(107.18 - 83.363) = \frac{23.818 \cdot 10^4}{li_0} = 0.844 \cdot 10^{-4}.
\end{aligned}
\tag{4}
$$

Let's calculate the point masses values (Figure 2, a):

$$m_1 = \frac{P_1}{g} = \frac{43.3 \cdot 10^3}{981} = 44.14\, kg \cdot s^2/cm;\; m_2 = \frac{P_2}{g} = 44.954\ kgs^2/cm;$$

$$m_3 = \frac{P_3}{g} = 43.83\ kgs^2/cm;\; m_4 = \frac{P_4}{g} = 38.84\ kgs^2/cm;\; m_5 = \frac{P_5}{g} = 39.9\ kgs^2/cm$$

Let's calculate the approximate value of the oscillation frequency response for free oscillations of the cantilever bar (Figure 2, a) according to formula (3).

$$\frac{1}{\omega_1^2} = m_1\delta_{11} + m_2\delta_{22} + m_3\delta_{33} + m_4\delta_{44} + m_5\delta_{55} =$$
$$= 10^{-4}\,(37.25 + 170.83 + 400.93 + 658.73 + 1005.89)\ = 2273.63 \cdot 10^{-4}$$

$\omega_1 = 10^2 \cdot 0.020973 = 2.0973\ s^{-1}$ is the oscillation frequency response of the cantilever bar (Figure 1,a).

To estimate reliability of the result obtained, let's calculate the (ω_1) value through the reduced mass (M) (Figure 3) the coefficient of reduction of the distributed mass to the end of the cantilever bar [14].

$$M = \beta\frac{\left(\sum m_i\right) H}{H} = \beta\sum m_i H = 0.23\,(m_1 + m_2 + m_3 + m_4 + m_5) = 47.99$$

According to formula 7.70 [1]:

$$\omega_1^2 = \frac{1}{\delta_{55}} = \frac{1}{47.99 \cdot 27.26 \cdot 10^{-4}} = 10^2 \cdot 0.000764;\;\; \omega_1^* = 2.764\ s^{-1}$$

Figure 3: The bar reduced mass

The ω_1 and ω_1^* values calculated by different methods (approaches) are sufficiently close which proves reliability of the proposed theory of calculating the cantilever bar of step-variable bending stiffness with point masses located along its length (height).

Let's study the effect of changing the scaling relative stiffness $i_0 = 8.06 \cdot 10^8\, kgcm$ on the oscillation frequency response (ω_1) of the cantilever bar (Figure 2, a) according to formulas (4):

$$\begin{aligned} &\delta_{55} = \frac{768.992 \cdot 10^4}{3.5 i_0} = \frac{219.71 \cdot 10^4}{i_0}; \quad \delta_{44} = \frac{136.692 \cdot 10^4}{i_0}; \\ &\delta_{33} = \frac{73.73 \cdot 10^4}{i_0}; \quad \delta_{22} = \frac{30.62 \cdot 10^4}{i_0}; \quad \delta_{11} = \frac{60.81 \cdot 10^4}{i_0}. \end{aligned} \tag{5}$$

According to formula (3) let's calculate taking into account expression (5) with $i_0 = (1, 3, 5, 7, 9, 11) \cdot 8.06 \cdot 10^8\, kgcm$ (Table 1).

Table 1 – Values of the oscillation frequency response for free oscillations of the cantilever bar

$10^{-8}\, i_0$	1.0	3.0	5.0	7.0	9.0	11.0
δ_{11}	6.81x10-4	2.27x10-4	1.36x10-4	0.97x10-4	0.76x10-4	0.62x10-4
δ_{22}	30.62x10-4	10.21x10-4	6.12x10-4	4.37x10-4	3.4x10-4	2.78x10-4
δ_{33}	73.73x10-4	24.5x10-4	14.75x10-4	10.53x10-4	8.19x10-4	6.70x10-4
δ_{44}	136,69x10-4	45.5x10-4	23.34x10-4	19.52x10-4	45.19x10-4	12.42x10-4
δ_{55}	219.71x10-4	73.24x10-4	43.94x10-4	31.39x10-4	24.41x10-4	19.97x10-4
ω_1, c^{-1}	5.954	3.44	2.652	2.242	1.977	1.789

According to Table 1, let's build the graphs of the $\omega_{1,i} = f(i_{0,i})$ $(i = 1, 3, 5, 7, 9, 11)$ dependence. This graph is presented in Figure 4.

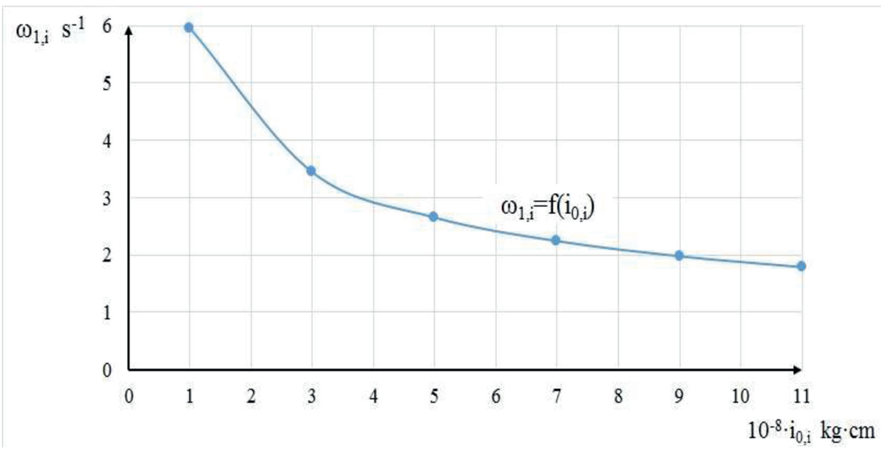

Figure 4: The oscillation frequency response dependence on the relative stiffness value of the cantilever bar

4 Conclusions

Based on the analytical operations, generalized formula (1) has been obtained for an approximate estimation of the oscillation frequency response with varying parameters of the section lengths, point mass values, and relative stiffness values of sections of a five-stage cantilever bar (Figure 1, a).

A numerical example (Figure 2, a) shows reliability of the proposed theoretical provisions; this is shown by the proximity of the oscillation frequency response values obtained by two independent methods of calculating $\omega_1 \approx \omega_1^*$.

The dependence of the oscillation frequency response value the cantilever bar (Figure 2, a) on changing the value of relative stiffness i_0 in the range from $1 \cdot 10^8 \, kgcm$ to $11 \cdot 10^8 \, kgcm$ has been studied, which is reflected graphically (Figure 4).

The dependence $\omega_{1,0} = f(i_{0,i})$ shown in Figure 4 can be used as a nomogram to determine the oscillation frequency response of various cantilever bars (Figure 1, a) at arbitrary values of the main relative stiffness of the lower section of the cantilever bar with step-variable bending stiffness.

References

[1] Kiselev V.A. Structural Mechanics: Spec. well. Dynamics and stability of structures. Moscow: Stroyizdat, 1980. 616 p.

[2] Numerical methods for solving differential and integral equations and quadrature formulas. Digest of articles. M.: Science. 1964.

[3] Doyev V.S., Doronin F.A., Indeikin A.V. Theory of vibrations in transport mechanics (under the editorship of A. V. Indeikin). M.: FGOU "Training and Methodological Center for Education in Railway Transport". 2011. 352 p.

[4] Gorelov Yu.N. Numerical methods for solving ordinary differential equations (the Runge-Kutta method): textbook. allowance. Samara: Samara University. 2006. 48 p.

[5] Konstantinov I.A., Lalina I.I. Structural mechanics. Calculation of rod systems. St. Petersburg: Publishing house of Politekhn. university 2005. 155 p.

[6] Mrdak Ivan, Rakocevic Marina, Zugic Ljiljana, Usmanov Rustam, Murgul Vera, Vatin Nikolay. Analysis of the influence of dynamic properties of structures on seismic response according to Montenegrin and European regulations. 2014. Vol. 633-634. pp. 1069-1076.

[7] Timoshenko S.P. Fluctuations in engineering. M.: Nauka, 1967. 444 p.

[8] Vatin N.I., Sinelnikov A.S. Long-span elevated pedestrian crossings made of light cold-formed steel profile // Construction of unique buildings and structures. 2012. No. 1. P. 47-52.

[9] Lyakhovich, Leonid Semyonovich. Special Characteristics of Forms of Bending of The Bars With Equal Resistance and Forms of Natural Oscillation Under Fundamental Tone Value Restriction for Linear Dependence of Moments of Cross-Section Inertia and Varied Parameter // Vestnik TGASU No 1, 2010, C. 102-109.

[10] Ufimtsev E.M., Voronin M.D. Dynamic Calculation of a Roof Truss during the Process of Free Structurally Nonlinear Oscillations // Bulletin of the South Ural State University. Ser. Construction Engineering and Architecture. 2016 Vol. 16, No. 3, PP. 18–25.

[11] IGNATIEV V.A., IGNATYEV A.V. Application of the mixed form of the finite element method to the calculation of bar systems for free oscillations. 2012. No. 16. pp. 101-110.

[12] Chernov S. A. Analysis of free oscillations of an arbitrary planar bar system on a computer // Bulletin of the Ulyanovsk State Technical University. 2015. №2. pp. 17-21.

[13] Postnoe V.A. Dynamic Stiffness Matrices of Beam Elements and their Use in the Finite Element Method in Calculating Forced Vibrations of Rod Systems // Bulletin of Civil Engineers. 2005. S. 42-45.

[14] Klein G. K., Rekach V. G., Rosenblat G. I. Guide to practical exercises in the course of structural mechanics. M.: Higher school, 1980. 320 p.

[15] Sovremennye metody proektirovaniya mostov [Modern methods of bridge design] // M.: Transport. – 2006. – 664.

IRSTI 41.03.02 DOI: https://doi.org/10.26577/JMMCS.2022.v116.i4.04

M.Zh. Minglibayev , A.B. Kosherbayeva*
al-Farabi Kazakh National University, Almaty, Kazakhstan
*e-mail: kosherbaevaayken@gmail.com

EVOLUTION EQUATIONS OF MULTI-PLANET SYSTEMS WITH VARIABLE MASSES

In celestial mechanics and astrodynamics, the study of the dynamical evolution of exoplanetary systems is the relevant topics. For today more than 3,000 exoplanetary systems are known. In this paper, we study the dynamic evolution of extrasolar systems, when the leading factor of evolution is the variability of the masses of gravitating bodies. The problem of $n+1$ spherically symmetric bodies with variable masses is considered in a relative coordinate system, this bodies inter-gravitating according to Newton's law. The quasi-elliptical motions of planets whose orbits do not intersect during evolution are investigated. It is believed that the mass of bodies under consideration varies isotropically by various known laws with different velocities. The mass of the parent star is considered to be the most massive than its planets and the origin of the relative coordinate system is in the center of the parent star. Due to the variability of the masses, the differential equations of motion become non-autonomous and the task is difficult. The problem is investigated by methods of perturbation theory. The canonical perturbation theory based on a periodic motion over a quasi-canonical section is used. Canonical equations of motion are obtained in analogues of the second Poincare system, which are effective in the case when the analogues of eccentricities and the analogues of the inclination of the orbital plane of planets are sufficiently small. The secular perturbations of the planets, which determine the behavior of the orbital parameters over long time intervals, are studied.
The evolutionary equations of many planetary systems with isotropically varying masses in analogues of the second system of Poincare variables are derived in an analytical form which are obtained using the Wolfram Mathematica computer algebra system. This takes into account the effects of the decreasing mass of the parent star and the growth of the masses of the planets due to the accretion of matter from the remnants of the protoplanetary disk. For the three-planetary problem of four bodies with variable masses, the evolutionary equations in dimensionless variables are obtained explicitly. In the future, these results will be used to study the dynamics of the three-planet system K2-3 in the non-stationary stage of its evolution.
Key words: variable mass, perturbation theory, evolutionary equations, exoplanetary systems, Poincare elements.

М.Дж. Минглибаев, А.Б. Кошербаева*
Әл-Фараби атындағы Казақ Ұлттық Университеті, Алматы қ., Қазақстан
*e-mail: kosherbaevaayken@gmail.com

Массалары өзгермелі көп планеталы жүйелердің эволюциялық теңдеулері

Аспан механикасында және астродинамикада экзопланеталы жүйенің динамикалық эволюциясын зерттеу өзекті тақырып. Қазіргі таңда 3000-нан артық экзопланеталы жүйе белгілі. Бұл жұмыста гравитация арқылы әсерлесетін денелердің массаларының айнымалылығы эволюцияның жетекші факторы ретінде қарастырылған кезде күн жүйесі сыртындағы басқа да жүйелердің динамикалық эволюциясы зерттеледі. Салыстырмалы координаталар жүйесінде ньютон заңы бойынша өзара әсерлесетін айнымалы массалы сфералық симметриялы денелер мәселесі қарастырылады. Эволюция кезінде планеталардың орбиталары бір-бірімен қиылыспайтын квазиэллиптикалық қозғалыс зерттеледі. Қарастырылатын денелердің массалары әртүрлі жылдамдықпен белгілі әртүрлі заңдылықтар бойынша изотропты түрде өзгереді деп саналады. Орталық жұлдыздың массасы оның планеталарының массаларынан әлде-қайда үлкен деп алынады, және салыстырмалы координаталар жүйесінің бас нүктесі орталық жұлдыздың центрінде орналасады. Массалардың айнымалылығa есебінде диффе-

ренциалды қозғалыс теңдеулері автономды емес түрге енеді және есеп қиындайды. Мәселе ұйытқу теориясы әдістерімен зерттеледі. Квазиконустық қима бойынша апериодты қозғалыс негізінде канондық ұйытқу теориясы қолданылады. Экцентриситет аналогтары мен планета орбитасының көлбеулік бұрышының аналогтары жеткілікті деңгейде кіші шама болған кезде тиімді болып табылатын Пуанкаренің екінші жүйесінің аналогтары арқылы канондық қозғалыс теңдеуі алынды. Уақыттың үлкен интервалында орбита параметрлерінің өзгерісін анықтауға мүмкіндік беретін планетаның ғасырлық ұйытқуы зерттелінеді.
"Wolfram Mathematica" компьютерлік алгебра көмегімен массалары изотропты өзгеретін көп планеталы жүйенің эволюциялық теңдеулері Пуанкаре айнымалыларының екінші жүйесі аналогтары арқылы аналитикалық түрде келтірілген. Сонымен қатар, протопланеталы диск қалдықтары бөлшектерінің аккрециясы есебімен планета массасының өсуі және орталық жұлдыздың массасының азаю әсерлері есепке алынады. Айнымалы массалы төрт дененің үш планеталы мәселесі үшін өлшемсіз шама арқылы эволюциялық теңдеулер анық түрде алынды. Ендігі кезекте алынған нәтижелер K2-3 үш планеталы жүйесінің стационар емес эволюция кезеңінде динамикалық эволюциясын зерттеу үшін қолданылады.
Түйін сөздер: айнымалы масса, ұйытқу теориясы, эволюциялық теңдеулер, экзопланеталы жүйелер, Пуанкаре элементтері.

М.Дж. Минглибаев, А.Б. Кошербаева*
Казахский Национальный Университет имени аль-Фараби, г. Алматы, Казахстан
*e-mail: kosherbaevaayken@gmail.com

Эволюционные уравнения много планетных систем с переменными массами

В небесной механике и в астродинамике изучение динамическую эволюцию экзопланетных систем актуальная тема. На сегодняшний день известно более 3000 экзопланетные системы. В настоящей работе исследуется динамическая эволюция внесолнечных систем, когда ведущим фактором эволюции является переменность масс гравитирующих тел. Рассматривается в относительной системе координат задача сферический симметрических тел с переменными массами, взаимогравитирующие по закону ньютона. Исследуется квазиэллиптические движения планет орбиты которых в ходе эволюции не пересекаются. Считается, что масса рассматриваемых тел изменяется изотропно по различным известным законам с различными скоростями. Масса родительской звезды считается наиболее массивным чем её планеты и начало относительной системы координат находится в центре родительской звезды. Из-за переменности масс дифференциальные уравнения движения становится неавтономными и задача усложняется. Проблема исследуется методами теории возмущения. Используется каноническая теория возмущения на базе апериодического движения по квазиконическому сечению. Канонические уравнения движения получены в аналогах второй системы Пуанкаре, которые эффективны в случае, когда аналоги эксцентриситетов и аналоги наклонности орбитальной плоскости планет достаточно малы. Исследуются вековые возмущения планет, которые определяют поведение орбитальных параметров на больших интервалах времени.
В аналитическом виде приведены эволюционные уравнения много планетных систем с изотропно изменяющимися массами в аналогах второй системы переменных Пуанкаре, которые получены с использованием системы компьютерной алгебры "Wolfram Mathematica". При этом учитываются эффекты убывания массы родительской звезды и роста масс планет из-за аккреции вещества из остатков протопланетного диска. Для трех планетной задачи четырех тел с переменными массами, в явном виде, получены эволюционные уравнения в безразмерных переменных. В дальнейшем эти результаты будет использованы для изучения динамику трех планетной системы K2-3 в нестацонарной этапе ее эволюции.

Ключевые слова: переменная масса, теория возмущения, эволюционные уравнения, экзопланетные системы, элементы Пуанкаре.

1 Introduction

Multi-body problem is one of the center problem in celestial mechanics. Let us short review of more interesting work about this problem that are close to our topic. In paper [1] three body problem was researched and algorithm of solving equation in osculating elements was given, here perturbing acceleration smaller than main acceleration caused by the induced of the central body gravity. In article [2] integrability of the N body problem was described. In [3] the problem of deriving theory of motion of four planet around center star was considered. Here Hamiltonian was given in the Poisson series in the osculating elements of the second Poincare systems. The expansion in series was constructed up to third power of a small parameter. A relevant problem is the problem of formation planetary systems. In work [4] the orbital evolution of two planetary system of three bodies Sun-Jupiter-Saturn was investigated. The Hamiltonian written in osculating elements is represented in Poisson series expansion over all elements.

In [5] orbital evolution of asteroids Phaethon clusters was studied, taking into account perturbations from eight major planets, the dwarf planet Pluto, the influence of the Yarkovsky effect, the flattened Sun and relativistic effects. In article [6] dynamical evolution of orbits due to pressure of solar radiation was investigated. In [7] the authors analyzed dynamical evolution of young pairs of asteroids in close orbits. In work [8] evolution of planetary systems was studied. The averaged equations of motion was derived analytically up to third power of a small parameter for the case of a four planetary system. Here the system of Sun-Jupiter-Saturn-Neptune is considered.

In [9] and [10] the authors described a methodology for detection the initial orbits of exoplanet using the curve radial velocity of parent star and obtained an algorithm for solving the equations of two body problem in the form of series and proved that the serieses converges to solving the equations for small values of eccentricity.

In work [11] the orbital evolution of the three-planet exosystem as HD 39194 and the four-planet exosystems as HD 141399 and HD 160691 (μ Ara) are studied. In result the authors have derived an averaged semi-analytical theory of second-order motion by the masses of exoplanets. Here multi-planetary problem is considered. The equations of motion are given in the Jacobi coordinates and written in the elements of the second Poincare system.

In celestial mechanics and astrodynamics one of the relevant topics is the study dynamical evolution of non-stationary gravitational exoplanetary systems. For today 3677 exo-systems and 4903 confirmed exoplanets are known [12].

In this paper, in difference to the above-mentioned works, the dynamical evolution of multi-planetary systems is researched, when the leading factor of evolution is the variability of the masses of the celestial bodies themselves.

The particular case – two planetary problem of three bodies with variable masses was considered in work [13].

The motions are studied in a relative coordinate system, with the origin in the center of the parent star. The canonical perturbation theory is used, which elaborated on the base a periodic motion over quasi-canonical section [14]. Dimensionless evolutionary equations are obtained in analogues of the second Poincare system.

2 Materials and methods

2.1 The problem statement and differential equations of motion

We will consider the motion of $n+1$ ($n \geq 3$) bodies, which inter-gravitating according to Newton's law, in a relative coordinate system with the origin in the center of the parent star, whose axes are parallel to the corresponding axes of the absolute coordinate system. The bodies will be considered spherical with isotropically varying masses. We introduce the following notation: S – the parent star of planetary system – the center body, P_i, ($i = 1, 2, \dots, n$) – planets. The positions of the planets are such that P_i – the inner planet relative to the P_{i+1} planets, but the outer, relative to P_{i-1}. We will assume that such positions of the planets are preserved during of the evolution and their orbits don't intersect.

The law of varying of mass is considered to be known and different:

$$m_0 = m_0(t), \quad m_1 = m_1(t), \dots, m_n = m_n(t) \tag{1}$$

where, $m_0 = m_0(t)$ – mass of parent star S, $m_i = m_i(t)$, – mass of planet P_i.

The motion equations of n planets in the relative coordinate system are written as the following [14-15]:

$$\ddot{\vec{r}}_i = -f\frac{(m_0+m_i)}{r_i^3}\vec{r}_i + f\sum_{j=1}^{n}{}' m_j\left(\frac{\vec{r}_j-\vec{r}_i}{r_{ij}^3} - \frac{\vec{r}_j}{r_j^3}\right), \quad (i, j = 1, 2, \dots, n) \tag{2}$$

where, f – the gravitational constant, $\vec{r}_i(x_i, y_i, z_i)$ – the radius-vector of planet P_i, in summing the sign "stroke" means that $i \neq j$, r_{ij} – the mutual distances of the center of spherical bodies:

$$r_{ij} = \sqrt{(x_j-x_i)^2 + (y_j-y_i)^2 + (z_j-z_i)^2} = r_{ji} \tag{3}$$

We will use the methods of the canonical perturbation theory, elaborated on the basis of the aperiodic motion over a quasi-canonical section [14]. Canonical equations are convenient for studying non-stationary gravitating systems.

Based on differential equations of planetary motion written in the relative coordinate system (2), it is possible to write the canonical equations of motion in the osculating analogues of the second system of canonical Poincare variables [16-17]:

$$\Lambda_i, \quad \lambda_i, \quad \xi_i, \quad \eta_i, \quad p_i, \quad q_i \tag{4}$$

The system of canonical equations has the form

$$\begin{aligned}
&\dot{\lambda}_i = \frac{\partial R_i^*}{\partial \Lambda_i} = \frac{\mu_{i0}^2}{\gamma_i^2\Lambda_i^3} - \frac{\partial W_i}{\partial \Lambda_i}, \qquad \dot{\Lambda}_i = \frac{\partial R_i^*}{\partial \lambda_i} = \frac{\partial W_i}{\partial \lambda_i},\\
&\dot{\eta}_i = \frac{\partial R_i^*}{\partial \xi_i} = -\frac{\partial W_i}{\partial \xi_i}, \qquad \dot{\xi}_i = \frac{\partial R_i^*}{\partial \eta_i} = \frac{\partial W_i}{\partial \eta_i},\\
&\dot{q}_i = \frac{\partial R_i^*}{\partial p_i} = -\frac{\partial W_i}{\partial p_i}, \qquad \dot{p}_i = \frac{\partial R_i^*}{\partial q_i} = \frac{\partial W_i}{\partial q_i}.
\end{aligned} \tag{5}$$

where, the Hamilton function has the form

$$R_i^* = -\frac{\mu_{i0}^2}{2\Lambda_i^2} \cdot \frac{1}{\gamma_i^2(t)} - W_i\left(t, \Lambda_i, \xi_i, p_i, \lambda_i, \eta_i, q_i\right), \quad \gamma_i = \frac{m_0(t_0) + m_i(t_0)}{m_0(t) + m_i(t)} = \gamma_i(t) \tag{6}$$

here, $\mu_{i0} = f(m_0(t_0) + m_i(t_0)) = const$ – gravitational parameter of unperturbed motion at the initial moment of time t_0, $W_i(t, \Lambda_i, \xi_i, p_i, \lambda_i, \eta_i, q_i)$ – perturbing function.

In work [16] a scheme for expressing perturbing functions via osculating elements was presented (4). In the article [18] obviously expansion of the perturbing function in analogues of the second system of canonical Poincare variables were obtained up to the second power of small parameters including, for n – planetary systems with variable masses. The equations of secular perturbations in the general case are also obtained

$$\begin{aligned} \dot{\lambda}_i &= \frac{\mu_{i0}^2}{\gamma_i^2 \Lambda_i^3} - \frac{\partial W_i^{(\mathrm{sec})}}{\partial \Lambda_i}, & \dot{\Lambda}_i &= 0, \\ \dot{\eta}_i &= -\frac{\partial W_i^{(\mathrm{sec})}}{\partial \xi_i}, & \dot{\xi}_i &= \frac{\partial W_i^{(\mathrm{sec})}}{\partial \eta_i}, \\ \dot{q}_i &= -\frac{\partial W_i^{(\mathrm{sec})}}{\partial p_i}, & \dot{p}_i &= \frac{\partial W_i^{(\mathrm{sec})}}{\partial q_i}. \end{aligned} \tag{7}$$

The obviously form of the obtained evolutionary equations of the problem of multi bodies with variable masses (7) is as following

$$\begin{aligned} \dot{\xi}_i &= f\sum_{s=1}^{i-1} m_s \left(\frac{\Pi_{ii}^{is}}{\Lambda_i}\eta_i + \frac{\Pi_{is}^{is}}{\sqrt{\Lambda_i\Lambda_s}}\eta_s\right) + f\sum_{k=i+1}^{n} m_k \left(\frac{\Pi_{kk}^{ik}}{\Lambda_i}\eta_i + \frac{\Pi_{ik}^{ik}}{\sqrt{\Lambda_i\Lambda_k}}\eta_k\right) - \frac{3\ddot{\gamma}_i\Lambda_i^3}{2\gamma_i\mu_{i0}^2}\eta_i, \\ \dot{\eta}_i &= -f\sum_{s=1}^{i-1} m_s \left(\frac{\Pi_{ii}^{is}}{\Lambda_i}\xi_i + \frac{\Pi_{is}^{is}}{\sqrt{\Lambda_i\Lambda_s}}\xi_s\right) - f\sum_{k=i+1}^{n} m_k \left(\frac{\Pi_{kk}^{ik}}{\Lambda_i}\xi_i + \frac{\Pi_{ik}^{ik}}{\sqrt{\Lambda_i\Lambda_k}}\xi_k\right) + \frac{3\ddot{\gamma}_i\Lambda_i^3}{2\gamma_i\mu_{i0}^2}\xi_i \\ \dot{p}_i &= -f\sum_{s=1}^{i-1} m_s B_1^{is}\left(\frac{q_i}{4\Lambda_i} - \frac{q_s}{4\sqrt{\Lambda_i\Lambda_s}}\right) - f\sum_{k=i+1}^{n} m_k B_1^{ik}\left(\frac{q_i}{4\Lambda_i} - \frac{q_k}{4\sqrt{\Lambda_i\Lambda_k}}\right) \\ \dot{q}_i &= f\sum_{s=1}^{i-1} m_s B_1^{is}\left(\frac{p_i}{4\Lambda_i} - \frac{p_s}{4\sqrt{\Lambda_i\Lambda_s}}\right) + f\sum_{k=i+1}^{n} m_k B_1^{ik}\left(\frac{p_i}{4\Lambda_i} - \frac{p_k}{4\sqrt{\Lambda_i\Lambda_k}}\right) \end{aligned} \tag{8}$$

$$\dot{\lambda}_i = \frac{\mu_{i0}^2}{\gamma_i^2 \Lambda_i^3} - \frac{\partial W_i^{(\mathrm{sec})}}{\partial \Lambda_i}, \quad \dot{\Lambda}_i = 0 \tag{9}$$

here, index s – denotes the inner planet relative to the investigated planet, and the index k – the outer one.

For n planetary problem of multi-bodies with variable masses the system of canonical equations (8) represent $4n$-linear non-autonomous equations with complex coefficients. The explicit form of non-autonomous coefficients of equations (8) – (9) are cumbersome, for internal and external perturbing planets they are written separately. They are described in detail and given in the work [18]. These coefficients, in turn, depend on the Laplace coefficients. The Laplace coefficients can be calculated exactly and expressed throughout elliptic integrals of the first and second kind [19].

The resulting system of canonical equations (8) is divided into two separate subsystems [18]. The first subsystem defines the equations of secular perturbations for eccentric elements (ξ_i, η_i), and the second one for oblique elements (p_i, q_i). The linearity of the system of non-autonomous differential equations (8) significantly ease the study of the canonical system of differential equations in the formulation under consideration.

From the last equation (9) follows

$$\Lambda_i = const \quad \text{or} \quad a_i = const \tag{10}$$

Note that λ_i is calculated after integrating equations (8).

Remark that when the analogues of eccentricities and the analogues of the inclination of the orbital planes of planets are small enough, the equations of secular perturbations (8) – (9) are convenient for describing the dynamic evolution of planetary systems with variable masses.

2.2 Dimensionless differential equations of motion

For the calculation we use the following dimensionless quantities:

$$t^* = \tau = \omega_1 t, \quad \left(\frac{d}{d\tau}\right) = (\ )', \quad a_i^* = \frac{a_i}{a_1}, \quad m_i^* = \frac{m_i}{m_{00}}, \tag{11}$$

where, t^* – dimensionless time, a_i^* – dimensionless distance, m_i^* – dimensionless mass, $m_{00} = m_0(t_0) = const$ – the mass of the parent star at the initial moment of time, $a_1 = a_1(t_0) = const$ – the semi major axis of the planet P_1 at the initial moment of time, the value of ω_1 is defined as follows:

$$\omega_1 = \frac{\sqrt{f m_{00}}}{a_1^{3/2}} = const. \tag{12}$$

Accordingly, we write down the period of the planet P_1 at the initial moment of time in Earth years

$$T_1 = \frac{2\pi}{\omega_1} = \frac{2\pi}{\sqrt{f m_{00}}} a_1^{3/2} = const = k_1. \tag{13}$$

Then, taking into account the relations [14], [16]

$$\begin{aligned}
&\Lambda_i = \sqrt{\mu_{i0}}\sqrt{a_i}, \quad \lambda_i = l_i + \pi_i \\
&\xi_i = \sqrt{2\sqrt{\mu_{i0}}\sqrt{a_i}(1-\sqrt{1-e_i^2})}\cos\pi_i, \quad \eta_i = -\sqrt{2\sqrt{\mu_{i0}}\sqrt{a_i}(1-\sqrt{1-e_i^2})}\sin\pi_i, \\
&p_i = \sqrt{2\sqrt{\mu_{i0}}\sqrt{a_i}\sqrt{1-e_i^2}(1-\cos i_i)}\cos\Omega_i, \quad q_i = -\sqrt{2\sqrt{\mu_{i0}}\sqrt{a_i}\sqrt{1-e_i^2}(1-\cos i_i)}\sin\Omega_i, \\
&l_i = M_i = n_i[\phi_i(t) - \phi_i(\tau_i)], \ \pi_i = \Omega_i + \omega_i,
\end{aligned} \tag{14}$$

where

$$a_i, \quad e_i, \quad i_i, \quad \omega_i, \quad \Omega_i, \quad \phi_i(\tau_i) \tag{15}$$

the osculating elements of the aperiodic motion over the quasi conic section, we can write

$$\xi_i = \xi_i^*(fm_{00}a_1)^{1/4}, \quad \eta_i = \eta_i^*(fm_{00}a_1)^{1/4}, \quad p_i = p_i^*(fm_{00}a_1)^{1/4}, \quad q_i = q_i^*(fm_{00}a_1)^{1/4} \tag{16}$$

$$\Lambda_i = \sqrt{fm_{00}}\sqrt{a_1}\Lambda_i^*, \quad \frac{3\ddot{\gamma}_i\Lambda_i^3}{2\gamma_i\mu_{i0}^2} = \omega_1\frac{3\gamma_i''}{2\gamma_i}\frac{\Lambda_i^{*3}}{\mu_{i0}^{*2}}. \tag{17}$$

At the same time, dimensionless eccentric and oblique elements have the form

$$\begin{aligned} \xi_i^* &= \sqrt{2\sqrt{\mu_{i0}^*}\sqrt{a_i^*}(1-\sqrt{1-e_i^2})}\cos\pi_i, \\ \eta_i^* &= -\sqrt{2\sqrt{\mu_{i0}^*}\sqrt{a_i^*}(1-\sqrt{1-e_i^2})}\sin\pi_i, \end{aligned} \tag{18}$$

$$\begin{aligned} p_i^* &= \sqrt{2\sqrt{\mu_{i0}^*}\sqrt{a_i^*}\sqrt{1-e_i^2}(1-\cos i_i)}\cos\Omega_i, \\ q_i^* &= -\sqrt{2\sqrt{\mu_{i0}^*}\sqrt{a_i^*}\sqrt{1-e_i^2}(1-\cos i_i)}\sin\Omega_i, \end{aligned} \tag{19}$$

$$\Lambda_i^* = \sqrt{\mu_{i0}^*}\sqrt{a_i^*}, \quad \mu_{i0}^* = 1 + \frac{m_{i0}}{m_{00}} = const. \tag{20}$$

Using the introduced notation (11) – (17) and the relations (18) – (20), we proceed to dimensionless variables.

In equations (8), by reducing the left and right sides of the equation by a common multiplier $\omega_1(fm_{00}a_1)^{1/4} = const$, we obtain the evolution equations in dimensionless quantities.

For the convenience of writing, omitting the symbol $(*)$, we rewrite the equations (8) in dimensionless variables in the following form

$$\begin{aligned} \xi_i' &= \sum_{s=1}^{i-1} m_s\left(\frac{\Pi_{ii}^{is}}{\Lambda_i}\eta_i + \frac{\Pi_{is}^{is}}{\sqrt{\Lambda_i\Lambda_s}}\eta_s\right) + \sum_{k=i+1}^{n} m_k\left(\frac{\Pi_{kk}^{ik}}{\Lambda_i}\eta_i + \frac{\Pi_{ik}^{ik}}{\sqrt{\Lambda_i\Lambda_k}}\eta_k\right) - \frac{3\gamma_i''}{2\gamma_i}\frac{\Lambda_i^3}{\mu_{i0}^2}\eta_i, \\ \eta_i' &= -\sum_{s=1}^{i-1} m_s\left(\frac{\Pi_{ii}^{is}}{\Lambda_i}\xi_i + \frac{\Pi_{is}^{is}}{\sqrt{\Lambda_i\Lambda_s}}\xi_s\right) - \sum_{k=i+1}^{n} m_k\left(\frac{\Pi_{kk}^{ik}}{\Lambda_i}\xi_i + \frac{\Pi_{ik}^{ik}}{\sqrt{\Lambda_i\Lambda_k}}\xi_k\right) + \frac{3\gamma_i''}{2\gamma_i}\frac{\Lambda_i^3}{\mu_{i0}^2}\xi_i, \\ p_i' &= -\sum_{s=1}^{i-1} m_s B_1^{is}\left(\frac{q_i}{4\Lambda_i} - \frac{q_s}{4\sqrt{\Lambda_i\Lambda_s}}\right) - \sum_{k=i+1}^{n} m_k B_1^{ik}\left(\frac{q_i}{4\Lambda_i} - \frac{q_k}{4\sqrt{\Lambda_i\Lambda_k}}\right), \\ q_i' &= \sum_{s=1}^{i-1} m_s B_1^{is}\left(\frac{p_i}{4\Lambda_i} - \frac{p_s}{4\sqrt{\Lambda_i\Lambda_s}}\right) + \sum_{k=i+1}^{n} m_k B_1^{ik}\left(\frac{p_i}{4\Lambda_i} - \frac{p_k}{4\sqrt{\Lambda_i\Lambda_k}}\right). \end{aligned} \tag{21}$$

At the same time, the expressions Π_{ii}^{is}, Π_{is}^{is}, Π_{kk}^{ik}, Π_{ik}^{ik} in equations (21) and the Laplace coefficients retain their form. But, they are already dimensionless quantities.

3 Results

3.1 Dimensionless evolutionary equations of the three-planetary problem of four bodies for numerical calculations

Now we will explicitly write dimensionless evolutionary equations for the special case when $n = 3$. The planet P_1 is affected only by the outer planets ($s = 0,\ k = 2, 3$), and for planet P_2 we take into account the influence of one inner planet ($s = 1$) and one outer planet ($k = 3$). For planet P_3, there is only the influence of the outer planets ($s = 1, 2,\ k = 0$).

The system of equations of eccentric elements consists of six equations

$$\begin{aligned}
\xi_1' &= (D_2^{1,2} + D_2^{1,3} + D_3^1) \cdot \eta_1 + D_1^{1,2} \cdot \eta_2 + D_1^{1,3} \cdot \eta_3,\\
\eta_1' &= -(D_2^{1,2} + D_2^{1,3} + D_3^1) \cdot \xi_1 - D_1^{1,2} \cdot \xi_2 - D_1^{1,3} \cdot \xi_3,\\
\xi_2' &= D_1^{2,1} \cdot \eta_1 + (D_2^{2,1} + D_2^{2,3} + D_3^2) \cdot \eta_2 + D_1^{2,3} \cdot \eta_3,\\
\eta_2' &= -D_1^{2,1} \cdot \xi_1 - (D_2^{2,1} + D_2^{2,3} + D_3^2) \cdot \xi_2 - D_1^{2,3} \cdot \xi_3,\\
\xi_3' &= D_1^{3,1} \cdot \eta_1 + D_1^{3,2} \cdot \eta_2 + (D_2^{3,1} + D_2^{3,2} + D_3^3) \cdot \eta_3,\\
\eta_3' &= -D_1^{3,1} \cdot \xi_1 - D_1^{3,2} \cdot \xi_2 - (D_2^{3,1} + D_2^{3,2} + D_3^3) \cdot \xi_3,
\end{aligned} \tag{22}$$

Similarly, we obtain a system of equations for oblique elements

$$\begin{aligned}
p_1' &= -(H_2^{1,2} + H_2^{1,3}) \cdot q_1 + H_1^{1,2} \cdot q_2 + H_1^{1,3} \cdot q_3,\\
q_1' &= (H_2^{1,2} + H_2^{1,3}) \cdot p_1 - H_1^{1,2} \cdot p_2 - H_1^{1,3} \cdot p_3,\\
p_2' &= H_1^{2,1} \cdot q_1 - (H_2^{2,1} + H_2^{2,3}) \cdot q_2 + H_1^{2,3} \cdot q_3,\\
q_2' &= -H_1^{2,1} \cdot p_1 + (H_2^{2,1} + H_2^{2,3}) \cdot p_2 - H_1^{2,3} \cdot p_3,\\
p_3' &= H_1^{3,1} \cdot q_1 + H_1^{3,2} \cdot q_2 - (H_2^{3,1} + H_2^{3,2}) \cdot q_3,\\
q_3' &= -H_1^{3,1} \cdot p_1 - H_1^{3,2} \cdot p_2 + (H_2^{3,1} + H_2^{3,2}) \cdot p_3,
\end{aligned} \tag{23}$$

The following notation is introduced in equations (22) and (23)

$$D_1^{ik} = \frac{m_k \Pi_{ik}^{ik}}{\sqrt{\Lambda_i \Lambda_k}}, \quad D_2^{ik} = \frac{m_k \Pi_{kk}^{ik}}{\Lambda_i}, \quad D_3^i = -\frac{3\Lambda_i^3}{2\mu_{i0}^2} \frac{\gamma_i''(t)}{\gamma_i}, \tag{24}$$

$$H_1^{i,k} = \frac{1}{4} \frac{m_k B_1^{i,k}}{\sqrt{\Lambda_i \Lambda_k}}, \quad H_2^{i,k} = \frac{1}{4} \frac{m_k B_1^{i,k}}{\Lambda_i}, \tag{25}$$

$$\begin{aligned}
\Pi_{ik}^{ik} &= \frac{1}{8}\left(9B_0^{ik} + B_2^{ik}\right) - \frac{9\,(1+\alpha_{ik}^2)}{8\alpha_{ik}} C_0^{ik} + \frac{21}{16} C_1^{ik} + \frac{3\,(1+\alpha_{ik}^2)}{8\alpha_{ik}} C_2^{ik} + \frac{3}{16} C_3^{ik},\\
\Pi_{kk}^{ik} &= -\frac{3}{4\alpha_{ik}} B_0^{ik} - \frac{1}{2} B_1^{ik} + \frac{15\alpha_{ik}^2 + 6}{8\alpha_{ik}^2} C_0^{ik} - \frac{3}{2\alpha_{ik}} C_1^{ik} - \frac{9}{8} C_2^{ik},
\end{aligned} \tag{26}$$

$$B_0^{ik} = \frac{2a_i\gamma_i}{\pi\,(a_k\gamma_k)^2} \int\limits_0^{\pi} \frac{d\lambda}{(1+\alpha_{ik}^2 - 2\alpha_{ik}\cos\lambda)^{3/2}}, \quad B_1^{ik} = \frac{2a_i\gamma_i}{\pi\,(a_k\gamma_k)^2} \int\limits_0^{\pi} \frac{\cos\lambda\, d\lambda}{(1+\alpha_{ik}^2 - 2\alpha_{ik}\cos\lambda)^{3/2}},$$

$$B_2^{ik} = \frac{2a_i\gamma_i}{\pi\left(a_k\gamma_k\right)^2}\int\limits_0^\pi \frac{\cos 2\lambda d\lambda}{\left(1+\alpha_{ik}^2-2\alpha_{ik}\cos\lambda\right)^{3/2}},$$

$$C_0^{ik} = \frac{2\left(a_i\gamma_i\right)^2}{\pi\left(a_k\gamma_k\right)^3}\int\limits_0^\pi \frac{d\lambda}{\left(1+\alpha_{ik}^2-2\alpha_{ik}\cos\lambda\right)^{5/2}},\quad C_1^{ik} = \frac{2\left(a_i\gamma_i\right)^2}{\pi\left(a_k\gamma_k\right)^3}\int\limits_0^\pi \frac{\cos\lambda d\lambda}{\left(1+\alpha_{ik}^2-2\alpha_{ik}\cos\lambda\right)^{5/2}},\tag{27}$$

$$C_2^{ik} = \frac{2\left(a_i\gamma_i\right)^2}{\pi\left(a_k\gamma_k\right)^3}\int\limits_0^\pi \frac{\cos 2\lambda d\lambda}{\left(1+\alpha_{ik}^2-2\alpha_{ik}\cos\lambda\right)^{5/2}},\quad C_3^{ik} = \frac{2\left(a_i\gamma_i\right)^2}{\pi\left(a_k\gamma_k\right)^3}\int\limits_0^\pi \frac{\cos 3\lambda d\lambda}{\left(1+\alpha_{ik}^2-2\alpha_{ik}\cos\lambda\right)^{5/2}},$$

where the following conditions are met for the outer planets $(i < k)$

$$\alpha_{ik} = \frac{\gamma_i a_i}{\gamma_k a_k} = \alpha_{ik}(t) < 1.\tag{28}$$

For the inner planets , the designations are as follows

$$D_1^{is} = \frac{m_s\Pi_{is}^{is}}{\sqrt{\Lambda_s\Lambda_i}},\quad D_2^{is} = \frac{m_s\Pi_{ii}^{is}}{\Lambda_i},\quad D_3^{i} = -\frac{3\Lambda_i^3}{2\mu_{i0}^2}\frac{\gamma_i''(t)}{\gamma_i},\tag{29}$$

$$H_1^{i,s} = \frac{1}{4}\frac{m_s B_1^{i,s}}{\sqrt{\Lambda_s\Lambda_i}},\quad H_2^{i,s} = \frac{1}{4}\frac{m_s B_1^{i,s}}{\Lambda_i},\tag{30}$$

$$\begin{aligned}\Pi_{is}^{is} &= \frac{1}{8}\left(9B_0^{is}+B_2^{is}\right) - \frac{9\left(1+\alpha_{is}^2\right)}{8\alpha_{is}}C_0^{is} + \frac{21}{16}C_1^{is} + \frac{3\left(1+\alpha_{is}^2\right)}{8\alpha_{is}}C_2^{is} + \frac{3}{16}C_3^{is},\\ \Pi_{ii}^{is} &= -\frac{3\alpha_{is}}{4}B_0^{is} - \frac{1}{2}B_1^{is} + \frac{15+6\alpha_{is}^2}{8}C_0^{is} - \frac{3\alpha_{is}}{2}C_1^{is} - \frac{9}{8}C_2^{is},\end{aligned}\tag{31}$$

$$B_0^{is} = \frac{2a_s\gamma_s}{\pi\left(a_i\gamma_i\right)^2}\int\limits_0^\pi \frac{d\lambda}{\left(1+\alpha_{is}^2-2\alpha_{is}\cos\lambda\right)^{3/2}},\quad B_1^{is} = \frac{2a_s\gamma_s}{\pi\left(a_i\gamma_i\right)^2}\int\limits_0^\pi \frac{\cos\lambda d\lambda}{\left(1+\alpha_{is}^2-2\alpha_{is}\cos\lambda\right)^{3/2}},$$

$$B_2^{is} = \frac{2a_s\gamma_s}{\pi\left(a_i\gamma_i\right)^2}\int\limits_0^\pi \frac{\cos 2\lambda d\lambda}{\left(1+\alpha_{is}^2-2\alpha_{is}\cos\lambda\right)^{3/2}},$$

$$C_0^{is} = \frac{2\left(a_s\gamma_s\right)^2}{\pi\left(a_i\gamma_i\right)^3}\int\limits_0^\pi \frac{d\lambda}{\left(1+\alpha_{is}^2-2\alpha_{is}\cos\lambda\right)^{5/2}},\quad C_1^{is} = \frac{2\left(a_s\gamma_s\right)^2}{\pi\left(a_i\gamma_i\right)^3}\int\limits_0^\pi \frac{\cos\lambda d\lambda}{\left(1+\alpha_{is}^2-2\alpha_{is}\cos\lambda\right)^{5/2}},\tag{32}$$

$$C_2^{is} = \frac{2\left(a_s\gamma_s\right)^2}{\pi\left(a_i\gamma_i\right)^3}\int\limits_0^\pi \frac{\cos 2\lambda d\lambda}{\left(1+\alpha_{is}^2-2\alpha_{is}\cos\lambda\right)^{5/2}},\quad C_3^{is} = \frac{2\left(a_s\gamma_s\right)^2}{\pi\left(a_i\gamma_i\right)^3}\int\limits_0^\pi \frac{\cos 3\lambda d\lambda}{\left(1+\alpha_{is}^2-2\alpha_{is}\cos\lambda\right)^{5/2}},$$

In formulas (29) – (32), the following conditions are met for the inner planets $(s < i)$

$$\alpha_{is} = \frac{\gamma_s a_s}{\gamma_i a_i} = \alpha_{is}(t) < 1\tag{33}$$

4 Discussion

The resulting system of canonical equations (19) is divided into two separate subsystems.

The first subsystem (22) defines the equations of secular perturbations for eccentric elements. The second subsystem (23) contains equations for oblique elements. The linearity of the obtained non-autonomous canonical systems of differential equations (22) – (23) significantly ease the study of the problem in the formulation under consideration.

Note that equations (9) determining the mean longitude λ_i of the planets is calculated after integrating equations (22) and (23).

The obtained systems of differential equations (22) – (23) in dimensionless variables will be further used to analyze the effects of mass variability on the dynamic evolution of specific planetary systems by numerical methods.

5 Conclusion

In the work using the symbolic computing system "Wolfram Mathematica" [20-21], evolutionary equations are obtained in explicit analytical form, in dimensionless variables for the three-planetary problem of four bodies system with isotropically varying masses. Differential equations are described in analogues of the second system of canonical Poincare elements.

The obtained evolutionary equations will be used to study the dynamic evolution of extrasolar planetary systems. This will take into account the effects of the decrease in the mass of the parent star and the increase in the mass of the planets due to the accretion of matter from the remnants of the protoplanetary disk.

Acknowledgments

This research has been funded by the Science Committee of the Ministry of Education and Science of the Republic of Kazakhstan (Grant No. AP14869472).

References

[1] Sannikova T.N., Kholshevnikov K.V., "Motion in a Central Field in the Presence of a Constant Perturbing Acceleration in a Co-moving Coordinate System" , *Astronomy Reports,* 59(8) (2015): 806–817.

[2] Sokolov L.L., Kholshevnikov K.V., "Ob integpipyemocti zadachi N tel [On the integrability of the N-body problem]" , *Astronomy Letters,* 12(7) (1986): 557–561.

[3] Perminov A.S., Kuznetsov E.D., "The Implementation of Hori–Deprit Method to the Construction Averaged Planetary Motion Theory by Means of Computer Algebra System Piranha" , *Mathematics in Computer Science,* 14(2) (2020): 305–316. DOI: 10.1007/s11786-019-00441-4.

[4] Kuznetsov E.D., Kholshevnikov K.V., "Orbital'naya evolyuciya dvuplanetnoj sistemy Solnce – YUpiter – Saturn [Orbital evolution of the Sun – Jupiter – Saturn bi - planetary system]" , *Vestniks of Saint Petersburg University,* 1(1) (2009): 139–150.

[5] Kuznetsov E.D., "Orbital evolution of phaethon cluster" , *Meteoritics & Planetary Science,* 56 (2021): 1.

[6] Belkina S.O., Kuznetsov E.D., "Orbital flips due to solar radiation pressure for space debris in near-circular orbits" , *Acta Astronautica,* 178 (2021): 360–369. https://doi.org/10.1016/j.actaastro.2020.09.025.

[7] Kuznetsov E.D., Rosaev A.E., Plavalova E., Safronova V.S., Vasileva M.A., "A Search for Young Asteroid Pairs with Close Orbits" , *Solar System Research,* 54(3) (2020): 236–252. DOI: 10.1134/s0038094620030077.

[8] Perminov A., Kuznetsov E., "The orbital evolution of the Sun–Jupiter–Saturn–Uranus–Neptune system on long time scales", *Astrophysics and Space Science,* 365(8) (2020): 144. DOI: 10.1007/s10509-020-03855-w.

[9] Kholshevnikov K.V., Mullari A.A., Tolumbaeva D.A., Vavilov D.E., "Opredelenie pervonachal'nyh orbit vnesolnechnyh planet metodom luchevyh skorostej: zamknutye formuly [Determination of the initial orbits of extrasolar planets by the method of radial velocities: closed formulas]", *Vestniks of Saint Petersburg University,* 1(3) (2011): 143–152.

[10] Kholshevnikov K.V., Tolumbaeva D.A., Mullari A.A., "Opredelenie pervonachal'nyh orbit vnesolnechnyh planet metodom luchevyh skorostej: stepennye ryady [Determination of the initial orbits of extrasolar planets by the method of radial velocities: power series]", *Vestniks of Saint Petersburg University,* 1(1) (2011): 166–172.

[11] Perminov A.S., Kuznetsov E.D., "Orbital'naya evolyuciya vnesolnechnyh planetnyh sistem HD 39194, HD 141399 I HD 160691 [Orbital evolution of extrasolar planetary systems HD 39194, HD 141399 and HD160691]", *The Astronomical Journal,* 96(10) (2019): 795–813. DOI: 10.1134/S1063772919090075.

[12] https://exoplanets.nasa.gov/.

[13] Prokopenya A., Minglibayev M., Shomshekova S., "Computing Perturbations in the Two-Planetary Three-Body Problem with Masses Varying Non-Isotropically at Different Rates", *Mathematics in Computer Science,* 14(2) (2020): 241–251. https://doi.org/10.1007/s11786-019-00437-0.

[14] Minglibayev M.Zh., *Dinamika gravitiruyushchikh tel s peremennymi massami i razmerami [Dynamics of gravitating bodies with variable masses and sizes]* (LAP LAMBERT Academic Publishing, 2012): 224. Germany. ISBN:978-3-659-29945-2.

[15] Minglibayev M.Zh., Kosherbayeva A.B., "Differential equations of planetary systems", *Reports of the National Academy of Sciences of the Republic of Kazakhstan,* 2(330) (2020): 14–20. https://doi.org/10.32014/2020.2518-1483.26.

[16] Minglibayev M.Zh., Kosherbayeva A.B., "Equations of planetary systems motion", *News of NAS RK. Physical-mathematical series,* 6 (2020): 53–60.

[17] Minglibayev M. Zh., Mayemerova G.M., "Evolution of the orbital-plane orientations in the two-protoplanet three-body problem with variable masses", *Astronomy Reports,* 58(9) (2014): 667–677. DOI: 10.1134/S1063772914090066.

[18] Prokopenya A.N., Minglibayev M.Zh., Kosherbayeva A.B., "Derivation of evolutionary equations in the multi-body problem with isotropically varying masses using computer algebra", *Programming and Computer Software,* 48(2) (2022): 1–11.

[19] Charlier K., *Nebesnaya mekhanika [Celestial mechanics]* [Текст] / Perevod s nem. V.G. Demina; Pod red. prof. B.M. Shchigoleva [Translated from German by V.G. Demin; Edited by prof. B.M. Shchigolev] (Moscow: Nauka, 1966): 627.

[20] Wolfram S., *An elementary introduction to the Wolfram Language* (New York: Wolffram Media, Inc., 2017): 324. ISBN: 978-1-944183-05-9.

[21] Prokopenya A.N., *Reshenie fizicheskih zadach c ispolzovaniem sistemy Mathematica [Solving physical problems using the Mathematica system]* (BSTU Publishing, Brest., 2005): 260.

IRSTI 30.03, 55.30.31, 55.30.13 DOI: https://doi.org/10.26577/JMMCS.2022.v116.i4.05

A. Rakhmatulina[1,2*], S. Ibrayev[1], N. Imanbaeva[3], A. Ibrayeva[1]
[1]U. Joldasbekov Institute of Mechanics and Engineering, Almaty, Kazakhstan
[2]Almaty Technological University, Almaty, Kazakhstan
[3]Satbayev University, Almaty, Kazakhstan
E-mail: *kazrah@mail.ru

SYNTHESIS OF THE TRANSFORMING MECHANISM OF THE ROCKING MACHINE

This article discusses the synthesis of a six-link transforming mechanism of a rocking machine. First, the problem of synthesizing a four-link articulated-lever mechanism for reproducing a vertical line was solved. For this purpose, the problem of synthesizing a rectilinear-guiding mechanism of the Evans type, which is a hinged-lever four-link mechanism with a straight vertical line drawing point, is considered. The task of synthesis is to implement the constraint equation. The geometric meaning of the constraint equation is to determine the hinge, the positions of which in the absolute coordinate system are equidistant from the origin of the OXY coordinate system.
The problem of synthesis is formulated as a problem of quadratic approximation. According to the found dimensions of the articulated four-link, performing the position analysis, the true positions of the suspension point of the rod column were determined. After that, the found parameters were refined using the output criterion directly, that is, the deviation from the given rectilinear trajectory.
After the synthesis of a straight-line guiding mechanism, a drive kinematic chain was synthesized, which consists of a crank and a connecting rod.
Thus, a rocking machine drive mechanism was obtained, containing a base, a crank pair connected to the main hinged four-link mechanism. The technical result is achieved by the fact that a two-link group is attached to the main four-link mechanism, forming a class III mechanism. The attached two-drive group is the leading crank connected to the rack and connecting rod.
Based on the obtained dimensions of the six-link converting mechanism, an experimental model was developed, which fully confirmed the efficiency of the transforming mechanism.
Key words: Synthesis, rocking machine, drive, connecting rod, four-link articulated-lever mechanism, converting mechanism.

А. Рахматулина[1,2*], С. Ибраев[1], Н. Иманбаева[3], А. Ибраева[1]
[1]Ө.А. Жолдасбеков атындағы Механика және машинатану институты, Алматы қ., Казақстан
[2]Алматы технологиялық университеті, Алматы қ., Казақстан
[3]Satbayev University, Алматы қ., Казақстан
E-mail: *kazrah@mail.ru

Сорғыш қондырғының түрлендіруші механизмінің синтезі

Бұл мақалада сорғыш қондырғының алты буынды түрлендіруші механизмінің синтезі талқыланады. Біріншіден, тік сызықты жаңғыртуға арналған төртбуынды топсалы-иінтіректі механизмнің синтез мәселесі қарастырылады. Осы мақсатта түзу тік сызықты сызу нүктесі бар топсалы иінтіректі төрт буынды механизм болып табылатын Эванс типті түзу сызықты бағыттаушы механизмді синтездеу мәселесі қарастырылған. Синтездің міндеті - шектеу теңдеуін жүзеге асыру. Шектеу теңдеуінің геометриялық мағынасы абсолютті координаталар жүйесіндегі орындары OXY координаталар жүйесінің басынан бірдей қашықтықта орналасқан топсаны анықтау болып табылады.

Синтез мәселесі квадраттық жуықтау есебі ретінде тұжырымдалған. Топсалы төрт буынның табылған өлшемдеріне сәйкес позициялық талдауды орындау арқылы өзек бағанының ілу нүктесінің шынайы позициялары анықталды. Осыдан кейін табылған параметрлер тікелей шығыс критерийін, яғни берілген түзу сызықты траекториядан ауытқуды пайдаланып нақтыланды.
Түзу сызықты бағыттаушы механизм синтезделгеннен кейін иінді және шатуннан тұратын жетекті кинематикалық тізбек синтезделді.
Осылайша, негізгі топсалы төрт буынды механизмге айналшақ-бұлғақты жұбы негізі қосылған, бар сорғыш қондырғының жетек механизмі алынды. Техникалық нәтижеге екі буынды топ негізгі төртбуынды механизмге бекітіліп, III класты механизмді құрайды. Бекітілген екі жетекті топ тірекке және шатунға қосылған жетекші айналшақ.
Алты буынды түрлендіру механизмінің алынған өлшемдері негізінде түрлендіру механизмінің тиімділігін толық растайтын тәжірибелік үлгі әзірленді.
Түйін сөздер: Синтез, тербелгіш машина, жетек, шатун, төртбуынды топсалы-иінтіректі механизм, түрлендіруші механизм.

А. Рахматулина[1,2*], С. Ибраев[1], Н. Иманбаева[3], А. Ибраева[1]
[1]Институт механики и машиноведения им. У.А. Джолдасбекова, г. Алматы, Казахстан
[3]Алматинский технологический университет, г. Алматы, Казахстан
[3]Satbayev University, г. Алматы, Казахстан
E-mail: *kazrah@mail.ru
Синтез преобразующего механизма станка качалки

В данной статье рассматривается синтез шестизвенного преобразующего механизма станка качалки. Сначало решена задача синтеза четырехзвенного шарнирно-рычажного механизма для воспроизведения вертикальной прямой. Для чего рассмотрена задача синтеза прямолинейно-направляющего механизма типа Эванса, который представляет собой шарнирно-рычажный четырехзвенный механизм с чертящей точкой прямую вертикальную линию. Задача синтеза заключается в реализации уравнения связей. Геометрический смысл уравнения связей заключается в определении шарнира, положения которых в абсолютной системе координат является равноудалеными от начала системы координат OXY.
Сформулирована задача синтеза в виде задачи квадратического приближения. По найденным размерам шарнирного четырехзвенника, выполняя анализ положений определен истинные положения точки подвеса колонны штанг. После этого произведен уточнение найденных параметров используя непосредственно выходной критерий, то есть отклонение от заданной прямолинейной траектории.
После синтеза прямолинейно - направляющего механизма, синтезирован приводная кинематическая цепь, которая состоит из кривошипа и шатуна.
Тем самым получен механизм привода станка качалки, содержащий основание, кривошипно-шатунную пару соединенный к основному шарнирно четырехзвенному механизму. Технический результат достигается тем, что на основной четырехзвенный механизм присоединяется двухповодковая группа, образуя механизм III класса. Присоединенная двухповодковая группа является ведущим кривошипом, связанное с стойкой и шатуном.
На основе полученных размеров шестизвенного преобразующего механизма разработан экспериментальный образец, который полностью подтвердил работоспособность преобразующего механизма.
Ключевые слова: Синтез, станок качалка, привод, шатун, четырехзвенный шарнирно-рычажный механизм, преобразующий механизм.

1 Introduction

Of the existing mechanized methods of oil production, the most common is the sucker-rod deep-pumping method with balancing individual drives of mechanical action.

As a converting mechanism connecting the gearbox with the balancer, a four-link crank mechanism is used, which converts the uniform rotation of the crank into the reciprocating movement of the plunger. At the same time, according to the location of the balancing load, the designs of pumping units with crank, rocker (balance) and combined balancing are distinguished. The most commonly used and well-studied are converting mechanisms with a two-arm load balancer and crank balancing, less common are designs with a single-arm load balancer with heavy loads on the balancer and traverse. An important advantage of such installations is the ability to control the pumping mode by changing the stroke of the plunger, for which the crank pin connecting the lower head of the connecting rod with the crank is put on different holes on the crank.

Meanwhile, the use of lever mechanisms, whose connecting rod point describes a straight path with high accuracy, could eliminate the arc head, and the rod string can be hung directly from the drawing point. Such a design could also solve another problem - reducing the metal consumption of the installation due to the possibility of reducing the height of the support frame. The fact is that a significant drawback of the existing design is the high location of the so-called "upper rack", on which the hinge of the balancer is located - the most loaded link. The large height of the balancer attachment point, which is affected by large support reactions, creates a significant swinging force on the rack, which makes it necessary to manufacture a massive foundation from high-quality concrete. This factor is largely due to the high metal consumption of the structure. This drawback can be overcome by synthesizing a lever system with a reduced mounting height of the rack hinges.

2 Analysis of literature data and problem statement

Displacement analysis for four-link linkages has been extensively covered in the technical literature [1, 2].

In terms of optimization, bioinspired techniques have expanded significantly over the past two decades. One of the earliest work on an evolutionary algorithm applied to the optimal synthesis of a four-link linkages generator [4]. The authors developed a genetic algorithm to solve three research cases with and without given time and considering different target points. In [5], a procedure for synthesizing the path to the generator connections using a neural network is proposed, it consists of a training stage, at which a large number of kinematic simulations with random dimensions are generated, and at the second stage, the neural network is used to approximate the synthesis of the solution to the problem. The article [6] describes the process of optimal synthesis of a four-link by the method of controlled deviations of variables using the differential evolution algorithm. In [7], the authors consider the Pareto optimal synthesis of four-link mechanisms for generating a path, taking into account the tracking error and the transmission angle error, it is solved using a multicriteria hybrid genetic algorithm. A hybrid evolutionary algorithm for synthesizing a four-link link path is presented in the study [8], where a hybridization between the genetic algorithm and the differential evolution algorithm is proposed. The authors state that the main advantages of this algorithm are the simplicity and ease of implementation and solving of complex optimization problems without the need for deep knowledge of the search space. In the article [9], the authors present a new approach to the multicriteria synthesis of the optimal four-link path and its application to the traditional problem with one, two, and three objective functions. A new algorithm called "Mechanism synthesis algorithm of the University of Malaga" for the synthesis of mechanism paths has been successfully applied to six cases of synthesis of paths and functions of four-bar and six-bar mechanisms [10].

Similar topics can be found in the titles of articles [11, 12, 13]. In the literature, the kinematic and optimization formulation of the four-rod generator is very similar. The kinematic setting in these papers is based on the traditional closed loop condition, and the objective function is the sum of squared Euclidean distances, where the main difficulty is the need for a penalty when the kinematics has no solution in two-dimensional real space.

For this reason, the formulation proposed here is based on the use of natural coordinates and the Hermitian Conjugate of an Operator to construct an objective function whose output is always a positive real number. It should also be noted that the statement proposed here can be extended to any problem of the synthesis of planar mechanisms with a closed solution.

3 Solution of the problem

Consider, for the synthesis of a four-link hinged-lever mechanism for reproducing a vertical straight line, the problem of synthesizing a straight-line-guiding mechanism of the Evans type, which is a four-link hinged-lever mechanism $ABCO$ with a drawing point D. We consider given N finitely distant positions of the point D along a vertical straight line in a section of length S (S is the stroke of the rod string, for example $S = 2500$ mm), given by the absolute coordinates X_i^*, Y_i^* :

$$X_i^* = X_k \tag{1}$$

$$Y_i^* = Y_k + S * \frac{i-1}{N-1}, i = 1, \ldots, \; N \tag{2}$$

We also assume that the parameters of the dyad ABD given by the values X_A, Y_A, a, b are also given. Where X_A, Y_A are the absolute coordinates of the hinge A relative to the fixed coordinate system OXY (Figure 1).

Behind each given position D_i^* of the point D along the straight line from the analysis of the dyad ABD with given dimensions, we determine the absolute coordinates X_{Bi}, Y_{Bi} of the hinge B_i. (Figure 2).

By solving a system of two equations (3) and (4) using the Maple program.

$$\begin{cases} (X_i^* - X)^2 + (Y_i^* - Y)^2 - b^2 = 0 \\ (X_A - X)^2 + (Y_A - Y)^2 - a^2 = 0 \end{cases} \tag{3}$$

$$X = X_{Bi}, \quad Y = Y_{Bi}$$

$$\alpha_i = \arctan(Y_i^* - Y_{B_i}, X_i^* - X_{B_i})$$

$$\begin{cases} X_{Ci} = X_{Bi} + x_C^{loc} \cos \alpha_i - y_C^{loc} \sin \alpha_i \\ Y_{Ci} = Y_{Bi} + x_C^{loc} \sin \alpha_i + y_C^{loc} \sin \alpha_i \end{cases} \tag{4}$$

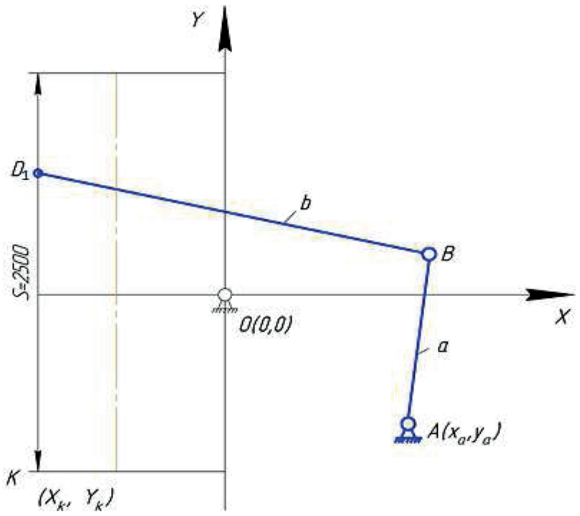

Figure 1: Geometric interpretation of the equation of connection of the synthesis problem.

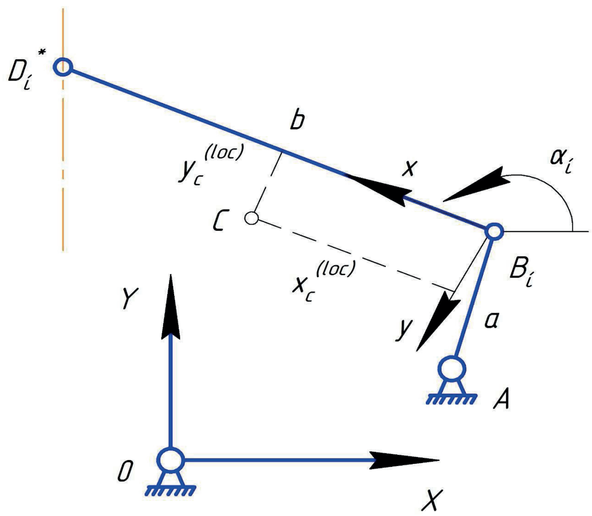

Figure 2: Geometric interpretation of the equation of connection of the problem of synthesis of a four-link mechanism.

According to the given absolute coordinates of the hinges B_i and D_i^*, it is possible to determine the angular positions α_i of the links BD. The Bxy coordinate system is rigidly connected with the BD link, while the Bx axis is directed along the vector $\overrightarrow{B_iD_i^*}$. Then the absolute coordinates of the hinge C with local coordinates x_C^{loc}, ${}_C^{loc}$ are determined from formula (4).

The task of synthesis is to implement the constraint equation of the form (5).

$$(X_{Ci} - X_0)^2 + (Y_{Ci} - Y_O)^2 - l_{OC}^2 = 0, \quad i = 1, \dots, N. \tag{5}$$

The geometric meaning of this equation is to determine the hinge , the positions of which in the absolute coordinate system C_i, $i = 1, \ldots, N$ are equidistant from the origin of the OXY coordinate system. Thus, the positions of the hinge C must approximately realize a circle centered at the point O and with a radius l_{OC}.

Substituting from (6) the absolute coordinates X_{Ci}, Y_{Ci} into (5), we obtain the equation of relations in the following form

$$[(X_{Bi}-X_O)\cos\alpha_i+(Y_{Bi}-Y_O)\sin\alpha_i]\,x_C^{loc}+[-(X_{Bi}-X_O)\sin\alpha_i+(Y_{Bi}-Y_O)\cos\alpha_i]\,y_C^{loc}+ \\ +x_C^{(loc)^2}+y_C^{(loc)^2}-\frac{1}{2}l_{OC}^2+\frac{1}{2}(X_{Bi}-X_O)^2+\frac{1}{2}(Y_{Bi}-Y_O)^2=0,\quad i=1,\ldots,N \tag{6}$$

Introduce the notation

$$a_i=(X_{Bi}-X_O)\cos\alpha_i+(Y_{Bi}-Y_O)\sin\alpha_i,$$

$$b_i=-(X_{Bi}-X_O)\sin\alpha_i+(Y_{Bi}-Y_O)\cos\alpha_i$$

$$c_i=1$$

$$d_i=\frac{1}{2}(X_{Bi}-X_O)^2+\frac{1}{2}(Y_{Bi}-Y_O)^2$$

Then in new variables $x_1 = x_C^{loc}$, $x_2 = y_C^{loc}$, $x_3 = x_C^{(loc)^2}+y_C^{(loc)^2}-\frac{1}{2}l_{OC}^2$ constraint equations in the form

$$\Delta_i \equiv a_i x_1 + b_i x_2 + c_i x_3 + d_i = 0,\quad i=1,\ldots,N \tag{7}$$

Here Δ_i is called a deviation from the implementation of the given equation of relations, then the synthesis problem will consist of approximate implementations of equation (7) for all, $i = 1, \ldots, N$ given positions of points.

In the general case, when $N > 3$, that is, when more than 3 positions of the points D_i^* are given, the exact implementation of equation (7) is not possible, and for their approximate implementations it is necessary to find the minimum of the function

$$S(x_1,\ x_2,\ x_3)=\sum_{i=1}^{N}\Delta_i^2 \to \min_{x_1,\,x_2,\,x_3} \tag{8}$$

Thus, the synthesis problem is formulated as a quadratic approximation problem. Equating the partial derivatives with respect to x_i to zero,

$$\frac{\partial S}{\partial x_i}=0$$

obtain a system of 3 linear equations for determining the variables x_1, x_2, x_3.

$$A\overrightarrow{X}=\overrightarrow{b} \tag{9}$$

where

$$A = \begin{bmatrix} \frac{1}{N}\sum a_i^2 & \frac{1}{N}\sum a_i b_i & \frac{1}{N}\sum a_i c_i \\ \frac{1}{N}\sum a_i b_i & \frac{1}{N}\sum b_i^2 & \frac{1}{N}\sum c_i b_i \\ \frac{1}{N}\sum a_i c_i & \frac{1}{N}\sum b_i c_i & \frac{1}{N}\sum c_i^2 \end{bmatrix}, \quad \overrightarrow{X} = \begin{bmatrix} x_1 \\ x_2 \\ x_3 \end{bmatrix}, \quad \overrightarrow{b} = \begin{bmatrix} -\frac{1}{N}\sum a_i d_i \\ -\frac{1}{N}\sum b_i d_i \\ -\frac{1}{N}\sum c_i d_i \end{bmatrix}$$

The solution of this equation for $\det A \neq 0$ is written as

$$\overrightarrow{X} = A^{-1}\overrightarrow{b} \tag{10}$$

It can be proved that the case $\det A = 0$ corresponds to the case of degeneracy of the system of linear equations (9). The geometric meaning of which is to replace the rotational kinematic pair with a translational one. In view of obtaining an infinite value of the radius of the circle. Based on the found values x_1, x_2, x_3, we determine the variables x_C^{loc}, $^{loc}_{C}$, and also

$$l_{OC} = \sqrt{(x_C^{loc})^2 + (y_C^{loc})^2 - 2x_3} \tag{11}$$

Based on the found dimensions of the $ABCO$ articulated four-link, performing the analysis of the positions, we determine the true positions of the point D of the suspension of the column of rods. After that, it is possible to refine the found parameters using the output criterion directly, that is, the deviation from the given rectilinear trajectory.

Let us introduce the local coordinate system $_{55}$ by directing the abscissa axis $_5$ along the link , the angular positions of the $_5$ axis relative to the absolute coordinate system will be denoted by α_{CD} (Figure 3). Absolute coordinates of the new suspension point of the rod column $_{D1}$, Y_{D1} according to the formula (12, 13).

After defining variables

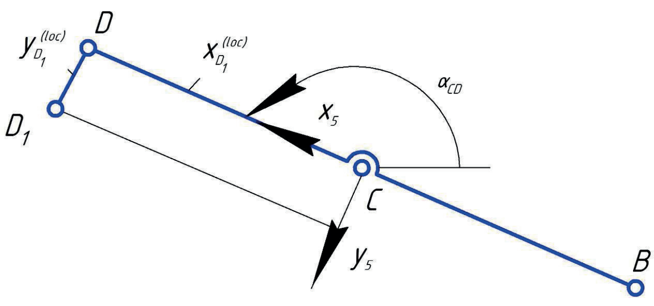

Figure 3: Local coordinate system $_{55}$.

$$X_{D_1} = X_C + x_{D_1}^{(loc)} \cos\alpha_{CD} - y_{D_1}^{(loc)} \sin\alpha_{CD} \tag{12}$$

$$Y_{D_1} = Y_C + x_{D_1}^{(loc)} \sin\alpha_{CD} + y_{D_1}^{(loc)} \cos\alpha_{CD} \tag{13}$$

Synthesis: Refinement

Then the constraint equation is written as

$$X_{D_{i1}} = X_O, \quad i = 1, \dots, N \tag{14}$$

which means the requirement for the constancy of the X coordinate of the points D_{1i} (Figure 4).

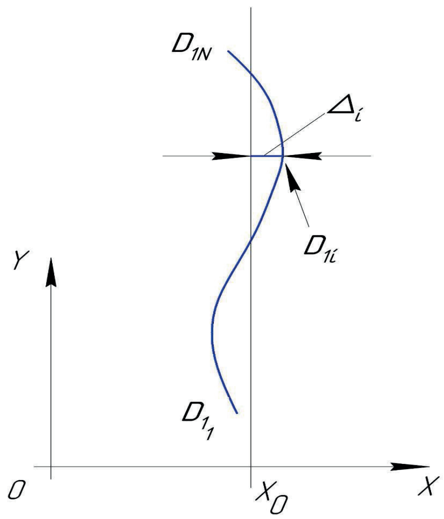

Figure 4: Approximation error – deviation of the true from the given vertical line.

Substituting the value of the absolute coordinates $_{D1}$ from formula (12) we obtain the relation equation in the form

$$-X_0 + x_{D_1}^{(loc)} \cos \alpha_{CDi} - y_{D_1}^{(loc)} sin\alpha_{CDi} = -X_{C_i} \tag{15}$$

Then introducing the notation

$$\begin{aligned} &x_1 = X_0, \quad x_2 = x_{D_1}^{(loc)}, \ x_3 = y_{D_1}^{(loc)} \\ &a_i = -1, \ b_i = \cos \alpha_{CDi}, \quad c_i = -\sin \alpha_{CDi}, \quad d_i = X_{C_i} \end{aligned} \tag{16}$$

We obtain the synthesis equation in the form

$$\Delta_i = a_i x_1 + b_i x_2 + c_i x_3 + d_i = 0 \tag{17}$$

Here Δ_i is the approximation error. The task of synthesis in the general case for $N > 3$ will be in the approximate implementation of these synthesis equations. To do this, it is necessary to solve the problem of quadratic approximation, which consists in minimizing the function S, of the form: problem (8).

The solution of this problem can be obtained by analogy with the solution of the previous problem of quadratic approximation in the form (9). This solution is the only solution to the system of linear equations (11), with $\det A \neq 0$.

4 Synthesis of a drive kinematic chain

After the synthesis of a straight-line guide mechanism, it is necessary to synthesize the drive kinematic chain GFE, which consists of a crank GF and a connecting rod FE connected to the connecting rod BC (Figure 5).

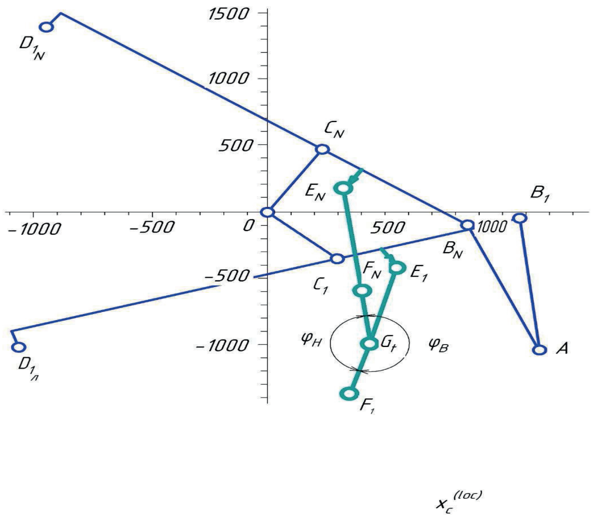

Figure 5: Synthesis of the crank group GFE.

Let us introduce the local coordinate system Bxy rigidly connected with the connecting rod BC by directing the Bx axis along the link BC. Let us introduce a hinge E on the connecting rod BC with local coordinates x_E^{loc}, ${}_E^{loc}$. Then, when the OC link moves from the lowest position OC_1 to the extreme upper position OC_N, the hinge occupies the positions $E_1, \ldots, E_N$. It is believed that a kinematic analysis of the four-link $ABCO$ has been performed and the angular positions of the connecting rod BC determined by the angle of rotation α_{BC} are known.

Then the absolute coordinates of the hinge E is determined through the absolute coordinates of the hinge B and the rotation angles α_{BC} according to the formulas

$$\begin{aligned} X_{E_i} &= X_{B_i} + x_E^{(loc)} \cos\alpha_{BC_i} - y_E^{(loc)} \sin\alpha_{BC_i} \\ Y_{E_i} &= Y_{B_i} + x_E^{(loc)} \sin\alpha_{BC_i} + y_E^{(loc)} \cos\alpha_{BC_i} \end{aligned} \tag{18}$$

Let's set the position of the hinge G relative to the fixed coordinate system OXY through the coordinates X_G, Y_G. Denote by ρ_i the distance between the hinges Gi and Ei and determine the minimum and maximum values of ρ:

$$\begin{aligned} \rho &= |GE_i| \\ \rho_{\min} &= \min_{i=1,\ldots,N} \rho_i \\ \rho_{\max} &= \max_{i=1,\ldots,N} \rho_i \end{aligned} \tag{19}$$

Then the required lengths l_1, l_2 of the crank GF and connecting rod FE are determined from the ratio

$$\begin{cases} l_1 + l_2 = \rho_{max} \\ l_2 - l_1 = \rho_{min} \end{cases} \tag{20}$$

From here we determine l_1, l_2 by the following formulas

$$l_1 = (\rho_{\max} - \rho_{\min})/2$$
$$l_2 = (\rho_{\min} + \rho_{\max})/2 \tag{21}$$

Points F_1, G, F_N define two angles $\varphi_{\text{в}}$ and $\varphi_{\text{н}}$ and $\varphi_{\text{в}} > \varphi_{\text{н}}$, $\varphi_{\text{в}} + \varphi_{\text{н}} = 2\pi$, where $\varphi_{\text{в}}$ corresponds to the angle of rotation of the crank when the rod string goes up, φ_n corresponds to the lowering of the plunger down.

The drive mechanism of the rocking machine, containing a base, a crank pair connected to the main articulated four-link mechanism, a balancer support, a two-arm balancer with a front arm and a rear arm, characterized in that it has a connecting rod consisting of two triangular contours, which is pivotally connected to the rear arm a double-arm balancer and with a rocker, and the front triangular contour, which serves as the front shoulder of the connecting rod, is connected to the suspension point of the column rods, and the counterweight is fixed on the front shoulder of the two-arm rocker.

The technical result is achieved by the fact that a two-link group is attached to the main four-link mechanism, forming a III class mechanism. The attached two-drive group is the leading crank connected to the rack and connecting rod.

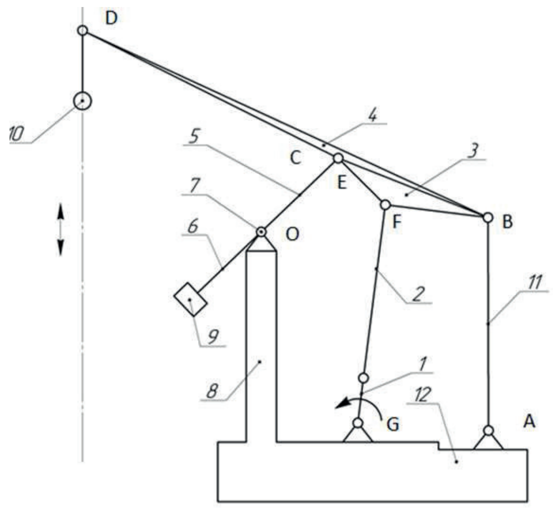

Figure 6: Scheme of the drive mechanism of sucker-rod pumping units in the upper position.

The sucker-rod pumping drive mechanism contains a crank 1 (Figure 6), a connecting rod 2 hinged on one side to the crank 1, and on the other side to the connecting rod, which consists of two triangular contours 3 and 4. The balancer 6 on the rear arm 5 is connected to the connecting rod 3, the middle hinge 7 is connected to the support 8, and the counterweight 9 is fixed on the front arm of the balancer-6. The connecting rod 3 is connected to the rocker arm 11, and the head 10 is fixed on the front arm 4 of the connecting rod 3. The rocker arm 11 and the crank 1 are pivotally connected to the rack 12.

Dimensions: L_{AB} = 1115 mm, L_{BD} = 2360.35 mm, L_{BD} = 1019.205 mm, L_{BC} = 868.28 mm, L_{CD} = 1494.10 mm, L_{BC} = 868.28 mm, L_{OC} = 548.95 mm, L_{CE} = 533.729 mm, L_{EF} = 1163.4655 mm, L_{FG} = 454.879 mm.

5 Discussion of experimental results

The analysis showed the possibility of using this mechanism as a converting mechanism for driving sucker-rod pumping units. Based on the obtained dimensions of the six-link converting mechanism, an experimental model was developed, which fully confirmed the efficiency of the transforming mechanism. For the manufacture of an experimental model of the design of a six-link rectilinearly guiding converting mechanism for the drive of sucker-rod pumping units, a geometric model of all structural components of the mechanism was designed in Kompas 3D as part of the work.

An experimental model of the converting mechanism for the drive of sucker-rod pumping units is shown in Figure 7.

Figure 7: Experimental model of a six-link rectilinearly guiding converting drive mechanism.

In addition to a significant gain in dimensions, the use of the mechanism leads to a significant simplification of the design, since the arc head is removed, the connecting rod point is directly connected to the stuffing box without the use of an intermediate flexible link. Reducing the hinges of the mechanism to the foundation leads to a significant reduction in the metal consumption of the foundation, since the rocking forces on the frame of the mechanism are reduced.

6 Conclusion

The problem of synthesis of a straight-line guiding mechanism has been solved, a drive kinematic chain has been synthesized, which consists of a crank and a connecting rod. The dimensions of the articulated four-bar linkage are found, by performing the position analysis, the true positions of the suspension point of the rod column are determined. The found parameters were refined using the output criterion directly, that is, the deviation from the given straight-line trajectory.

A rocking machine drive mechanism has been obtained, containing a base, a crank pair connected to the main hinged four-link mechanism. A four-link mechanism is joined by a two-link group, forming a class III mechanism. The attached two-drive group is the leading crank connected to the rack and connecting rod.

Based on the obtained dimensions of the six-link converting mechanism, an experimental model was developed, which fully confirmed the efficiency of the transforming mechanism.

Acknowledgments

This research has been funded by the Science Committee of the Ministry of Education and Science of the Republic of Kazakhstan (Grant No. AP08052127).

References

[1] Dukkipati R.V., *Spatial mechanisms: analysis and synthesis* (CRC Press, Boca Raton, 2001).

[2] McCarthy J.M., Soh G.S., *Geometric design of linkages* vol 11. (Springer, Berlin, 2010).

[3] Cabrera J., Simon A., Prado M., "Optimal synthesis of mechanisms with genetic algorithms", *Mech Mach Theory* 37(10) (2002): 1165–1177. https://doi.org/10.1016/S0094-114X(02)00051-4

[4] Vasiliu A., Yannou B. "Dimensional synthesis of planar mechanisms using neural networks: application to path generator linkages", *Mech Mach Theory* 36 (2001): 299–310. https://doi.org/10.1016/S0094-114X(00)00037-9

[5] Bulatović R.R., Dordević S.R, "On the optimum synthesis of a four-bar linkage using differential evolution and method of variable controlled deviations", *Mech Mach Theory* 44(1) (2009): 235–246. https://doi.org/10.1016/j.mechmachtheory.2008.02.001

[6] Nariman-Zadeh N., Felezi M., Jamali A., Ganji M., "Pareto optimal synthesis of four-bar mechanisms for path generation", *Mech Mach Theory* 44(1)(2009): 180–191. https://doi.org/10.1016/j.mechmachtheory.2008.02.006

[7] Lin W.Y. "A GA-DE hybrid evolutionary algorithm for path synthesis of four-bar linkage", *Mech Mach Theory* 45(8) (2010): 1096–1107. https://doi.org/10.1016/j.mechmachtheory.2010.03.011

[8] Khorshidi M., Soheilypour M., Peyro M., Atai A., Shariat Panahi M., "Optimal design of four-bar mechanisms using a hybrid multi-objective GA with adaptive local search", *Mech Mach Theory* 46(10)(2011): 1453–1465. https://doi.org/10.1016/j.mechmachtheory.2011.05.006

[9] Cabrera J.A., Ortiz A., Nadal F., Castillo J.J., "An evolutionary algorithm for path synthesis of mechanisms", *Mech Mach Theory* 46(2) (2011): 127–141. https://doi.org/10.1016/j.mechmachtheory.2010.10.003

[10] Bulatović R.R., Miodragović G., Bošković M.S., "Modified Krill Herd (MKH) algorithm and its application in dimensional synthesis of a four-bar linkage", *Mech Mach Theory* 95 (2016): 1–21. https://doi.org/10.1016/j.mechmachtheory.2015.08.004

[11] Chanekar P.V., Fenelon M.A.A., Ghosal A., "Synthesis of adjustable spherical four-link mechanisms for approximate multi-path generation", *Mech Mach Theory* 70 (2013): 538–552. https://doi.org/10.1016/j.mechmachtheory.2013.08.009

[12] Kim B.S., Yoo H.H., "Body guidance syntheses of four-bar linkage systems employing a spring-connected block model", *Mech Mach Theory* 85 (2014): 147–160. https://doi.org/10.1016/j.mechmachtheory.2014.11.022

3-бөлім **Раздел 3** **Section 3**

Информатика **Информатика** **Computer Science**

IRSTI 28.23.15 DOI: https://doi.org/10.26577/JMMCS.2022.v116.i4.06

Zh. Yessenbayev[1*], **Zh. Kozhirbayev**[2], **A. Shintemirov**[3]
[1]Atyrau oil and gas university, Atyrau, Kazakhstan
[2]National Laboratory Astana, Astana, Kazakhstan
[3]Nazarbayev University, Astana, Kazakhstan
*e-mail: zh.yessenbayev@aogu.edu.kz

DEVELOPMENT OF A COMPUTER VISION MODULE FOR AUTONOMOUS VEHICLES

The favorable geopolitical position and very large transit potential of the Republic of Kazakhstan in the field of land freight traffic between China and Europe makes the transport logistics industry one of the most promising areas for the development of the country's economy. In this context, deployment of unmanned cargo vehicles to minimize the costs of fuel consumption and use of human labor in labor-intensive and routine operations of logistic processes both inside warehouses and during freight transportation on public roads seems natural and efficient as ever.
This paper describes the results of a research work on development of a computer vision module for an autonomous truck prototype. The performed project stages include installation of the necessary equipment, training of computer vision models and development of a mapping between cameras and LIDAR sensor for object classification and localization purposes.
Key words: Computer vision, autonomous vehicle, vehicle trajectory planning, real-time trajectory planning, unmanned solution.

Ж.А. Есенбаев[1*], Ж.М. Кожирбаев[2], А.М. Шинтемиров[3]
[1]Сафи Өтебаев атындағы Атырау мұнай және газ университеті, Атырау қ., Қазақстан
[2]National Laboratory Astana, Астана қ., Қазақстан
[3]Назарбаев Университет, Астана қ., Қазақстан
*e-mail: zh.yessenbayev@aogu.edu.kz

Автономды көліктер үшін компьютерлік көру модулін әзірлеу

Қазақстанның оңтайлы геосаяси жағдайы мен Қытай мен Еуропа арасындағы жүк тасымалы саласында Қазақстан Республикасының үлкен транзиттік әлеуеті көліктік-логистикалық саланы ел экономикасын дамыту үшін перспективалы бағыттардың бірі болып табылады. Осы тұрғыда отын тұтыну шығындарын азайту және адам еңбегін пайдаланудың логистикалық үдерістердің ішінде, сондай-ақ қоғамдық көліктердегі жүктерді тасымалдау кезінде пайдаланбайтын жүктердің технологиясын пайдалану табиғи және тиімді болып көрінеді. Бұл мақалада автономды жүк көлігінің прототипі үшін компьютерлік көру модулін әзірлеу бойынша зерттеу жұмысының нәтижелері сипатталған. Орындалған жоба кезеңдері қажетті жабдықты орнатуды, компьютерлік көру үлгілерін дайындау және объектілерді жіктеу және локализациялау мақсатында камералар мен LIDAR сенсоры арасындағы картаны әзірлеуді қамтиды.

Түйін сөздер: Компьютерлік көру, автономды көлік, көлік траекториясын жоспарлау, нақты уақыттағы траекторияны жоспарлау, адамсыз шешім.

Ж.А. Есенбаев[1*], Ж.М. Кожирбаев[2], А.М. Шинтемиров[3]
[1]Атырауский университет нефти и газа имени Сафи Утебаева, г. Атырау, Казахстан
[2]National Laboratory Astana, г. Астана, Казахстан
[3]Назарбаев Университет, г. Астана, Казахстан
*e-mail: zh.yessenbayev@aogu.edu.kz

Разработка модуля компьютерного зрения для автономных транспортных средств

Выгодное геополитическое положение и огромный транзитный потенциал Республики Казахстан в сфере наземных грузоперевозок между Китаем и Европой делает отрасль транспортной логистики одним из самых перспективных направлений развития экономики страны. В этом контексте, применения технологий беспилотного грузового транспорта для минимизации издержек от расходования топлива и использования человеческого труда в трудоёмких и рутинных операциях логистических процессов как внутри складских помещений, так и при грузоперевозках по дорогам общего пользования, видится как никогда естественным и эффективным.

В данной статье описаны результаты научно-исследовательской работы по разработке модуля компьютерного зрения для прототипа автономного грузового автомобиля. Выполненные этапы проекта включают в себя установку необходимого оборудования, обучение моделей компьютерного зрения и разработку сопоставления между камерами и датчиком LIDAR для целей классификации и локализации объектов.

Ключевые слова: Компьютерное зрение, автономное транспортное средство, планирование траектории транспортного средства, планирование траектории в реальном времени, беспилотное решение.

1 Introduction

The global transport market is estimated at about 3 trillion USD, which is almost 7% of the global GDP. For example, in Germany this figure reaches 13%, and in Ireland it reaches 14.2%, in Singapore - 13.9%, Hong Kong - 13.7%. This indicates that countries pay special attention to the development of this sector as one of the sources of national income [1]. Favorable geopolitical position and very large transit potential of the Republic of Kazakhstan in the field of land transportation between China and Europe makes the transport logistics industry one of the most promising areas for the development of the country's economy. To this end, Kazakhstan sets the task to increase transit traffic through the country by 10 times by 2050 [2].

To achieve this goal, Kazakhstan is actively putting into operation large transport and logistics centers (TLC) in key regions of the country. The development of the transport corridor "Western Europe - Western China" will allow it to become a new Silk Road, which may become a competitor to the maritime route of cargo transportation from the countries of Southeast Asia to Europe. Thus, cargo transportation along the sea route takes an average of 35-40 days, while along the transport corridor "Western Europe - Western China" the time of delivery of goods by road can be reduced by 2-3 times [3]. Such indicators, along with an increase in the volume of transit traffic, can be achieved through the digitalization and automation of the processes of cargo transportation and logistics operations. Part of the measures to develop the infrastructure of transport corridors is planned for implementation within the framework of the state program "Digital Kazakhstan" [4]. Further development of the industry involves the introduction of robotic systems to minimize or completely eliminate the use of human labor and ensure long-term or round-the-clock operation in the TLC by logistics robots, as well as autonomous cargo transportation by autonomous vehicles along transit highways [5].

Currently, mobile robots and autonomous vehicles are increasingly being used in various sectors of the economy in developed countries. The world's leading automakers such as Tesla, Nissan, Volvo and others are already testing and offering autonomous systems to customers in serial models of cars and trucks [6–8]. The world's leading innovative companies Waymo, Yandex, Uber and others are also developing and testing technologies for autonomous vehicles.

On the other hand, unmanned technologies for the autonomy of trucks are widely used in the mining industry. Volvo was one of the first companies to implement an autonomous transport project in a mine in Norway, where six unmanned trucks operated on a 5 km long route, of which 4.7 km were tunnels. This solution made it possible to increase safety in tunnels and organize round-the-clock work [8]. Since 2015, the British mining company Rio Tinto has been using a fleet of unmanned cargo vehicles in its quarries and mines in Australia, and thereby increased productivity and reduced the cost of the extraction of natural resources [9]. In Russia, ZyfraGroup is actively engaged in the development and implementation of autonomous mining dump trucks in commercial operation [10].

The active promotion of unmanned solutions in the mining industry is associated with the relative ease of ensuring safety measures during the operation of autonomous vehicles by minimizing the presence of a person in the area of operation, the cyclicity and repeatability of operations, etc. At the same time, a much higher level of safety of autopilot systems for trucks is required for facilitating movement of autonomous vehicles on transit roads and TLC territories, along with conventional human-controlled passenger cars and trucks, with pedestrian presence in the traffic area. This area of research is currently under active development in various countries with varying degrees of readiness for testing in real conditions. One of the fewexamples is the successfully launched North American startup Embark Trucks, which is realizing a project for cargo transportation along the highway from El Paso (Texas) to Palm Springs (California) [11] along a 650 miles (about 1000 km) long route.

In view of the prospects for the introduction of autonomous vehicles technologies in Kazakhstan, Nazarbayev University (NU), together with the Russian company Zyfra (VIST) Group [10], with the support of KAMAZ PJSC, has recently completed a a industrial project on development of an autonomous truck on the basis of a modern KAMAZ NEO platform [12].

As part of the project, partners from Zyfra (VIST) Group have equipped a test KAMAZ NEO truck with their own autopilot system for autonomous vehicle movement along a predetermined trajectory or to a specified target position with the possibility of remote control by a person from the control panel (Fig. 1). These technologies have been tested on KAMAZ and BELAZ trucks and will be adapted for a new model of the KAMAZ NEO 5490 truck (Fig. 1) with an automatic transmission. The task of the NU project group was to develop software and hardware modules for computer vision, vehicle trajectory planning with the ability to replan the trajectory in real-time to avoid obstacles and respond to the infrastructure of the traffic system (traffic signs, traffic lights, etc.). The results of the project work on vehicle trajectory planning were reported in [13].

For experimental testing of the developed software and hardware solutions on an experimental KAMAZ vehicle, a test site was created at NU on the basis of an open car parking area on the NU campus.

Figure 1: Autonomous truck based on KAMAZ Neo 5490 platform (left) and Remote control cabin designed by VIST Group (right)

The test site was equipped with road signs, dummy people and cars.

2 Hardware Setup

The hardware part of the computer vision module is a set of interconnected hardware, which is a single system designed to collect, store, process and transmit data from video cameras. The main components are:

1. Video cameras Logitech C922;
2. Wi-Fi/4G router;
3. Laptop;
4. Remote computing server.

Next, we describe the process of integrating these equipment within the truck's cabin.

The bracket and fasteners for the Logitech C922 cameras of the autopilot system inside the cabin of the Kamaz truck were assembled as shown in Fig. 2. The parts were designed in SolidWorks and made on a 3D printer from aluminum profile 40 × 40 mm. The cameras were attached to the frame, which, in turn, was attached to the regular power fasteners of the Kamaz cabin ceiling sheething. The stock ceiling mount is a power mount that will not deform due to the added weight of the camera mount assembly and the cameras themselves and the gravitational forces acting on them.

3 Data synchronization between cameras and the LIDAR

The task of localizing objects using RGB cameras, installed inside the test truck cabin,and the LIDAR sensor, mounted in front of the vehicle, involves the transformation from one coordinate system to another. For this, the cameras and LIDAR were calibrated. For automatic calibration, the algorithm needs to find a specific image template. A chamotte board is usually used as the image, since the computer vision algorithm is able to easily find corners.

Figure 2: Finished assembly of fasteners for the cameras

Using the found coordinates of the corners, the matrix of internal parameters K was calculated (Equation 1). The matrix K for a hole camera consists of 5 parameters: (u_0, v_0) - optical center (principal point) in pixels; (α_x, α_y) - focal length in pixels with $\alpha_x = F/p_x$ and $\alpha_y = F/p_y$, where F is the focal length in real units, usually expressed in millimeters (p_x, p_y) is the pixel size in real units; γ is the skew factor, which is non-zero, if the image axes not perpendicular (Fig. 3).

$$K = \begin{bmatrix} \alpha_x & \gamma & u_0 & 0 \\ 0 & \alpha_y & v_0 & 0 \\ 0 & 0 & 1 & 0 \end{bmatrix} \tag{1}$$

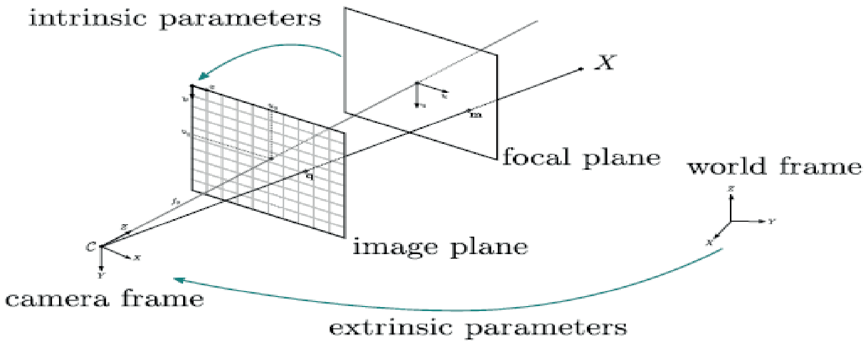

Figure 3: Point camera model

Using internal camera parameters, you can convert points from the real-space coordinate system R3 (x, y, z) to the camera coordinate system R2 (w, h).

$$Z_c \begin{bmatrix} u \\ v \\ 1 \end{bmatrix} = K[R \;\; T] \begin{bmatrix} x_w \\ y_w \\ z_w \\ 1 \end{bmatrix} \tag{2}$$

The Equation 2 shows the formula for converting points in the real space coordinate system to the camera coordinate system, where $[x_w\ y_w\ z_w\ 1]$ is a point in the world coordinate system, $[u\ v\ 1]$ is a point in the camera coordinate system, K are the internal parameters of the camera, z_c is arbitrary scale parameter. $[R\ \ T]$ - are external parameters that denote the transformation of the coordinate system from the coordinates of the three-dimensional world to the coordinates of the three-dimensional camera. Equivalently, the extrinsic parameters define the position of the camera's center and the direction of the camera in world coordinates. T is the position of the center of the world coordinate system, expressed in the coordinates of the camera-centered coordinate system.

The Zhang's model was used for calibration [14], which is a camera calibration method that uses traditional calibration methods (known calibration points) and self-calibration methods (correspondence between calibration points when they are in different positions). To perform a full Zhang calibration, it requires at least three different images of the calibration object, either by moving the object or the camera itself. If some of the intrinsic parameters are given (image orthogonality or optical center coordinates), the number of required images can be reduced to two.

At the first stage, the approximation of the estimated projection matrix H between the calibration target and the image plane is determined using the DLT (Direct linear transformation) method [15]. Subsequently, self-calibration methods are applied to obtain an image of an absolute conical matrix.

Several 4×8 chessboards were printed on A1 sheets. These chessboards were placed in the field of view of the both RGB cameras, mounted in the truck cabin, to calculate the corresponding internal parameters. Figure 4 shows 4 calibration boards.

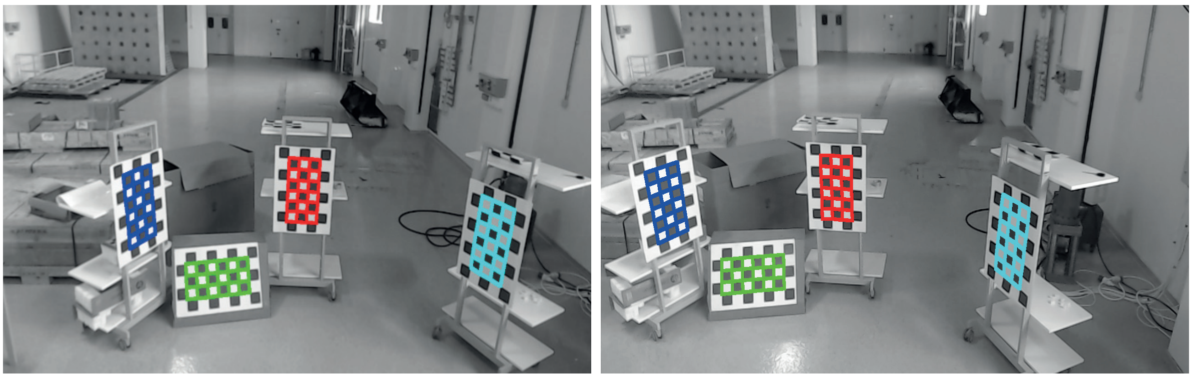

Figure 4: Example of the installed calibration chessboards

At the first stage of calibration the cvlib toolbox was used [16]. This toolbox defines the internal parameters of the cameras and determines the position and rotation between two cameras. To work, several boards were placed ce for the entire size of the frame in different orientations. The figure shows the result of finding the corners of cells in chessboards. Different colors represent different boards found. Figure 5 shows the result of matching the left and right cameras. Thus, the external parameters of both cameraswere computed

In order to achieve accurate results of object recognition, the algorithms for overlaying 2D segments on 3D data from the LIDAR system were developed. To transform the coordinate

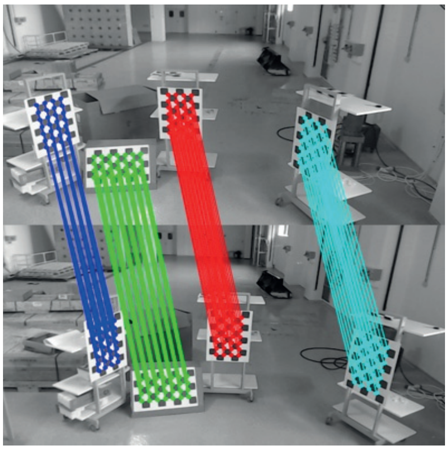

Figure 5: The result of matching two frames of the left and right cameras

system, it was necessary to calibrate the cameras and the LIDAR in order to build the transformation matrix.

Transformation matrices allow arbitrary linear transformations to be displayed in a consistent format suitable for computation. It also makes it easy to combine transformations (by multiplying their matrices).

Linear transformations are not the only ones that can be represented by matrices. Some transformations that are non-linear in the n-dimensional Euclidean space R_n can be represented as linear transformations in the $(n+1)$-dimensional space R_{n+1}. These include both affine transformations (such as translation) and projective transformations. For this reason, 4×4 transformation matrices are widely used in 3D computer graphics. These $n+1$-dimensional transformation matrices are called affine transformation matrices, projective transformation matrices, or, more generally, non-linear transformation matrices. As for an n-dimensional matrix, an $n+1$-dimensional matrix can be described as an augmented matrix.

In the physical sciences, an active transformation is one that actually changes the physical position of the system and makes sense even in the absence of a coordinate system, while a passive transformation is a change in the description of the coordinates of the physical system (change of base). The distinction between active and passive transformations is important. By default, by transformation the mathematicians usually mean active transformations, while physicists can mean both.

Calibration was done using the Aruco calibration toolbox [17] which provides a graphical interface for interacting with 2D and 3D images. Calibration takes place in 2 stages. The first stage is to select points in the 2D image and their corresponding points in the 3D LIDAR image. This step must be repeated several times to increase the accuracy of the results.

At the second stage, the algorithm calculates the transformation matrix from the LIDAR coordinate system to the camera coordinate system. This matrix is also known as the external parameters of the camera. An example of a calibration process we made is shown in Fig. 6.

The complete calibration scene is shown in Fig. 7. In the center, data from the LIDAR system is presented in Point Cloud format, where the intensity of each reflected beam is shown in color. The lower left picture shows data from the left camera fixed inside the truck

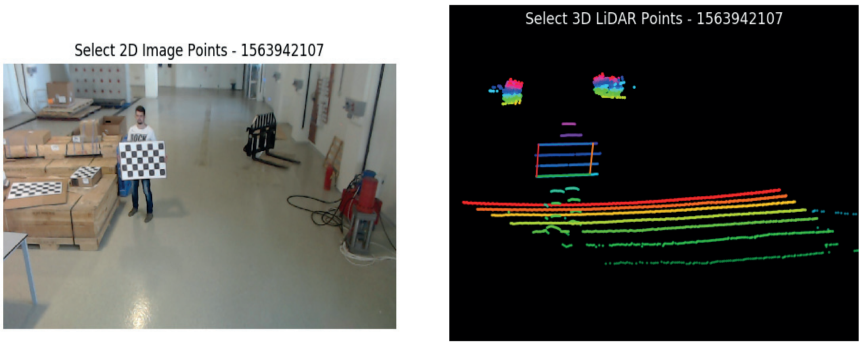

Figure 6: Aruco calibration toolbox example

cabin. The lower right picture shows data from the right camera fixed inside the truck cabin.

Points with the LIDAR are filtered based on the visibility area, which are set as parameters. We consider only points in front of the test truck Then, they are transferred to the camera coordinate system using the matrix obtained earlier. Based on the segments obtained during object detection, the points are filtered again. The resulting points are the basis for the final clustering.

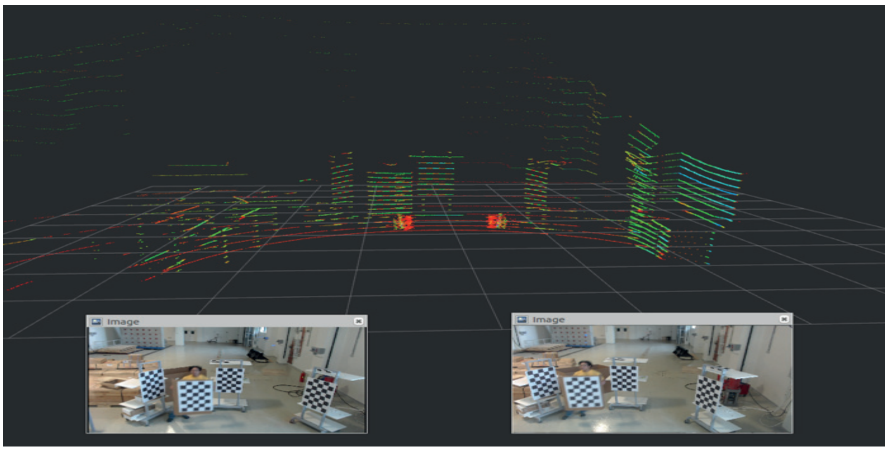

Figure 7: Full calibration scene

4 Datasets

One of the most important parts of machine learning using artificial neural networks is the collection and processing of large amounts of data. To train the object detection and localization model, it was decided to use COCO dataset [18]. The COCO (Common Objects in COntext) dataset is a dataset for training models based on different tasks: object recognition, localized objects, keypoint identification, segmentation, etc. It contains 80 classes, 80,000 training images, and 40,000 images to test the accuracy of the model (Fig. 8).

The dataset consists of several parts. The first part is the images themselves containing the objects. The second part depends on which problem the dataset is applied to. In our case, we use annotations to localize objects. Each object instance contains an annotation with a number of fields, which include a class identifier and a designation of the object's boundaries in the format of x, y coordinates, width and height.

The processing process is divided into several steps. At first, the image must be scaled using an interpolation algorithm. Secondly, it is necessary to use algorithms for data augmentation. We used a random image cropping algorithm to obtain different regions. Also, some images were mirrored horizontally. To annotate the data that was collected manually, the YoloMark tool is used [19].

Figure 8: Examples of images in the COCO Dataset database

For a full-fledged computer vision system that will be able to move along the roads of Kazakhstan in real time, it is necessary to collect additional data on road signs. By training the traffic sign recognition model, the computer vision module can detect traffic signs and send the position of the sign relative to the vehicle to the trajectory planning module. Next, the planner must take certain actions that were prescribed for a particular sign.

After searching and analyzing existing databases, it was decided to use the RTSD road sign database [20]. The database has similar road signs as in Kazakhstan. There are 156 traffic sign classes and 104358 sign images in this dataset.

As you can see in Figure 9, the RTSD dataset has very diverse seasons and also different times of day, which of course helps retrain the model on the same type of data and increases the accuracy of sign detection.

5 Development of an object detection model

During the development of the object detection model, two models were used: YOLOv3 [21] and CenterNet [22]. Both models were trained on COCO public data.

Figure 9: Examples of images in the RTSD database

Figure 10 shows the result of the YOLOv3 recognition algorithm on data collected with an analog camera. It was revealed that the both models were able to constantly find objects in the image for classification (detection stage). A distinctive feature of these methods is that they perform detection and classification at the same time, thereby eliminating the need for re-classification. This allows the models to be suitable for real-time tasks.

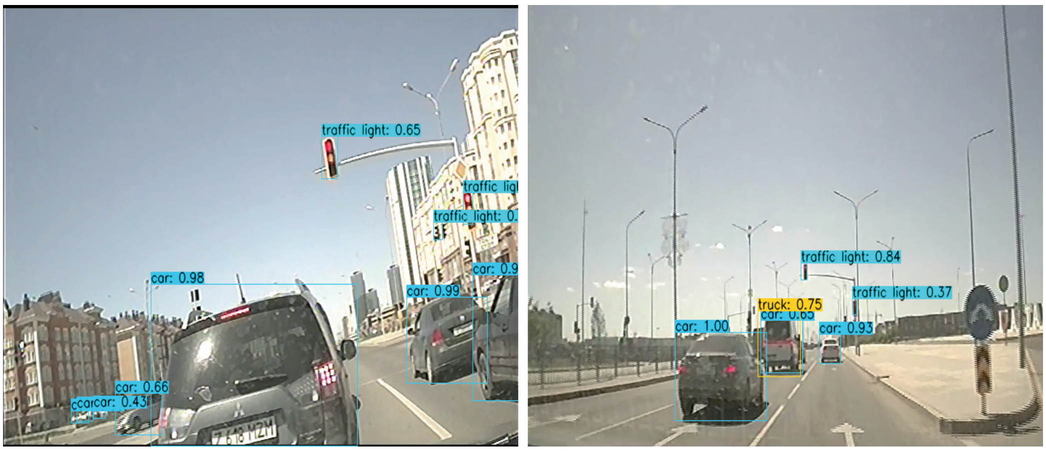

Figure 10: The result of the classification algorithm

The models were trained on the COCO dataset using data augmentation algorithmsfor recognition of people, cars, fire hydrants and US-style road signs. The “training” of the machine learning models were carried out on the DGX-1 deep learning cluster from NVIDIA, which consists of 8 video cards with a total video memory of 64 GB. Both models were able to recognize all the necessary objects that are found on the roads, namely cars, trucks, buses, people, signs, traffic lights, etc.

Table 1: Results of comparing the YOLOv3 and CenterNet models

Model	**Size of input frame**	**Time to process**	**Average accuracy on dataset MS COCO (AP)**
YOLOv3	416x416	40ms	31.0
CenterNet	511x511	60ms	37.4

During the experiments the main characteristics of the two above-mentioned algorithms were identified. The comparison result is presented in Table 1. CenterNet showed a more accurate classification. YOLOv3, in turn, is the faster model of the two presented.

6 Model training

To recognize objects with an RGB camera, it was decided to use a convolutional neural network with the CenterNet architecture (Fig. 11). CenterNet uses a system similar to YOLO. This network is a state-of-the-art architecture capable of classifying and localizing objects in 2D RGB images. CenterNet accepts a fixed-size 2D image as input, and an interpolation algorithm is used to resize the images coming from the camera. As output, CenterNet provides a 2D bounding box of objects found in the image. Unlike YOLO, CenterNet is based on a central point. The implementation of CenterNet for PyTorch was used.

CenterNet consists of several parts. The first part is preprocessing, in which the images are converted to the required format that the neural network accepts. At this stage, the image is interpolated to the dimensions 511×511. Each of the three RGB channels of the image is normalized according to the parameters of the dataset on which the network was trained.

In the second step, the algorithm uses an autoencoder/decoder-based neural network architecture to perform semantic segmentation. The hourglass architecture with 54 convolutional layers is used as a basis.

At the third stage, the corners of the bounding box are found in parallel using the cascade pooling algorithm and the centers are found. After that, a heatmap is built for the found centers and angles. Heatmap contains information about the probability of each pixel to contain the corners and centers of objects. The data from both heatmaps are combined to get the final bounding box.

The network was trained and tested on MS COCO datasets with 50 classes of everyday objects and KITTI dataset [23] with three classes: cars, pedestrians, bicycles, collected using a car with 2 RGB cameras and equipped with a LIDAR system and designed for training and testing machine algorithms with self-government.

7 Development of methods and algorithms for localization of detected objects

After converting the points from 2D to 3D and segmenting them, it was necessary to select clusters that correspond only to the objects that need to be defined. The first step in achieving this was the segmentation of the plane that corresponds to the ground. For this, parameters were found to describe the plane. All points that lie below a certain distance are filtered. This distance can be set as a separate parameter. The remaining points are passed on. To determine the parameters of the plane, the formula was used:

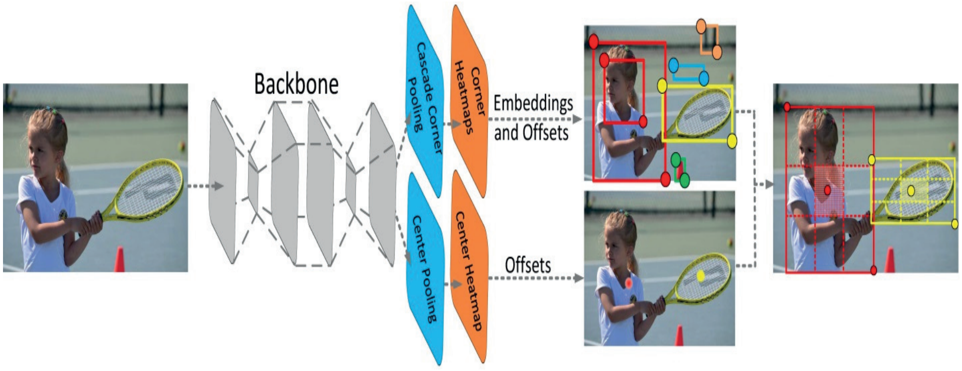

Figure 11: Stages of object detection in the CenterNet architecture

$$fit = (A^T * A)^{-1} * A^T * b \tag{3}$$

where A - x and y coordinates are a set of points belonging to the plane, b - z coordinates are a set of points belonging to the plane, fit - parameters of the plane in the format:

$$ax + by + cz + d = 0 \tag{4}$$

The remaining points can be grouped together to form separate objects. We use the Euclidean Clustering Extraction algorithm to separate points into clusters based on their proximity to each other. The algorithm uses the Euclidean distance to determine if the points belong to the same cluster. Points are considered to be in the same cluster if they are within radius r from each other. The radius r is set as a parameter. By changing it, we can control the size of the clusters. It should be noted that in our case, r must be larger than the voxel size used in the VoxelGrid downsampling step. Brute force search of points within a radius is very expensive, so the point cloud library uses the Kd tree structure to optimize the algorithm. The modified version creates a kdtree from all input points. The tree is used to find the closest points and check their relative distance. This eliminates the need to check all points in the set. At the end, the algorithm extracts a set of clusters that contain points for each feature. The clustering method divides the disorganized point cloud model P into smaller parts, so that the overall processing time for P is greatly reduced. A simple approach to data clustering in the Euclidean sense can be implemented by using a 3D grid subdivision of space using fixed-width blocks or, more generally, an octree data structure. Such a particular representation is very quick to construct and is useful in situations where either a three-dimensional representation of the occupied space is needed, or the data in each resulting 3D block (or octree leaf) can be approximated with a different structure. More generally, however, we can use nearest neighbors and implement a clustering method that is essentially similar to the flooding algorithm. Let's assume we've given a point cloud with a table and objects on top of it. We want to find and segment individual point clusters of an object that lie on a plane. Assuming we are using a Kd tree structure to find nearest neighbors, the algorithmic steps for this would be:

1. Create a tree view Kd for the input point cloud dataset P;
2. Initialize an empty list of clusters C and a queue of points Q to be checked;
3. Then for each point $\boldsymbol{p_i} \in P$, do the following;
   (a) add $\boldsymbol{p_i}$ in the current queue Q;
   (b) for each point $\boldsymbol{p_i} \in Q$ perform:
      i. find a set P_i^k of point neuighbors $\boldsymbol{p_i}$ in the sphere of radius $r < d_{th}$;
      ii. for each neighbor $\boldsymbol{p_i^k} \in P_i^k$, check if the point has already been processed and if not add it to Q;
   (c) when the list of all points in Q has been processed, add Q to the list of clusters C and reset Q to an empty list;
4. The algorithm terminates when all points $\boldsymbol{p_i} \in P$ have been processed and are now part of the list of point clusters C.

For each segment, the algorithm finds several clusters. By choosing the largest cluster, i.e. the cluster with the most points is the desired object. Using these points, you can find the position of the object relative to LIDAR The position is found using the cluster centroid. The centroid is the average value of all the coordinates of a given cluster. To test the algorithm, data was collected from the test KAMAZ truck: images from the two installed RGB cameras and Point Cloud data from the LIDAR sensor The data was written using the rosbag utility that comes with the Robot Operating System (ROS) robotics software development framework. To visualize the work of the algorithm for converting data from a 3D LIDAR coordinate system to a 2D coordinate system, an algorithm was written that, using the calibration parameters, overlays the LIDAR data and the image from the camera. An example is shown in Fig. 12.

Fig. 15 shows the visualization result of object detection and classification. In this example, the pedestrian classes have been filtered out. Fig. 16 shows the visualization of the result of the object localization algorithm. The objects are localized based on the segments shown in Fig. 13. The dots of different colors show the centers of the segmented objects.

8 Conclusion

In this paper we developed a computer vision module for an autonomous vehicle prototype based on a KAMAZ NEO chassis which was provided by our industry partners. The module is aimed at object detection and localization using an integrated system with two video cameras and a LIDAR sensor. The first task was to design and install the necessary hardware equipment. Thus, the cameras and the fasteners were installed inside the cabin whereas the LIDAR sensor with its brackets was installed on the front bumper outside the cabin. Next,

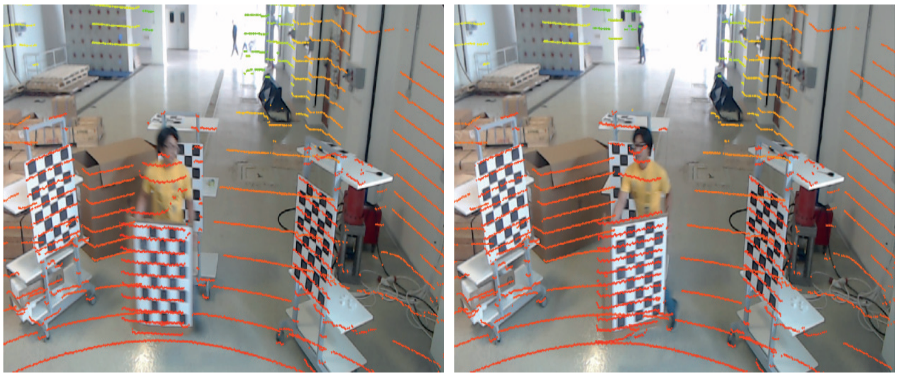

Figure 12: Visualization of the overlay algorithm

Figure 13: Visualization of the detection (left) and localization (right) algorithms

we performed the tasks of calibration and synchronization of two independent data streams, namely, 2D images from the cameras and 3D point clouds from the LIDAR sensor. Once the data streams were fully calibrated and synchronized, we developed the algorithms and trained the models for object detection in the 2D images and localized them in 3D space using information coming from LIDAR.

All the tasks were successfully completed. Currently, our computer vision module is able to detect and classify people, cars, road signs and traffic lights as well as to identify the distance to the detected object. It should be noted that the developed algorithms are suitable for any type of vehicle or mobile robotic systems that employ RGB cameras and a LIDAR sensor as their primary sources of visialinformation.

As a future work, we plan to develop the algorithms for obstacle avoidance, i.e., we need to replan the trajectory or stop the truck based on the situation on the road. This work was partially done but still needs to be improved.

9 Acknowledgement

The project team was partially supported by the Ministry of Education and Science of the Repubic of Kazakhstan (grant project IRN AP08052091), Nazarbayev University CRP project (project №11022021CRP1502) and the industrialgrant funded by Zygra (VIST) Group.

References

[1] Iskaliyev Y., "Transport logistics today сегодня is the key component in implementing of the State program Forced Industrial Development", accessed: 07.07.2022, URL: http://portal.kazlogistics.kz/analytics/95/708/.

[2] Nazarbayev N., "State program «Strategy «Kazakhstan — 2050»: new political course of a developed country", accessed: 07.07.2022, URL: https://online.zakon.kz.

[3] "What is the importance of logistics development for the economy of Kazakhstan", accessed: 07.07.2022, URL: https://forbes.kz/finances/markets/birthday/.

[4] "Official website of the State program «Digital Kazakhstan»", accessed: 07.07.2022, URL: https://digitalkz.kz.

[5] "Transport logistic centers of Kazakhstan, what was done?", accessed: 07.07.2022, URL: http://atameken.kz/ru/articles/27077-transportkazakhstana.

[6] "Official website of Tesla", accessed: 07.07.2022, URL: https://www.tesla.com/autopilot.

[7] "Nissan tests fully autonomous prototype technology on streets of Tokyo?", accessed: 07.07.2022, URL: https://newsroom.nissan-global.com/releases/release-1fc537356ae3aaf048d0201b77013bf9.

[8] "Autonomous trucks in real operation", accessed: 07.07.2022, URL: https://www.volvotrucks.com/en-en/news/volvo-trucks-magazine/2019/feb/bronnoy.html.

[9] "Mining automation: The be all and end all?", accessed: 07.07.2022, URL: https://www.australianmining.com.au/features/mining-automation-the-be-all-and-end-all/.

[10] "Robotized technique for mining and industrial companies", accessed: 07.07.2022, URL: https://vistgroup.ru/solutions/robotizirovannaya-tekhnika/.

[11] "Self-Driving Trucks Are Now Delivering Refrigerators", accessed: 07.07.2022, URL: https://www.wired.com/story/embark-self-driving-truck-deliveries/.

[12] "A new project for development of an autonomous vehicle based on KAMAZ NEO platform started at Nazarbayev University", accessed: 07.07.2022, URL: https://nu.edu.kz/ru/news-ru/v-nazarbaev-universitete-startoval-proekt-po-sozdaniyu-robotizirovannogo-avtomobilya-kamaz-neo.

[13] Abilkassov Sh., Nurlybayev A., Soltan S., Kim A., Shpieva E., Yesmagambet N., Yessenbayev Zh., Shintemirov A., "Facilitating Autonomous Vehicle Research and Development Using Robot Simulators on the Example of a KAMAZ NEO Truck", *2020 IEEE 23rd International Conference on Intelligent Transportation Systems (ITSC),* (2020):1-8.

[14] Zhang Zh, "A Flexible New Technique for Camera Calibration", *IEEE Trans. Pattern Anal. Mach. Intell.,* 22(11), (2000):1330-1334.

[15] Abdel-Aziz Y.I., Karara H.M., "Direct linear transformation from comparator coordinates into object space coordinates in close-range photogrammetry", *In Proceedings of the Symposium on Close-Range Photogrammetry,* 8 (1971):1-18.

[16] "cvlib - a simple, high level, easy to use, open source Computer Vision library for Python", accessed: 07.07.2022, URL: https://www.cvlib.net/.

[17] "ArUco: a minimal library for Augmented Reality applications based on OpenCV", accessed: 07.07.2022, URL: https://www.uco.es/investiga/grupos/ava/node/26.

[18] Lin T.Y., Maire M., Belongie S., Hays J., Perona P., Ramanan D., Doll?r P., Zitnick C.L., "Microsoft COCO: Common Objects in Context", *European conference on computer vision,* (2014):740-755.

[19] "YoloMark - Windows and Linux GUI for marking bounded boxes of objects in images for training Yolo v3 and v2", accessed: 07.07.2022, URL: https://github.com/AlexeyAB/Yolo_mark.

[20] "Russian Traffic Sign Dataset", accessed: 07.07.2022, URL: http://graphics.cs.msu.ru/en/research/projects/rtsd.

[21] Redmon J., Divvala S., Girshick R., Farhadi A., "You only look once: Unified, real-time object detection", *In Proceedings of the IEEE conference on computer vision and pattern recognition,* (2016):779-788.

[22] Duan K., Bai S., Xie L., Qi H., Huang Q.,Tian Q., "CenterNet: Keypoint Triplets for Object Detection", *In Proceedings of the IEEE/CVF international conference on computer vision,* (2019):6569-6578.

[23] Geiger A., Lenz P., Stiller C., Urtasun R., "Vision meets robotics: The KITTI dataset", *International Journal of Robotics Results,* 32(11)(2013):1231–1237.

4-бөлім **Раздел 4** **Section 4**

Қолданбалы математика **Прикладная математика** **Applied Mathematics**

IRSTI 27.31.44 DOI: https://doi.org/10.26577/JMMCS.2022.v116.i4.07

Sh. Akimzhanova[1*], G. Yesbotayeva[2], A. Sakabekov[1]
[1]Satbayev University, Almaty, Kazakhstan
[2]Almaty University of Power Engineering and Telecommunication, Almaty, Kazakhstan
[*]e-mail: shinar_a@mail.ru

FINITE DIFFERENCE METHOD FOR NUMERICAL SOLUTION OF THE INITIAL AND BOUNDARY VALUE PROBLEM FOR BOLTZMANN'S SIXMOMENT SYSTEM OF EQUATIONS

Boltzmann's one-dimensional non-linear non-stationary moment system of equations in the third approximation is presented, in which the first, third and fourth equations corresponds to the laws of conservation of mass, momentum and energy, respectively. This system contains six equations and represents a nonlinear system of hyperbolic type equations. For the Boltzmann's six-moment system of equations an initial and boundary value problem is formulated. The macroscopic boundary condition contains the moments of the incident particles distribution function on the boundary and moments of the reflected particles distribution function from the boundary. The boundary condition depends on the temperature of the wall (boundary).
In this work, using the finite-difference method, an approximate solution of the mixed problem for the Boltzmann system of moment equations is constructed in the third approximation under the boundary conditions obtained by approximating the Maxwell boundary condition. For given values of the coefficients included in the moments of the nonlinear collision integral and the parameter depending on the wall temperature, as well as for fixed values of the initial conditions, a numerical experiment was carried out. As a result, the approximate values of the particle distribution function incident on the boundary and reflected from the boundary, as well as the density, temperature and average velocity of gas particles, as moments of the particle distribution function, are obtained.
Key words: Boltzmann's moment system of equations, microscopic Maxwell boundary condition, macroscopic Maxwell-Auzhan boundary conditions.

Ш. Акимжанова[1*], Г. Есботаева[2], А. Сақабеков[1]
[1]Сәтбаев Университеті, Алматы қ., Қазақстан
[2]Алматы энергетика және байланыс университеті, Алматы қ., Қазақстан
[*]e-mail: shinar_a@mail.ru

Бөлшектердің шекарадан айна және диффузия шағылысу жағдайында Больцманның алты моменттік теңдеулер жүйесі

Больцманның бір өлшемді сызықсыз стационар емес моменттік теңдеулер жүйесінің үшінші жуықтауы келтірілген, онда бірінші, үшінші және төртінші теңдеулер тиісінше массаның, импульстің және энергияның сақталу заңдарына сәйкес келеді. Бұл жүйе алты теңдеуден тұрады және гиперболалық типті теңдеулердің сызықсыз жүйесін құрайды. Больцманның алты моменттік теңдеулер жүйесі үшін алғашқы-шекаралық есеп құрастырылды. Макроскопиялық шекаралық шарт шекараға түскен бөлшектердің таралу функциясының моменттерін және шекарадан шағылысқан бөлшектердің таралу функциясының моменттерін қамтиды. Шекаралық шарт қабырғаның (шекараның) температурасынан тәуелді.

Жұмыста ақырлы-айырым әдісімен Максвелдің шекаралық шартын аппроксимациялау арқылы алынған шекаралық шартты қанағаттандыратын Больцманның теңдеулер жүйесінің үшінші жуықтауы үшін қойылған аралас есептің жуық сан шешуі алынған. Сызықсыз соқтығысу интегралының моменттеріндегі коэффициенттер мен шекараның температурасынан тәуелді параметрдің берілген мәндеріне сай және алғашқы шарттың нақты мәндері үшін сан эксперимент жүргізілді. Нәтижесінде, шекараға түскен (құлаған) және шекарадан шағылысқан молекулалардың үлестіру функциясының,сонымен бірге, газ молекулалар тығыздығының, температурасының және орта жылдамдығының жуық мәндері анықталды.
Түйін сөздер: Больцманның моменттік теңдеулер жүйесі, Максвелдің микроскопиялық шекаралық шарты, Максвел-Аужанның макроскопиялық шекаралық шарты.

Ш. Акимжанова[1*], Г. Есботаева[2], А. Сакабеков[1]
[1]Satbayev University, г. Алматы, Казахстан
[2]Алматинский университет энергетики и связи, г. Алматы, Казахстан
*e-mail: shinar_a@mail.ru

Метод конечных разностей для численного решения начально-краевой задачи для шестимоментной системы уравнений Больцмана

Приведена одномерная нелинейная нестационарная система моментных уравнений Больцмана в третьем приближении, в которой первое, третье и четвертое уравнения соответствуют законам сохранения массы, импульса и энергии соответственно. Эта система содержит шесть уравнений и представляет нелинейную систему уравнений гиперболического типа. Для шестимоментной системы уравнений Больцмана сформулирована начально-краевая задача. Макроскопическое граничное условие содержит моменты функции распределения падающих на границу частиц и функции распределения отраженных от границы частиц. Граничное условие зависит от температуры стенки (границы).
В работе с помощью конечно-разностного метода построено приближенное решение смешанной задачи для системы моментных уравнений Больцмана в третьем приближении при граничных условиях, полученных аппроксимацией граничного условия Максвелла. При заданных значениях коэффициентов, входящих в моменты нелинейного интеграла столкновений и параметра, зависящего от температуры стенки, а также при фиксированных значениях начальных условий проведен численный эксперимент. В результате, приближенные значения падающих на границу и отраженных от границы функции распределения частиц, а также плотность, температура и средняя скорость частиц газа, как моменты функции распределения частиц, получены.

Ключевые слова: Система моментных уравнений Больцмана, микроскопические граничные условия Максвелла, макроскопические граничные условия Максвелла-Аужана.

1 Introduction

The physical state of a system consisting of monatomic molecules can be described with varying degrees of accuracy. The state of the system has a variable meaning depending on what information about the system is useful for the purposes in question. The state of the system is usually determined by the values of some variables – state parameters. Depending on how these options are chosen, information about the system can be quite detailed. In other words, the description of a physical system is possible with varying degrees of accuracy. In order for the description of a non-equilibrium state to be satisfactory with a sufficient level of precision, equations must be known that allow one to determine their changes in time from the given initial the state parameters' values. The particle distribution function can be used to describe the state of the system, which satisfies the nonlinear Boltzmann equation. Boltzmann equation satisfies the rules of mass, momentum, and energy conservation. These conservation laws correspond to five partial differential equations, which contain thirteen unknowns. This system of equations is not closed, since the conservation equations include additional variables – stresses and heat flux. Assuming that the particle distribution function has a special form depending only on thermodynamic variables and their derivatives, one can express stresses and heat flux in terms of these thermodynamic variables. Thus, the system of conservation equations is brought to a closed form. Within the framework of such a scheme, various approximations are possible, leading, respectively, to the equations of Euler, Navier-Stokes, Barnett, etc. Moment equations, which are a series of nonlinear equations represented in partial derivatives, can be used to characterize the state of the system in the transition phase. Between the kinetic (Boltzmann equation) and hydrodynamic (Euler and Navier-Stokes equations, etc.) levels of characterizing the state of a gas lies the system of moment equations. Different basis function systems, the degree of arbitrariness of the particle distribution function, and the procedures for calculating the coefficients of the expansion of the particle distribution function in a Fourier series set apart the various moment approaches. Expanding the particle distribution function in terms of Hermite polynomials around a local Maxwellian distribution produced the Grad system of moment equations in [1] and [2]. By expanding the particle distribution function in terms of the eigenfunctions of the linearized collision operator [5],[6], the moment system of equations, which is distinct from the Grad system, was constructed in [3,[4]. The Boltzmann system of moment equations was the name given to this set of equations. The moment system's and the Boltzmann equation's structures are comparable. Calculating the collision integral's moments is the source of the entire challenge [7]. Solution The mixed value problem for the nonlinear nonstationary moment system of equations of Boltzmann's existence and uniqueness in three dimensions were established [3],[4].

The design and operation of aircraft at high altitudes requires the calculation of aerodynamic characteristics in a wide range of determining parameters (flight altitude, atmospheric parameters, flight speed, spacecraft orientation, aircraft configuration, etc.).

The aerodynamic characteristics of the flow around bodies in the upper layer of the atmosphere in the transition mode are obtained by calculation. On the basis of the kinetic theory of gases, computational investigations of the flow around bodies in the transitional regime are conducted. The condition at the moving boundary, more specifically the interaction of a gas with a moving solid surface, is important in aerospace engineering [8]. If the gas's initial state is known and the condition on the moving boundary is defined, the integra-differential Boltzmann equation can characterize the gas' evolution. The moment method stands out among the approximate methods for resolving the Boltzmann equation.

The system of moment equations contains all the macroscopic quantities that are of primary interest when it comes to rarefied gas theory. Therefore, moment equations are sufficient to determine the macroscopic quantities characterizing the state of gas molecules. However, boundary conditions must be formulated for a set of partial differential equations. As a result, the issue of estimating the Boltzmann equation's boundary condition approximation emerges. Additionally, the moment equations' ensuing problem needs to be properly phrased.

In [9], the macroscopic boundary conditions for the Boltzmann's nonstationary one-dimensional moment system of equations were used to approximate the Maxwell's microscopic boundary conditions for the Boltzmann's nonlinear equation. Maxwell-Auzhan conditions were given to new macroscopic boundary conditions.

In problems of atmospheric optics, the theory of radiative transfer, and the rarefied gas dynamics moment equations are often used. As a result, it is a crucial and pressing issue to design approximate solutions to the mixed problem for the system of moment equations.

2 Materials and methods

2.1 Numerical experiment for Boltzmann's six-moment one- dimensional system of equations with macroscopic boundary conditions

We investigate the mixed problem for the third approximation of the Boltzmann system of moment equations under the approximate Maxwell boundary condition. The third approximation of the mixed problem for the Boltzmann system of moment equations is created through the finite-difference method.

We take into account the third approximation of the Boltzmann's moment system equations [4]

$$\begin{gathered}
\frac{\partial \varphi_{00}}{\partial t}+\frac{1}{\alpha}\frac{\partial \varphi_{01}}{\partial x}=0,\\
\frac{\partial \varphi_{02}}{\partial t}+\frac{1}{\alpha}\frac{\partial}{\partial x}\left(\frac{2}{\sqrt{3}}\varphi_{01}+\frac{3}{\sqrt{5}}\varphi_{03}-\frac{2\sqrt{2}}{\sqrt{15}}\varphi_{11}\right)=J_{02},\\
\frac{\partial \varphi_{10}}{\partial t}+\frac{1}{\alpha}\frac{\partial}{\partial x}\left(-\sqrt{\frac{2}{3}}\varphi_{01}+\sqrt{\frac{5}{3}}\varphi_{11}\right)=0,\\
\frac{\partial \varphi_{01}}{\partial t}+\frac{1}{\alpha}\frac{\partial}{\partial x}\left(\varphi_{00}+\frac{2}{\sqrt{3}}\varphi_{02}-\sqrt{\frac{2}{3}}\varphi_{10}\right)=0,\\
\frac{\partial \varphi_{03}}{\partial t}+\frac{1}{\alpha}\frac{\partial}{\partial x}\frac{3}{\sqrt{5}}\varphi_{02}=J_{03},\\
\frac{\partial \varphi_{11}}{\partial t}+\frac{1}{\alpha}\frac{\partial}{\partial x}\left(-\frac{2\sqrt{2}}{\sqrt{15}}\varphi_{02}+\sqrt{\frac{5}{3}}\varphi_{10}\right)=J_{11},\\
x\in(-a,a),\quad t>0,
\end{gathered} \tag{1}$$

where $\varphi_{00}=\varphi_{00}(t,x)$, $\varphi_{01}=\varphi_{01}(t,x)$, $\dots,\varphi_{11}=\varphi_{11}(t,x)$ are the coefficients of particle distribution function's expansion to Fourier series;

$$I_{02}=(\sigma_2-\sigma_0)(\varphi_{00}\varphi_{02}-\varphi_{01}^2/\sqrt{3})/2,$$

$$I_{03}=\frac{1}{4}(\sigma_3+3\sigma_1-4\sigma_0)\varphi_{00}\varphi_{03}+\frac{1}{4\sqrt{5}}(2\sigma_1+\sigma_0-3\sigma_3)\varphi_{01}\varphi_{02},$$

$I_{11}=(\sigma_1-\sigma_0)(\varphi_{00}\varphi_{11}+\frac{1}{2}\sqrt{\frac{5}{3}}\varphi_{10}\varphi_{01}-\frac{\sqrt{2}}{\sqrt{15}}\varphi_{01}\varphi_{02})$ – are the nonlinear collision integral's moments, where σ_0, σ_1, σ_2, σ_3 are constants, $\alpha=\frac{1}{R\Theta}$, Θ is the reflective wall temperature and Θ is the constant. Three homogeneous equations that represent the laws of conservation of mass, momentum, and energy can be found in the system of equations (1).

The system of equations (1) under the boundary conditions obtained by approximating the Maxwell boundary condition write in vector-matrix form

$$\begin{aligned} &\frac{\partial u}{\partial t}+\frac{1}{\alpha}C\frac{\partial w}{\partial x}=I_1(u,\ w)\\ &\frac{\partial w}{\partial t}+\frac{1}{\alpha}C'\frac{\partial u}{\partial x}=I_2(u,\ w),\ t\in(0,T],\quad x\in(-a,a), \end{aligned} \tag{2}$$

$$u\Big|_{t=0}=u_0(x),\quad w\Big|_{t=0}=w_0(x),\quad x\in[-a,a], \tag{3}$$

$$\frac{1}{\alpha}(Cw^-+Du^-)\Big|_{x=-a}=\frac{1}{\alpha\beta}(Cw^+-Du^+)\Big|_{x=-a}-\frac{(1-\beta)}{\alpha\beta\sqrt{\pi}}F,\quad t\in[0,T], \tag{4}$$

$$\frac{1}{\alpha}(Cw^--Du^-)\Big|_{x=a}=\frac{1}{\alpha\beta}(Cw^++Du^+)\Big|_{x=a}+\frac{(1-\beta)}{\alpha\beta\sqrt{\pi}}F,\quad t\in[0,T], \tag{5}$$

where

$$C=\begin{pmatrix}1&0&0\\ \frac{2}{\sqrt{3}}&\frac{3}{\sqrt{5}}&-\frac{2\sqrt{2}}{\sqrt{15}}\\ -\sqrt{\frac{2}{3}}&0&\sqrt{\frac{5}{3}}\end{pmatrix},\quad D=\frac{1}{\sqrt{\pi}}\begin{pmatrix}\sqrt{2}&\sqrt{\frac{2}{3}}&-\frac{1}{\sqrt{3}}\\ \sqrt{\frac{2}{3}}&2\sqrt{2}&-1\\ -\frac{1}{\sqrt{3}}&-1&3\sqrt{2}\end{pmatrix}$$

$$I_1(u,\ w)=(0,\ I_{02},\ 0)',\quad I_2(u,\ w)=(0,\ I_{03},\ I_{11})',$$

$$u=(\varphi_{00},\varphi_{02},\varphi_{10})',\quad w=(\varphi_{01},\varphi_{03},\varphi_{11})',\ F=\left(\frac{1}{4\sqrt{2}},\frac{1}{8\sqrt{6}},\frac{1}{8\sqrt{3}}\right)',$$

C' is the transpose matrix, while D is the positive definition matrix;

$u_0(x)=(\varphi^0_{00}(x),\ \varphi^0_{02}(x),\varphi^0_{10}(x))'$, $w_0(x)=(\varphi^0_{01}(x),\ \varphi^0_{03}(x),\varphi^0_{11}(x))'$ are the moments of initial function provided; $w^+,\ u^+$ are the falling vectors to the moments of the boundary distribution function; $w^-,\ u^-$ – are the reflection vector from the moments of the boundary distribution function. Pure mirror reflection is represented by the value of $\beta\in[0,1]$ and parameter value of $\beta=1$.

Through straightforward calculations, it is feasible to verify

$$\det C_1=\det\begin{pmatrix}0&C\\ C'&0\end{pmatrix}\neq 0,$$

hence the matrix C_1 has eigenvalues are real, with an equal number of positive and negative eigenvalues. Macroscopic boundary conditions correspond to the number of positive and negative eigenvalues of matrix C_1. Correctness of the problem (2) – (5) in $C([0,T];L^2[-a,a])R$ was proved in [10-11].

As a result, system (2) is a hyperbolic type system of nonlinear partial differential equations. To define approximate solution of the problem (2) – (5) we use finite-difference method.

Divide the segment [0, T] into N_1 equal parts, and divide the segment $[-a, a]$ into N_2 equal parts. Let us consider the grid functions $u_{ij} = u(t_i, x_j)$ and $w_{ij} = w(t_i, x_j)$. We approximate the differential problem (2) – (5) by the following finite-difference scheme [12, 13]

$$\frac{u_{i+1,j}^{n+1} - u_{ij}^{n+1}}{\tau} + \frac{1}{\alpha} C \frac{w_{ij}^{n+1} - w_{i,j-1}^{n+1}}{h} = I_1(u_{ij}^n, w_{ij}^n), \quad i = 0, 1, \ldots, N_1 - 1;\ j = 1, \ldots, N_2; \tag{6}$$

$$\frac{w_{i+1,j}^{n+1} - w_{ij}^{n+1}}{\tau} + \frac{1}{\alpha} C' \frac{u_{i,j+1}^{n+1} - u_{i,j}^{n+1}}{h} = I_2(u_{ij}^n, w_{ij}^n), \quad i = 0, 1, \ldots, N_1 - 1;\ j = N_2 - 1, \ldots, 0; \tag{7}$$

$$u_{0j}^{n+1} = u_j^0, \quad w_{0j}^{n+1} = w_j^0, \quad j = 0, 1, \ldots, N_2; \tag{8}$$

$$\frac{1}{\alpha}(Cw^- - Du^-)_{i,0}^{n+1} = \frac{1}{\alpha\beta}(Cw^+ + Du^+)_{i,0}^n - \frac{1-\beta}{\alpha\beta\sqrt{\pi}} F, \ i = 0, 1, \ldots, N_1, \tag{9}$$

$$\frac{1}{\alpha}(Cw^- + Du^-)_{i,N_2}^{n+1} = \frac{1}{\alpha\beta}(Cw^+ - Du^+)_{i,N_2}^n + \frac{1-\beta}{\alpha\beta\sqrt{\pi}} F, \ i = 0, 1, \ldots, N_1, \tag{10}$$

τ is time step, h is spatial variable step.

From the difference equations (6) – (7) it follows that the derivatives on t and x are approximated by the first order.

In order to find a numerical solution of the problem (6) – (10), we use the iterative method. We start the iterative process by n and continue calculations until we achieve the following conditions

$$|u_{ij}^{n+1} - u_{ij}^n| < \varepsilon, \quad |w_{ij}^{n+1} - w_{ij}^n| < \varepsilon, \quad i = 0, 1, \ldots, N_1 - 1; \quad j = 1, \ldots, N_2,$$

where ε is a given sufficiently small number.

Numerical experiment.

With the following data, a numerical experiment was performed: $[-a, a] \cong [0, 1]$,

$$u_0(x) = \begin{pmatrix} x \\ 1 - x \\ x(1-x) \end{pmatrix}, \quad w_0(x) = \begin{pmatrix} 1 + x, \\ (1-x)/2 \\ x(1-x)/2) \end{pmatrix}, \quad x \in [0, 1],$$

$$\alpha = 38.681, \quad \sigma_0 = 1.333, \quad \sigma_1 = \sigma_3 = 0, \quad \sigma_2 = -0.266;$$

$$h = \frac{1}{10}, \quad \tau = \frac{2}{100}.$$

Interval $[0, 1]$ is divided into 10 equal parts, h is the step in the spatial variable x, τ is the time step. The relation $\frac{\tau}{h}$ satisfied the stability condition. Let us present the graphs of the vectors u and w for value of $\beta = 1$.

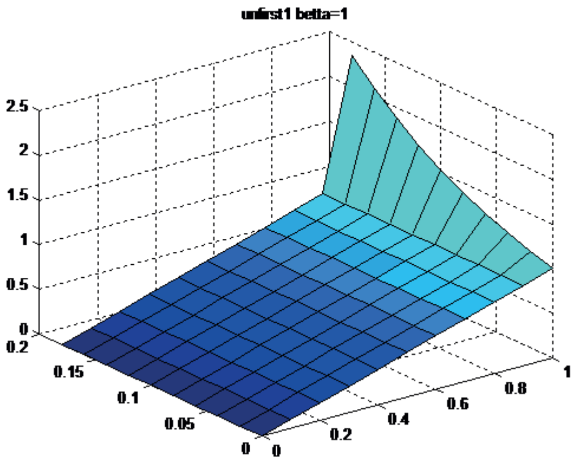
unfirst1 betta=1
2.5
2
1.5
1
0.5
0
0.2
0.15
0.1
0.05
0
0
0.2
0.4
0.6
0.8
1

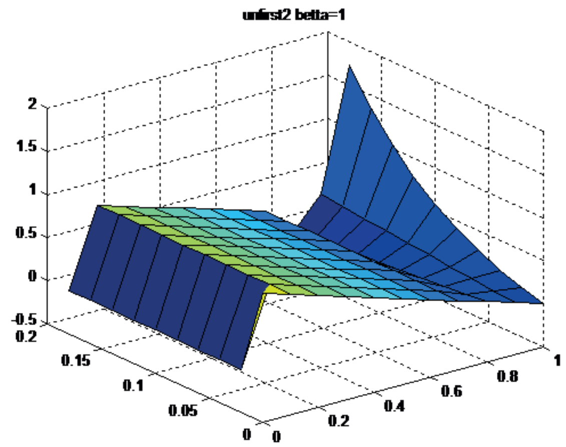
unfirst2 betta=1
2
1.5
1
0.5
0
-0.5
0.2
0.15
0.1
0.05
0
0
0.2
0.4
0.6
0.8
1

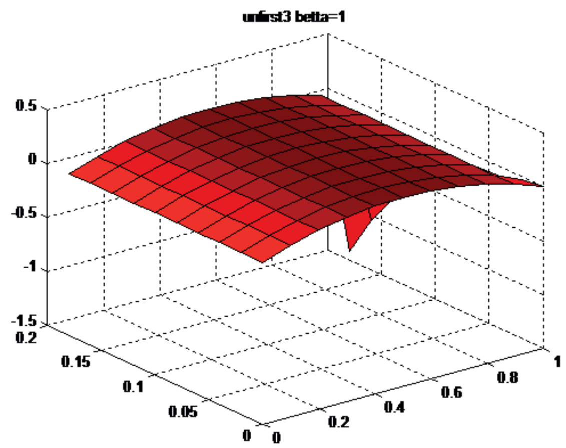
unfirst3 betta=1
0.5
0
-0.5
-1
-1.5
0.2
0.15
0.1
0.05
0
0
0.2
0.4
0.6
0.8
1

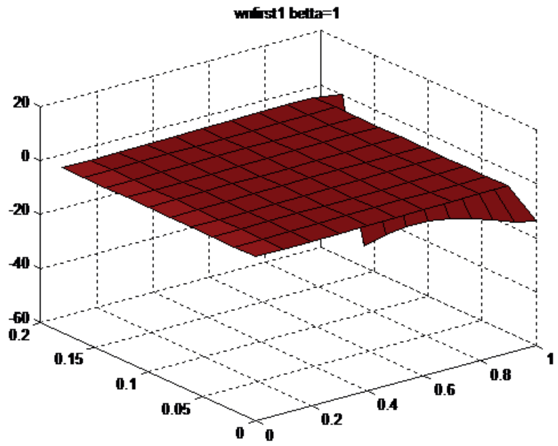
wnfirst1 betta=1
20
0
-20
-40
-60
0.2
0.15
0.1
0.05
0
0
0.2
0.4
0.6
0.8
1

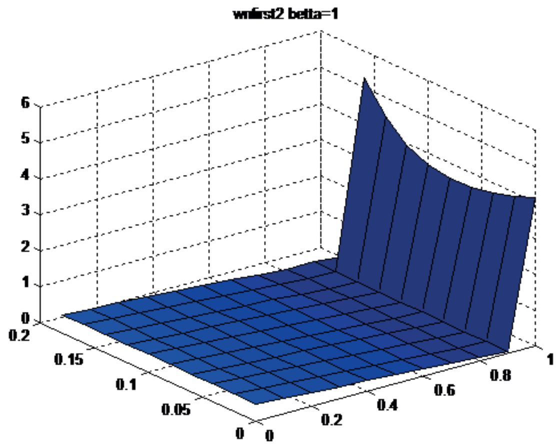
wnfirst2 betta=1
6
5
4
3
2
1
0
0.2
0.15
0.1
0.05
0
0
0.2
0.4
0.6
0.8
1

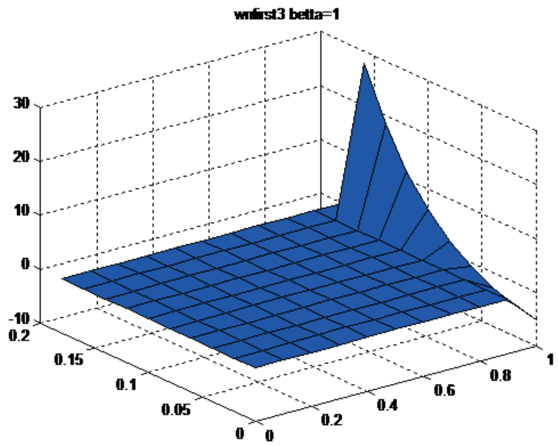
wnfirst3 betta=1
30
20
10
0
-10
0.2
0.15
0.1
0.05
0
0
0.2
0.4
0.6
0.8
1

3 Conclusion

The moments φ_{00}, φ_{01}, φ_{10} expressed by the macroscopic characteristics of the gas such that density, average speed and temperature. More exactly, we have following equalities $\varphi_{00} = \rho$, $\varphi_{01} = \alpha\rho V$, $\varphi_{10} = \sqrt{\frac{3}{2}}\rho - \sqrt{\frac{2}{3}}\alpha^2\rho(\frac{3}{2}k\theta + \frac{1}{2}V^2)$, where ρ is the gas density, V is the gas average speed, θ is the gas temperature and $\alpha = 38.681$ is the constant. On the plot unfirst1 $= \varphi_{00}$, unfirst3 $= \varphi_{10}$, wnfirst1 $= \varphi_{01}$. $\beta = 1$ corresponds to pure specular reflection. The value of the parameter β appreciable affected to the values of moments φ_{00}, φ_{01}, φ_{10}. Moreover we define approximate values of

$$\varphi_3(t,x,v) = f_0(\alpha|v|) \sum_{2n+1=0}^{3} \varphi_{n1}(t,x) g_{n1}(\alpha v),$$

$f_0(\alpha|v|)$ – is global Maxwell distribution, more exactly we define following functions

$$\varphi_3^{\pm}(t,\mp a,v) = \varphi_{00}^{\pm}(t,\mp a)g_{00}(\alpha v) + \varphi_{01}^{\pm}(t,\mp a)g_{01}(\alpha v) + \varphi_{02}^{\pm}(t,\mp a)g_{02}(\alpha v) +$$

$$+\varphi_{10}^{\pm}(t,\mp a)g_{10}(\alpha v) + \varphi_{03}^{\pm}(t,\mp a)g_{03}(\alpha v) + \varphi_{11}^{\pm}(t,\mp a)g_{11}(\alpha v),$$

where $\varphi_3^{+}(t,\mp a,v)$ is the distribution function of falling to the boundary particles, $\varphi_3^{-}(t,\mp a,v)$ is the distribution function of reflecting from boundary particles,

$$g_{00}(\alpha v) = 1, \quad g_{01}(\alpha v) = \alpha|v|\cos\theta, \quad g_{02}(\alpha v) = \frac{1}{\sqrt{3}}\left(\frac{\alpha|v|}{\sqrt{2}}\right)^2 (3\cos^2\theta - 1),$$

$$g_{10}(\alpha v) = \sqrt{\frac{2}{3}}\left(\frac{3}{2} - \frac{\alpha^2 v^2}{2}\right), \quad g_{03}(\alpha v) = \sqrt{\frac{2}{15}}\left(\frac{\alpha|v|}{\sqrt{2}}\right)^3 (5\cos^3\theta - 3\cos\theta),$$

$$g_{11}(\alpha v) = \sqrt{\frac{4}{5}}\frac{\alpha|v|}{\sqrt{2}}\left(\frac{5}{2} - \frac{\alpha^2 v^2}{2}\right)\cos\theta.$$

Acknowledgements

This work was financially supported by the Science Committee of the Ministry of Education and Science of the Republic of Kazakhstan, scientific project No. AP08856926.

References

[1] Grad G., "Kinetic theory of rarefied gases", *Comm. Pure Appl. Math* 2 (331) (1949).

[2] Grad G., "Principle of the kinetic theory of gases", *Handuch der Physik, Springer, Berlin* 12 (1958): 205–294.

[3] Sakabekov A., "Initial-boundary value problems for the Boltzmann's moment system equations in an arbitrary approximation", *Sb. Russ. Acad. Sci. Math.* 77(1) (1994): 57–76.

[4] Sakabekov A., *Initial-boundary value problems for the Boltzmann's moment system equations* (Gylym, Almaty, 2002).

[5] Cercignani C., *Theory and application of Boltzmann's equation* (Milano, Italy, 1975).

[6] Kogan M.N., *Dynamic of rarefied gas* (Moscow, Nauka, 1967): 440.

[7] Kumar K., "Polynomial expansions in Kinetic theory of gases", *Annals of physics* 57 (1966): 115–141.

[8] Barantcev R.G., *Interaction of rarefied gases with streamlined surfaces* (Moscow, Nauka, 1975): 343.

[9] Sakabekov A., Auzhani Y., "Boundary conditions for the onedimensional nonlinear nonstationary Boltzmann's moment system equations", *J. Math. Phys.* 55 (2014): 123507.

[10] Sakabekov A., Auzhani Y., "Boltzmann's Six-Moment One-Dimensional Nonlinear System Equations with the Maxwell-Auzhan Boundary Conditions", *Hindawi Publishing Corporation Journal of Applied Mathematics* 5834620 (2016): 8. http://dx.doi.org/10.1155/2016/5834620.

[11] Auzhani Y., Sakabekov A., "Mixed value problem for nonstationary nonlinear one-dimensional Boltzmann moment system of equations in the first and third approximations with macroscopic boundary conditions", *Kazakh Math. Journal* 20(1) (2020): 54–66.

[12] Samarskiy A.A., *Difference sheme theory* (Moscow, Nauka 1977): 656.

[13] Richtmyer Robert D., Morton K.W., *Difference methods for boundary value problems* (Moscow, 1972): 418.

IRSTI 27.39.21 DOI: https://doi.org/10.26577/JMMCS.2022.v116.i4.08

S.Ya. Serovajsky*, **O. Turar**, **T. Imankulov**
Al-Farabi Kazakh National University, Almaty, Kazakhstan
*e-mail: serovajskys@mail.ru

MATHEMATICAL MODELING OF THE EPIDEMIC PROPAGATION WITH LIMITED TIME SPENT IN COMPARTMENTS AND VACCINATION

The paper proposes discrete and continuous mathematical models of epidemic development. A division of the population into nine compartments is suggested: susceptible, exposed, vaccinated, contact vaccinated, undetected patients, isolated patients, hospitalized patients, recovered and deceased. At the same time, the time spent in exposed and infected compartments is considered limited. According to the assumptions made in the models, a susceptible person can encounter the patient and go into the exposed compartment, and be vaccinated, and then also encounter the infection and go into the contact vaccinated compartment. Exposed people may become ill to any degree of severity or not, returning to the susceptible group. A contact vaccinated either does not become ill or becomes undetected or isolated patient. Every patient can recover. An undiagnosed patient may develop symptoms of the disease, because of which he moves into the isolated compartment. An isolated patient may be hospitalized, and a hospitalized patient may die. In the discrete model, discrete quantitative data for each day of the epidemic are considered, in the continuous one, these indicators are considered continuous functions. The article provides a qualitative and quantitative analysis of the proposed models. The influence of all parameters on the process under study is investigated.

Key words: mathematical model, epidemic, vaccination.

С.Я. Серовайский*, О.Н. Тұрар, Т.С. Иманкулов
әл-Фараби атындағы Қазақ ұлттық университеті, Алматы қ., Қазақстан
*e-mail: serovajskys@mail.ru

ЭПИДЕМИЯНЫҢ ДАМУЫН ТОПТАРДА ОТЫРУ УАҚЫТЫ ШЕКТЕУЛІ БОЛУДЫ ЖӘНЕ ВАКЦИНАЦИЯЛАУДЫ ЕСКЕРЕ ОТЫРЫП МАТЕМАТИКАЛЫҚ МОДЕЛЬДЕУ

Эпидемия дамуының дискретті және үздіксіз математикалық модельдері ұсынылған. Олар халықты тоғыз топқа бөлуді ұсынады: сезімтал, контактілі, вакцинацияланған, вакцинацияланған контактілі, анықталмаған науқастар, оқшауланған науқастар, ауруханаға жатқызылған науқастар, сауығып кеткендер және қайтыс болғандар. Бұл модельдерде контактілі және ауру топтарында болу уақыты шектеулі болып саналады. Модельдерде жасалған болжамдарға сәйкес, сезімтал адам науқаспен байланыста болу арқылы байланыс тобына кіруі, және вакцинациялануы, содан кейін науқаспен байланыста болу арқылы вакцинацияланған контакт тобына өтуі мүмкін болады. Контактілі сезімтал топқа қайта оралуы, немесе кез келген ауру дәрежесімен ауруы мүмкін. Вакцинацияланған контактілі ауырмай сезімтал тобына қайта оралуы немесе анықталмай немесе оқшауланып ауыруы мүмкін. Әрбір науқас сауығып кете алады. Анықталмаған науқаста аурудың белгілері пайда болуы мүмкін, нәтижесінде ол оқшауланған топқа ауысады. Оқшауланған науқас ауруханаға жатқызылуы мүмкін, ал ауруханада жатқан науқас өлуі мүмкін. Дискретті модельде эпидемияның әрбір күні үшін дискретті сандық деректер қарастырылады, үздіксіз модельде бұл көрсеткіштер үздіксіз функциялар болып саналады. Мақалада ұсынылған модельдердің сапалық және сандық талдауы берілген. Барлық параметрлердің зерттелетін процеске әсері зерттеледі.

Түйін сөздер: математикалық модель, эпидемия, вакцинация.

С.Я. Серовайский*, О.Н. Турар, Т.С. Иманкулов
Казахский национальный университет имени аль-Фараби, г. Алматы, Казахстан
*e-mail: serovajskys@mail.ru

МАТЕМАТИЧЕСКОЕ МОДЕЛИРОВАНИЕ РАЗВИТИЯ ЭПИДЕМИИ С УЧЕТОМ ВАКЦИНАЦИИ И ОГРАНИЧЕННОГО ВРЕМЕНЕМ ПРЕБЫВАНИЯ В ГРУППАХ

Предлагаются дискретная и непрерывная математические модели развития эпидемии. Они предполагают разбиение популяции на девять групп: восприимчивые, контактные, вакцинированные, вакцинированные контактные, невыявленные больные, изолированные больные, госпитализированные больные, выздоровевшие и умершие. При этом время пребывания в группах контактных и больных считается ограниченным. Согласно допущениям, принятым в моделях, восприимчивый может войти в контакт с больным, перейдя в группу контактных, а также вакцинироваться, после чего также войти в контакт с больным, перейдя в группу контактных вакцинированных. Контактные могут заболеть в любой степени тяжести или не заболеть, вернувшись в группу восприимчивых. Контактный восприимчивый либо не заболевает, либо становится невыявленным или изолированным больным. Каждый больной может выздороветь. У невыявленного больного могут появиться симптомы болезни, в результате чего он переходит в группу изолированных. Изолированный больной может быть госпитализирован, а госпитализированный – умереть. В дискретной модули рассматривается дискретные количественные данные по каждому дню эпидемии, в непрерывной, данные показатели считаются непрерывными функциями. В статье проводится качественный и количественный анализ предлагаемых моделей. Исследуется влияние всех параметров на исследуемый процесс.

Ключевые слова: математическая модель, эпидемия, вакцинация.

1 Introduction

The development of the COVID-19 pandemic has largely updated the development of mathematical models of epidemic development. The first application of mathematical methods in the analysis of epidemics is associated with the works of outstanding mathematicians of the second half of the 18th and early 19th centuries D. Bernoulli, I. Lambert, P.S. Laplace. Modern mathematical models of epidemiology go back to the work of R. Ross, published in 1911, on the study of the spread of malaria [1] and, to an even greater extent, to the SIR model proposed in 1927 by W. Kermack and A. McKendrick [2]. This model is based on the division of the entire population into three compartments of susceptible, infected and recovered. The model is a system of non-linear differential equations and describes the change in the number of these population compartments over time.

The main drawback of the SIR model is that it does not take into account the presence of an incubation period, i.e. it assumes that a person who has had contact with a sick person immediately falls ill. To eliminate it the SEIR model was proposed, in which a compartment of exposed was added, see, for example, [3]. Thus, in the process of infection, a person susceptible to the disease first becomes exposed and only then becomes infected. There are a significant number of SEIR model modifications. Thus, the SEIRD model additionally includes a compartment of deceased [4, 5]. In the MSEIR model in addition to the compartments of the SEIR model, people endowed with immunity from birth (maternally derived immunity) are added [6]. In [7], a model which additionally takes into account patients in whom the disease proceeds in an asymptomatic form (asymptomatic) is considered. The SEIRHCD model also has compartments of hospitalized and critical patients [8, 9]. Along with continuous models, discrete models, in which time is an integer variable, are also considered, see, for example, [10].

These models do not take into account the limited stay in exposed and infected compartments. In particular, any person who has been in contact with a sick person, after some time, will most likely either get sick or not get sick, which means that they will certainly leave the exposed compartment. Anyone who falls ill after some time will surely either recover or die, i.e. will definitely leave the compartment of infected. This shortcoming is overwhelmed in [8, 9, 11] for continuous systems and in [11–13] for discrete systems. There are also models that take into account the vaccination of the population [14–22]. In this case, vaccination is considered at certain points in time (impulsive vaccination), as well as vaccination of newborns. Here, vaccinated susceptible people go directly into the compartment of recovered, see [15–18]. In the SIRV model [19], the vaccinated are treated as an independent compartment. The SEIRV model also uses a separate compartment of vaccinated people, some of whom may become infected in the future, and birth and natural mortality are also taken into account [20]. In [21], a model is proposed in which there is an additional compartment of people in quarantine. [22] explores the SUIHTER model, which also includes compartment of asymptomatic and hospitalized patients, and separately considers people received one and two doses of the vaccine.

This paper proposes discrete and continuous models for the development of the epidemic, providing for vaccination and limited time spent in compartments, which are a generalization of the models described in [11] for the case of vaccination. They assume the division of the entire population into nine compartments: susceptible, exposed, vaccinated, contact vaccinated, undetected, isolated and hospitalized patients, as well as recovered and deceased. A qualitative and quantitative analysis of the models is carried out. The influence of various parameters of the system on the process is investigated.

2 Description of models

An isolated population under the conditions of an epidemic is considered. The entire population is divided into the following compartments:

S: susceptible (healthy, but potentially sick);

V: vaccinated (healthy vaccinated);

E: exposed (healthy, in contact with sick);

C: contact vaccinated (vaccinated, who were in contact with patients);

U: undetected (infected with an asymptomatic course of the disease and mildly ill with an undiagnosed disease);

I: isolated (patients in a mild form, undergoing treatment at home);

H: hospitalized (seriously ill, hospitalized);

R: recovered (recovered from illness, who do not have any signs of illness);

D: died.

The sum of N numbers of people in all compartments is considered unchanged, i.e. natural births and deaths are not taken into account in the model.

The change in the number of people in each compartment is carried out due to intercompartment transitions, see Fig. 1.

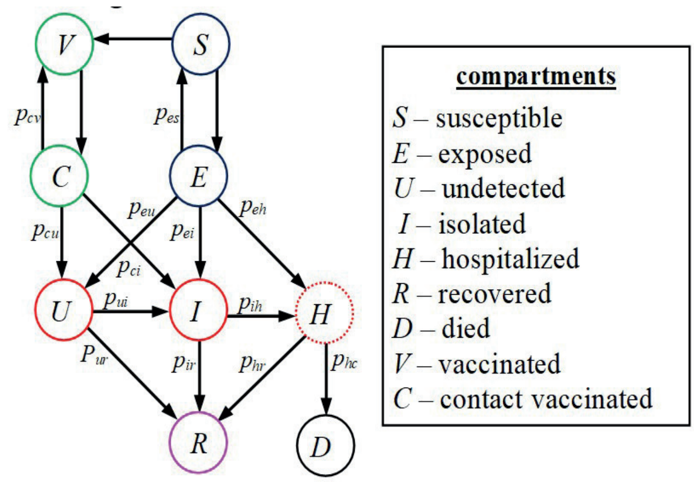

Figure 1: Graph of intercompartment transitions.

According to the accepted assumptions, a susceptible person can come into contact with the patient by moving to the exposed compartment, and also be vaccinated. A vaccinated person can also encounter a sick person and move into compartment of contact vaccinated people. The exposed may become ill in any degree of severity or not get ill, returning to the susceptible compartment. A contact vaccinated either does not become ill or becomes undetected or isolated sick. Every patient can recover. An undiagnosed patient may develop symptoms of the disease moving into the isolated compartment in result. An isolated patient may be hospitalized, and a hospitalized patient may die.

The number of days spent in all compartments of contact and patients is considered fixed and is indicated as follows n_e, n_c, n_u, n_i and n_h, where the index corresponds to the name of the compartment (the first letter of the compartment name). For vaccinated contacts, the time spent in the compartment is assumed to be the same as for unvaccinated contacts, i.e. $n_c = n_e$. At the end of the time spent in the compartment, each person in it goes into one of the possible compartments in accordance with the above figure. In this case, $p_{\alpha\beta}$ denotes the proportion of people in the compartment indicated as α passing into the compartment β. In this case, the conditions

$$\sum_{\beta} p_\alpha \beta = 1 \forall \alpha,$$

where the sum is taken over all compartments β, to which you can go from the compartment α.

Sources of infection are people in undetected (to a greater extent) and isolated (to a lesser extent) compartments, but not hospitalized. The degree of infectivity is described by the coefficients of contagiousness k_u and k_i undetected and isolated patients, and $k_u > k_i$. Vaccination of the population is characterized by the rate of vaccination v.

The mathematical model of the process is a system of equations for the number of people in each compartment that changes over time. In this case, the number of people in each compartment is indicated by the first letter of the compartment name, i.e. S, V, etc. These quantities are functions of a continuous argument t or an integer argument n, written as an index. Thus, S_k, V_k, etc. characterize the number of susceptible, vaccinated, etc. at the k-th time step (on the k-th day from the beginning of the study). In the continuous model, the values of $S(t)$, $V(t)$, etc. characterize the number of susceptible, vaccinated, etc. at time t (after t time from the start of the study).

Let us formulate a description of the discrete model. The number of all categories of contacts and patients at a given point in time is the sum of their numbers by the days they were in the compartment, i.e. following equalities are true

$$Z_k = \sum_{j=1}^{n_z} z_k^j, Z = E, C, U, I, H, \tag{1}$$

where z_k^j denotes the number of people in compartment Z at time k on the j-th day of being in this compartment. Here, any compartment of exposed and patients is chosen as Z, i.e. Z can take the values E, C, U, I, H. In this case, each member of Z of the j-th day of being in this compartment passes to the category of the $j+1$st day of being in the compartment every day, if this was not the last day of being in the compartment, which corresponds to the equalities

$$z_{k+1}^{j+1} = z_k^j, j = 2, ..., n_z - 1, z = e, c, u, i, h. \tag{2}$$

The susceptible number on the following day is equal to the susceptible number on the previous day minus the number of those vaccinated on that day, minus the susceptible number who contacted infection on that day, plus the number of contacts of the last day of stay in the exposed compartment who did not get infected. At the same time, the vaccinated number is directly proportional to the susceptible number, and the susceptible number contacted with infection is directly proportional to the susceptible number, as well as the number of undetected and isolated patients who are sources of infection. As a result, we obtain the equality

$$S_{k+1} = S_k - vS_k - \frac{k_u U_k + k_i I_k}{N} S_k + p_{es} e_k^{n_e}. \tag{3}$$

The division by the size of the entire population is carried out for reasons of normalization (otherwise, the numbers of two compartments, which are sufficiently large values, are multiplied).

The vaccinated number on the following day is equal to the vaccinated number on the previous day plus the number of new susceptible people who were vaccinated that day minus the number of vaccinated people contacted with infection on that day plus the number of people on the last day of stay in the contact vaccinated compartment who did not get infected. The corresponding quantities are determined in the same way as in the previous formula. As a result, we obtain the equality

$$V_{k+1} = V_k + vS_k - \frac{k_u U_k + k_i I_k}{N} V_k + p_{cv} c_k^{n_c}. \tag{4}$$

The number of all people in compartments of exposed and infected patients on the next day is equal to their number on the previous day plus the number of people who entered this compartment this day, minus the number of people who left the compartment the previous day

$$Z_{k+1} = Z_k + z_{k+1}^1 - z_k^{n_z}, \; Z = E, C, U, I, H. \tag{5}$$

The recovery number of at the next time point is equal to their number on the previous day plus the number of patients of all compartments who recovered on the previous day.

$$R_{k+1} = R_k + p_{ur} u_k^{n_a} + p_{ir} i_k^{n_i} + p_{hr} h_k^{n_h}. \tag{6}$$

The death number at a subsequent point in time is equal to their number on the previous day plus the number of people that died on this day

$$D_{k+1} = R_k + p_{hd} h_k^{n_h}. \tag{7}$$

The number of new exposed (exposed of the first day of being in the compartment), both unvaccinated and vaccinated, is exactly equal to the number, respectively, susceptible and vaccinated, who had contact with patients on the previous day

$$e_{k+1}^1 = (k_u U_k + k_i I_k) \frac{S_k}{N}, \; c_{k+1}^1 = (k_u U_k + k_i I_k) \frac{V_k}{N}, \tag{8}$$

The number of new undetected is the sum of both exposed compartments of the last day of being in the compartment, who fell ill with an undetected form of the disease

$$u_{k+1}^1 = p_{eu} e_k^{n_e} + p_{cu} c_k^{n_c}. \tag{9}$$

The number of new isolated patients is the sum of the number of both exposed compartments of the last day being in the compartment who fell ill with an isolated form of the disease, and the number of undetected contacts of the last day being in the compartment in whom the disease was detected

$$i_{k+1}^1 = p_{ei} e_k^{n_e} + p_{ci} c_k^{n_c} + p_{ui} u_k^{n_u}. \tag{10}$$

The number of new hospitalized patients is the sum of exposed and isolated patients of the last day of being in the compartment, in which the disease turned into a severe form, as a result of which they were hospitalized

$$h_{k+1}^1 = p_{eh} e_k^{n_e} + p_{ih} i_k^{n_i}. \tag{11}$$

The initial states of the system S_0, E_0, U_0, V_0, C_0, I_0, H_0, R_0, D_0 are known, and the distribution of all forms of exposed and patients at the initial moment of time by days of being in compartments is considered uniform, i.e. taken according equalities

$$z_0^j = Z_0/n_z, \quad j = 1, ..., n_z, \ \ z = e, c, u, i, h. \tag{12}$$

Relations (1) - (12) constitute a discrete model of the process under study.

Let us proceed to the description of the corresponding continuous model. The change in the number of susceptible people is its decrease due to vaccination and the fact that a certain number of susceptible people contacted with infection, and an increase, since some of the exposed do not get sick. At the same time, the new vaccinated number is directly proportional to the susceptible number and the number of susceptible who became exposed is directly proportional to the susceptible number, as well as the number of undetected and isolated patients. The number of non-diseased exposed is proportional to the exposed number and inversely proportional to the number of days spent in the exposed compartment. As a result, we obtain the equation

$$\frac{dS(t)}{dt} = -vS(t) - \frac{k_u U(t) + k_i I(t)}{N} S(t) + p_{es} \frac{E(t)}{n_e}. \tag{13}$$

The change in the vaccinated number is its decrease due to the fact that some part of the vaccinated who contacted with patients, and the increase due to vaccination and the fact that part of the contact vaccinated people does not get sick. The corresponding quantities are determined in the same way as in the previous formula. As a result, we obtain the equality

$$\frac{dV(t)}{dt} = vS(t) - \frac{k_u U(t) + k_i I(t)}{N} V(t) + p_{cv} \frac{C(t)}{n_v}. \tag{14}$$

The change in the number of contacts, both unvaccinated and vaccinated, increases due to, respectively, susceptible and vaccinated, who had contact with patients, and decreases due to the limited time spent in these compartments. Thus, we have the equalities

$$\frac{dE(t)}{dt} = \frac{k_u U(t) + k_i I(t)}{N} S(t) - \frac{E(t)}{n_e}, \tag{15}$$

$$\frac{dC(t)}{dt} = \frac{k_u U(t) + k_i I(t)}{N} V(t) - \frac{C(t)}{n_c}. \tag{16}$$

The number of undetected patients increases due to the disease of both exposed compartments and decreases due to the limited time spent in this compartment:

$$\frac{dU(t)}{dt} = p_{eu} \frac{E(t)}{n_e} + p_{cu} \frac{C(t)}{n_c} - \frac{U(t)}{n_u}. \tag{17}$$

The number of isolated patients increases due to the disease of both exposed compartments and the detection of the disease in some of the undetected and decreases due to the limited time spent in this compartment:

$$\frac{dI(t)}{dt} = p_{ei} \frac{E(t)}{n_e} + p_{ci} \frac{C(t)}{n_c} + p_{ui} \frac{U(t)}{n_u} - \frac{I(t)}{n_i}. \tag{18}$$

The number of hospitalized increases due to infection of people in exposed compartment in a severe form and the hospitalization of a part of the isolated ones and decreases due to the limited time spent in this compartment:

$$\frac{dH(t)}{dt} = p_{eh} \frac{E(t)}{n_e} + p_{ih} \frac{I(t)}{n_i} - \frac{H(t)}{n_h}. \tag{19}$$

The number of recovered patients is increasing due to the recovery of patients of all categories:

$$\frac{dR(t)}{dt} = p_{ur} \frac{U(t)}{n_u} + p_{ir} \frac{I(t)}{n_i} + p_{hr} \frac{H(t)}{n_h}. \tag{20}$$

The number of deaths increases due to the death of a part of the hospitalized:

$$\frac{dD(t)}{dt} = p_{hd} \frac{H(t)}{n_h}. \tag{21}$$

The initial states of the system S_0, E_0, U_0, V_0, C_0, I_0, H_0, R_0, D_0 are known, i.e. the following equalities hold

$$Z(0) = Z_0. \tag{22}$$

where $Z = S, E, U, V, C, I, H, R, D$. The system of differential equations (13) – (21) with initial conditions (22) constitutes a continuous model of the system.

3 Analysis of mathematical models

Let us establish the simplest qualitative properties of the models under consideration. The discrete model is characterized by the following statement.

Theorem 1. *For any values of the parameters, the system has a unique equilibrium position, and the limiting values of the numbers of all categories of exposed and infected people are equal to zero, and the functions R and D are increasing.*

To prove it, it suffices to pass to the limit in recurrence relations (3) – (7), taking into account that the sequences $\{Z_k\}$ and $\{Z_{k+1}\}$ have the same limit. At the same time, the zero limit values of the numbers of all categories of exposed and patients indicate the end of the epidemic. The monotonicity of the functions R and D (growth in the number of recovered and deceased) is due to the negativity of all expressions on the right side of equalities (6) and (7).

Theorem 2. *For any values of the system parameters, problem (13) - (22) has a unique equilibrium position, and the limiting values of the numbers of all categories of contact and patients is equal to zero, and the functions R and D are increasing.*

To prove it, it suffices to equate all derivatives to zero in differential equations (13) - (21). The results obtained indicate that the qualitative properties of the continuous and discrete models generally coincide.

The quantitative analysis of both models was carried out at the same parameter values, and the continuous model was implemented using the 4th order Runge - Kutta method. In doing so, the following numbers of days spent in compartments have been taken:$n_e = 14, n_u = 3, n_i = 5, n_h = 7, n_c = n_e = 7$. The coefficients of the equations take the following values: $k_u = 3.180, k_i = 0.171, p_{es} = 0.679, p_{eu} = 0.154, p_{ei} = 0.145, p_{eh} = 0.022, p_{cv} = 0.9, p_{cu} = 0.05, p_{ci} = 0.05, p_{ui} = 0.03, p_{ur} = 0.97, p_{ih} = 0.021, p_{ir} = 0.979, p_{hr} = 0.982, p_{hd} = 0.018, v = 0.0005$. The calculations were carried out at the initial stage of the epidemic, and $N = 18699640$, which corresponded to the population of Kazakhstan at the time of the start of the COVID-19 epidemic. In addition, it was assumed that at the initial moment of time there are 140 contact people, and all the rest are susceptible. Graphs of the obtained solutions are shown in Fig. 2, where the red curves correspond to the discrete model, and the blue curves to the continuous one.

Based on the results obtained, the following conclusions can be made. The qualitative properties of the solutions of both models are almost the same, and the corresponding functions for the continuous model are smoother. For some time, the number of exposed and patients has been growing. Then the epidemic reaches its peak, after which the incidence decreases. Over time, the system is observed to reach a position of equilibrium, and the number of all compartments of exposed and patients tends to zero, which corresponds to the end of the epidemic. The susceptible number decreases monotonously as more and more people get sick or get vaccinated over time. The number of vaccinated, recovered and dead people is gradually increasing, which is quite natural, since the vaccinated people will no longer become usually susceptible, the recovered acquire immunity.

Table. 1 shows the most important quantitative characteristics corresponding to the selected computation variant. According to the results obtained, the general characteristics of the discrete and continuous models are approximately the same. However, for the discrete model, the epidemic proceeds somewhat less intensively than for the continuous model. In

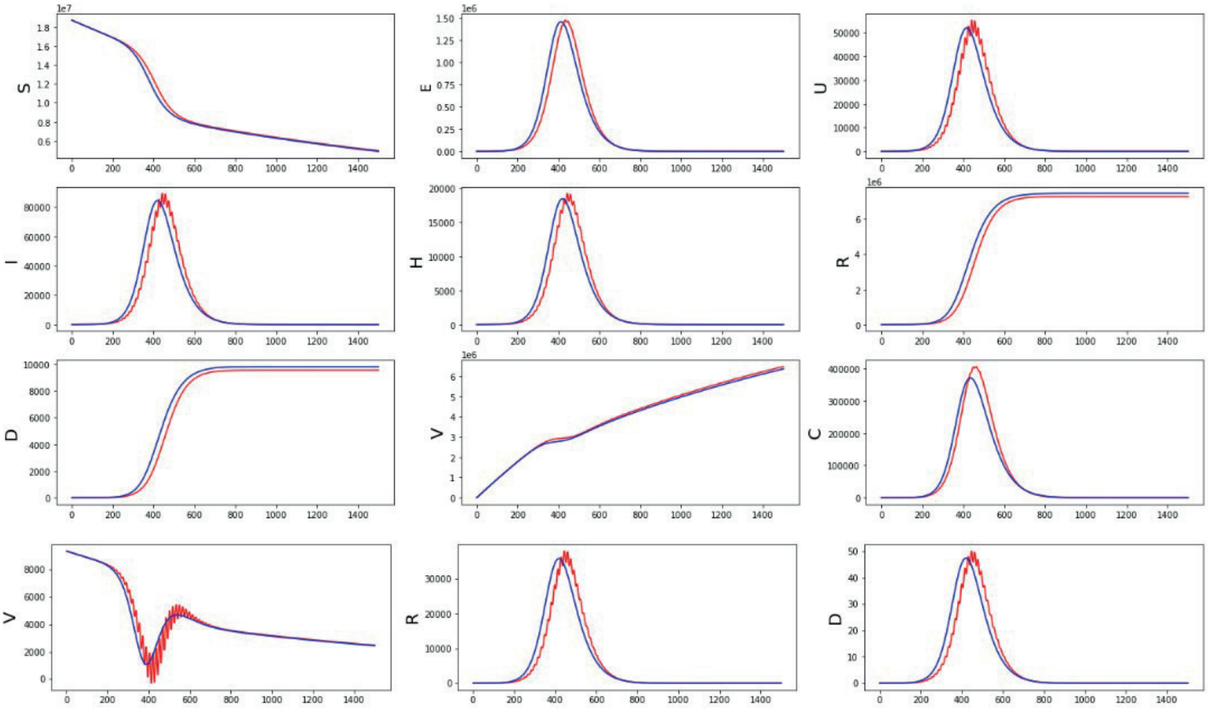

Figure 2: System states for discrete (red) and continuous (blue) models.

particular, the duration of the epidemic is shorter (by about two months), the time of the peak of the epidemic comes later (almost a month), the total number of cases and deaths is slightly less. However, the observed difference is insignificant, as a result of which we can conclude that the considered models are equivalent.

Let us now estimate the influence of system parameters on the considered process. Each of the tables below shows the values of the most important characteristics of the system for three counting options. The first of them corresponds to the main variant of the computation given above, and the next two correspond to the specified parameter, increased and decreased by some value.

Table. 2 evaluates the impact of the coefficient of contagiousness of undiagnosed patients. It turns out to be about the same for both models. In particular, an increase in the contagiousness coefficient leads to a reduction in the duration of the epidemic and the time it takes to reach its peak, as well as an increase in the number of simultaneously ill people, the total number of ill people and deaths. Such changes indicate a greater intensity of the epidemic development, which seems quite logical. At the same time, the percentage of recovered and dead people remains unchanged, since these characteristics are determined by the transition coefficients in the compartments of patients. Comparing the degree of influence of the parameter on the models under consideration, we note, for example, that an increase (respectively, a decrease) in the coefficient by 10% leads to a decrease in the duration of the epidemic by 11.8% for the discrete model and 11.6% for the continuous model (respectively,

Table 1: The most important quantitative characteristics of the system

	Discrete model	**continuous model**
Epidemic end time	1101	1154
Peak time of the epidemic	442	419
Total number of cases and % of the total population	7284183 (38.95%)	
The total number of recovered and % of the total number of cases	7274363 (99.87%)	7456303 (39.93%)
The total number of deaths and % of the total number of cases	9546 (0.13%)	9822 (0.13%)
The maximum number of patients at the same time	163412 (0.87%)	154790 (0.83%)

an increase of 20.5% for the discrete model and 20.4% for the continuous model). At the same time, the total number of cases increases by 21.3% for the discrete model and 21.2% for the continuous model (respectively, it decreases by 32.2% for the discrete model and by 32.4% for the continuous model). Thus, the degree of influence of the parameter on both models is almost the same.

Table 2: Influence of the coefficient of contagiousness of undiagnosed patients

Parameter ku	**Epidemic end time**		**Peak time of the epidemic**		**Total number of cases and % of the population**	
	Discrete	continuous	Discrete	continuous	Discrete	continuous
3.18	1101	1154	442	419	7284183 (38.95%)	7466126 (39.93%)
3.48	972	1020	377	344	8833599 (47.24%)	9047409 (48.38%)
2.88	1327	1389	571	547	4939864 (26.42%)	5049614 (27%)

Table 3 shows the results of assessing the impact of the contagiousness coefficient of isolated patients with an increase and decrease in this parameter by 58.8%. With its increase, there is a decrease in the duration of the epidemic and the time it takes to reach its peak, with an increase in the total number of cases of simultaneously infected, the percentage of recovered and dead remains unchanged. However, with the indicated increase (respectively, decrease) in the contagiousness coefficient of isolated patients, there is a reduction in the duration of the epidemic by 6.8% for the discrete model and by 6.5% for the continuous model (respectively, it increases by 9.1% for the discrete model and by 8.8% for the continuous model). Under the same conditions, there is an increase in the death number by 13.1% for the discrete model and by 13.0% for the continuous model (respectively, a decrease of 16.1% for the discrete model and 16.0% for continuous model). The weaker effect on the process of the contagiousness coefficient of isolated patients compared to the similar coefficient for unidentified patients is explained by the fact that isolated patients are a significantly less important source of infection compared to unidentified ones.

Table. 4 examines the effect of the recovering proportion of hospitalized patients when it changes by 1.5%. This parameter does not affect the duration of the epidemic, the time of its

Table 3: Influence of the contagiousness coefficient of isolated patients

Parameter ku	**Epidemic end time**		**Peak time of the epidemic**		**Total number of cases and % of the population**	
	Discrete	continuous	Discrete	continuous	Discrete	continuous
0.171	1101	1154	442	419	7284183 (38.95%)	7466126 (39.93%)
0.271	1026	1079	410	376	8187581 (43.78%)	8384067 (44.84%)
0.071	1201	1255	505	474	6160891 (32.95%)	6322669 (33.81%)

peak, the total number of cases and the maximum number of cases at a time, since it only applies to those patients who have already been hospitalized. Thus, it can only influence the ratio between the recovered and the dead. In particular, an increase (respectively, a decrease) in this parameter leads to a decrease (respectively, an increase) in the number of deaths by 83.3% for both models. It is clear that a reduction in the death number by a certain amount means an increase in the recovered number by the same amount.

Table 4: Influence of recovering rate of hospitalized patients

Parameter p_{hr}	**The total number of recovered and % of the total number of cases**		**The total number of deaths and % of the total number of cases**	
	Discrete	continuous	Discrete	continuous
0.982	7274636 (99.87%)	7456303 (99.87%)	9546 (0.13%)	9822 (0.13%)
0.997	7282592 (99.98%)	7464489 (99.98%)	1591 (0.02%)	1637 (0.02%)
0.967	7266681 (99.76%)	7448118 (99.76%)	17501 (0.24%)	18007 (0.24%)

Table. 5 examines the impact of the proportion of isolated patients who were hospitalized, with a change of 71.4%. This parameter does not affect the duration of the epidemic and the time of its peak, as well as the total number of cases, however, it affects the further fate of the patient. In particular, an increase (respectively, a decrease) in this parameter indicates a more severe (respectively, milder) course of the epidemic. This is reflected in the fact that the number of deaths increased by 9.7% for the discrete model and 9.6% for the continuous model (respectively, it decreased by 9.7% for both models).

Table. 6 assesses the impact of the proportion of undetected patients who subsequently developed symptoms of the disease and were isolated. A change in this parameter slightly affects the duration of the epidemic, the maximum number of patients at a time, as well as the proportion of recovered and dead. With an increase (respectively, decrease) of this parameter by 66.7%, there is an increase (respectively, a decrease) in the total number of cases by 0.5% for both models. At the same time, the number of deaths increases (respectively, decreases) by 0.8% for both models.

Table. 7 examines the effect of the proportion of contact vaccinated pcv who do not

Table 5: Influence of isolated patients proportion who were hospitalized

Parameter p_{ih}	**The total number of recovered and % of the total number of cases**		**The total number of deaths and % of the total number of cases**	
	Discrete	continuous	Discrete	continuous
0.021	7274636 (99.87%)	7456303 (99.87%)	9546 (0.13%)	9822 (0.13%)
0.036	7273712 (99.86%)	7455356 (99.86%)	10471 (0.14%)	10769 (0.14%)
0.006	7275561 (99.88%)	7457251 (99.88%)	8621 (0.12%)	8874 (0.12%)

Table 6: Impact of the proportion of undetected patients who were isolated

Parameter p_{ui}	**Total number of cases and % of the population**		**The total number of recovered and % of the total number of cases**		**The total number of deaths and % of the total number of cases**	
	Discrete	continuous	Discrete	continuous	Discrete	continuous
0.03	7284183 (38.95%)	7466126 (39.93%)	7274636 (99.87%)	7456303 (99.87%)	9546 (0.13%)	9822 (0.13%)
0.05	7318481 (39.14%)	7500949 (40.11%)	7308861 (99.87%)	7491052 (99.87%)	9620 (0.13%)	9897 (0.13%)
0.01	7249636 (38.77%)	7431047 (39.74%)	7240163 (99.87%)	7421300 (99.87%)	9472 (0.13%)	9746 (0.13%)

become ill. This value does not affect the temporal characteristics of the epidemic, as well as the percentage of recovered and dead, but affects their number. In particular, with an increase (respectively, decrease) in this value by 3.3%, the number of cases decreases by 2.9% for the discrete model and 2.8% for the continuous model (respectively, an increase of 2.8% for the discrete model and 2.7% for the continuous model). This is explained by the fact that with such a change, the number of cases among those who have been vaccinated decreases (respectively, increases). As a result, the number of recovered and dead people also decreases (respectively, increases).

Table 7: Impact of the proportion of contact vaccinated who did not infected

Parameter p_{cv}	**Total number of cases and % of the population**		**The total number of recovered and % of the total number of cases**		**The total number of deaths and % of the total number of cases**	
	Discrete	continuous	Discrete	continuous	Discrete	continuous
0.90	7284183 (38.95%)	7466126 (39.93%)	7274636 (99.87%)	7456303 (99.87%)	9546 (0.13%)	9822 (0.13%)
0.93	7071716 (37.82%)	7260647 (38.83%)	7062295 (99.87%)	7250946 (99.87%)	9421 (0.13%)	9701 (0.13%)
0.87	7486743 (40.04%)	7661702 (40.97%)	7477078 (99.87%)	7651766 (99.87%)	9665 (0.13%)	9936 (0.13%)

Table. 8 evaluates the impact of the exposed compartment proportion who did not infected. An increase in this parameter leads to an increase in the duration of the epidemic and the time it takes to reach its peak and a decrease in the number of ill, and therefore recovered and died. This suggests that with less infection, the epidemic becomes less intense, i.e. its terms are stretched, and fewer people get infected overall. In particular, with an increase (respectively, decrease) of this parameter by 1.5%, the duration of the epidemic increases by 12.5% for the discrete model and 13.3% for the continuous model (respectively, a decrease of

9.6% for the discrete model and 9.4% for the continuous model). Under the same conditions, there is a decrease in the number of cases by 19.2% for the discrete model and 19.3% for the continuous model (respectively, an increase of 15.1% for both models). Roughly the same effect has the proportion of exposed that get infected and isolated.

Table 8: Impact of the proportion of exposed who do not get sick

Parameter p_{es}	**Epidemic end time**		**Peak time of the epidemic**		**Total number of cases and % of the population**	
	Discrete	continuous	Discrete	continuous	Discrete	continuous
0.679	1101	1154	442	419	5887261 (31.48%)	6024809 (32.22%)
0.689	1249	1307	522	497	8385774 (44.84%)	8596170 (45.97%)
0.669	996	1045	393	363	5887261 (31.48%)	6024809 (32.22%)

Table. 9 evaluates the impact of the rate of vaccination on the overall process. An increase in this parameter leads to an increase in the duration of the epidemic and the time of its peak and a significant reduction in the total number of cases and those who are simultaneously ill, with a slight decrease in mortality. In particular, with an increase (respectively, a decrease) of this parameter by 80%, it leads to an increase in the duration of the epidemic by 5% for a discrete model and by 4% for a continuous model (respectively, a decrease in the duration of an epidemic by 1.6% for a discrete model and by 0.3% for a continuous model). At the same time, the total number of cases decreases by 36.8% for the discrete model and by 34.9% for the continuous one (respectively, the total number of cases increases by 32.4% for the discrete model and by 30.3% for the continuous model). The number of deaths is reduced by 41.2% for the discrete model and 39.3% for the continuous model (respectively, increases by 40.6% for the discrete model and 37.9% for the continuous model). The results obtained indicate the extreme importance of maintaining a high rate of vaccination of the population.

Table 9: Impact of vaccination rate

Parameter v	**Epidemic end time**		**The total number of deaths and % of the total number of cases**		**Total number of cases and % of the population**	
	Discrete	continuous	Discrete	continuous	Discrete	continuous
0.0005	1101	1154	7284183 (38.95%)	7466126 (39.93%)	9546 (0.13%)	9822 (0.13%)
0.0009	1157	1201	4601617 (24.61%)	4857401 (25.98%)	5610 (0.12%)	5961 (0.12%)
0.0001	1083	1151	9645972 (51.58%)	9730947 (52.04%)	13420 (0.14%)	13548 (0.14%)

4 Conclusion

The results obtained indicate a fairly high efficiency of the proposed models and can be used to predict the development of epidemics. In this case, in each specific case, the system is first identified based on the available statistical information, after which the forecasting problem is solved. For models of epidemic development in the absence of vaccination, this procedure is implemented in [5, 9, 11].

Further refinement of the models can be carried out by considering the possibility of re-infection of those who have been ill due to the mutation of the virus and the gradual decrease of immunity in recovered people, as well as the limited duration of the vaccine. In this case all considered population compartments are preserved, but intercompartment transitions are added, taking into account the possibility of transition from the compartments of recovered and vaccinated to the susceptible compartment.

Acknowledgments

This research was supported by the Grant No. AP09260317 “Development of an intelligent system for assessing the development of COVID-19 epidemics and other infections in Kazakhstan” of Al-Farabi Kazakh National University.

References

[1] Ross, R. The Prevention of Malaria. – London: John Murray, 1911.

[2] Kermack, W.O. and McKendrick, A.G. A Contribution to the Mathematical Theory of Epidemics. – Proc. Roy. Soc. Lond. A, 1927, 115, 700–721.

[3] Keeling, M.J. and Rohani, P. Modeling Infectious Diseases in Humans and Animals Illustrated Edition. – Princeton: Princeton University Press, 2007.

[4] Sameni R. Mathematical Modeling of Epidemic Diseases; A Case Study of the COVID-19 Coronavirus. – arXiv:2003.11371. 2020.

[5] Krivorotko O.I., Kabanikhin S.I., Ziatkov N. Iu. et al. Shishlenin M.A., Matematicheskoe modelirovanie i prognozirovanie COVID-19 v Moskve i Novosibirskoi oblasti. (Mathematical modeling and forecasting COVID-19 in Moscow and Novosibirsk regions). – 2020 https://arxiv.org/pdf/2006.12619.pdf

[6] Almeida, R., Cruz, A., Martins, N., and Monteiro N. An epidemiological MSEIR Model Described by the Caputo Fractional Derivative. – Int. J. of Dynamics and Control, 2019, 7, 776–784.

[7] Mwalili, S., Kimathi, M., Ojiambo, V. et al. SEIR model for COVID-19 dynamics incorporating the environment and social distancing. – BMC Res Notes 13, 352,2020. https://doi.org/10.1186/s13104-020-05192-1

[8] Unlu, E., Leger, H. Motornyi, O. et al Epidemic Analysis of COVID-19 Outbreak and Counter-Measures in France. – 2020. medRxiv. 2020.04.27.20079962. DOI: 10.1101/2020.04.27.20079962.

[9] Krivorotko O.I., Kabanikhin S.I. Matematicheskie modeli rasprostranenia COVID-19. (Mathematical models of COVID-19 development) – Mathematical town in Academcity, Novosibirsk, 2021. – arXiv:2112.05315v1 [q-bio.PE] 10 Dec 2021.

[10] Brauer, F., Feng, Z. and Castillo-Chavez, C. Discrete epidemic models // Math. Biosci. Eng. – 2010, 7. – P. 1–15.

[11] Turar, O., Serovajsky, S., Azimov, A. and Mustafin M Mathematical modeling of the epidemic propagation with a limited time spent in compartments / Proceedings of the 13th International ISAAC Congress, Birkhauser, Springer Int. Publ., Ghent, 2022 (to appear).

[12] Serovajsky, S. Turar, O. Mathematical Model of the Epidemic Propagation with Limited Time Spent in Exposed and Infected Compartments // Journal of Mathematics, Mechanics and Computer Science. – 2021. – No. 4 (112). – P. 162–169.

[13] Serovajsky, S. Mathematical modelling. – Chapman and Hall/CRC, London, 2021.

[14] Vynnycky, E. and White, R.G., eds. An Introduction to Infectious Disease Modelling. – Oxford: Oxford University Press, 2010.

[15] D'Onofrio, A. Stability properties of pulse vaccination strategy in SEIR epidemic model // Math. Biosci. – 2002, vol. 179, P. 57–72. [CrossRef]

[16] Gao, S., Teng, Z., Nieto, J. and Torres, A. Analysis of an SIR Epidemic Model with Pulse Vaccination and Distributed Time Delay. – Journal of Biomedicine and Biotechnology. 2007, 64870. doi:10.1155/2007/64870. PMC 2217597. PMID 18322563.

[17] De La Sen, M., Agarwal, R.P., Ibeas, A. and Alonso-Quesada, S. On a Generalized Time-Varying SEIR Epidemic Model with Mixed Point and Distributed Time-Varying Delays and Combined Regular and Impulsive Vaccination // Controls. Adv. Differ. Equ. 2010, 2010, 281612.

[18] Etxeberria-Etxaniz, M., Alonso-Quesada S. and De la Sen, M. On an SEIR Epidemic Model with Vaccination of Newborns and Periodic Impulsive Vaccination with Eventual On-Line Adapted Vaccination Strategies to the Varying Levels of the Susceptible Subpopulation // Appl. Sci. 2020, 10, 8296; doi:10.3390/app10228296. – 24 p.

[19] Schlickeiser, R. and Kroger, M. Analytical Modeling of the Temporal Evolution of Epidemics Outbreaks Accounting for Vaccinations // Physics. – 2021, 3: 386. doi:10.3390/physics3020028. S2CID 233589998.

[20] Li-Ming Cai, Zhaoqing Li, and Xinyu Song. Global Analysis of an Epidemic Model with Vaccination // J. Appl. Math. Comput. – 2018. – 57(1). – P. 605–628.

[21] Ghostine, R., Gharamti M., Hassrouny, S. and Hoteit, I. An Extended SEIR Model with Vaccination for Forecasting the COVID-19 Pandemic in Saudi Arabia Using an Ensemble Kalman Filter // Mathematics 2021, 9, 636. – 16 p. https://doi.org/10.3390/math9060636

[22] Parolinia, N., Luca Dede'a L., Ardenghia G., and Quarteroni A. Modelling the COVID-19 Epidemic and the Vaccination Campaign in Italy by the SUIHTER Model / arXiv:2112.11722v1 [q-bio.PE] 22 Dec 2021. https://arxiv.org/pdf/2112.11722.pdf

МАЗМҰНЫ – СОДЕРЖАНИЕ – CONTENTS